NTNU

Norwegian University of
Science and Technology

Numerical modelling and photo-electrochemical characterization of dye sensitized solar cells

Jacob Hadler-Jacobsen

Chemical Engineering and Biotechnology
Submission date: June 2017
Supervisor: Svein Sunde, IMA

Norwegian University of Science and Technology
Department of Materials Science and Engineering

Preface

The presented master thesis was carried out at the Department of Materials Science and Engineering at the Norwegian University of Science and Technology during the spring 2017. The assembly of the solar cells and the absorbance measurements were done at the department of chemistry by Audun Formo Buene. All the other work was carried out by the author.

Trondheim, June 2017

Jacob Hadler-Jacobsen

Acknowledgements

I would like to thank my supervisor Professor Svein Sunde for good guidance and advice, technical assistance and for giving me much freedom on how to shape this thesis.

I would like to thank Audun Formo Buene, for assembling and lending me the solar cells, for providing absorbance measurements, and for helpful discussions and insight into the world of organic dyes.

Furthermore, I would like to thank the Department of Chemistry which has provided the materials and dyes for the solar cells.

Last, but not least, would I like to thank technical staff at the Department of Materials Science and Engineering for help and for providing a good laboratory.

Abstract

Dye sensitized solar cells (DSSC) represent a potential low-cost alternative to the traditional silicon solar cells. DSSC's do not have the need for ultra-pure semiconductor material, and they are easy to assemble. However, they need very specialized dyes to work well. These dyes have typically been dependent on the expensive noble metal ruthenium. Recently however, there has been a new category of promising ruthenium-free dyes emerging. It is important to understand how the DSSC's and the new dyes work, so that they can be improved further. One way to understand this, is to use photo-electrochemical methods in combination with numerical modelling.

Current-potential characteristics were recorded, and intensity modulated photocurrent spectroscopy (IMPS), intensity modulated photovoltage spectroscopy (IMVS), and electrochemical impedance spectroscopy (EIS) was performed on two DSSC's. The two DSSC's were made identical, except that one was made with a well-known ruthenium dye (N719), and the other one with a novel ruthenium-free purely organic dye (AFB5-098, abbreviated AFB8). Anta et al.'s numerical version of the diffusion model[1] was extended to include small amplitude perturbation and used to interpret the experimental data. This made a basis from which the solar cells could be characterized and compared, and suggestions for ways to improve the cells were presented.

The extended numerical model reproduced both the experimental IV-characteristic and the IMPS and IMVS spectra with good, if not perfect, accuracy. It was further revealed by the model that the N719- DSSC had poor charge capture efficiency, but excellent injection and absorption efficiency. The AFB8-DSSC on the other hand, had excellent charge collection efficiency, but seemed to have sub-optimal injection and/or absorbance efficiency. There were strong indications that the N719-DSSC could benefit significantly from decreased thickness of the titanium dioxide layer and quicker diffusion. There were some indications that the AFB8- DSSC could increase its efficiency moderately from a thicker titanium dioxide layer. Both cells would gain a higher potential from slower recombination, while the N719-DSSC would also gain increased current density from it. All in all, the combination of the numerical modelling and the photo-electrochemical experimental work was successful at both characterizing and suggesting ways to optimize the solar cells.

Sammendrag

Fargestoffbaserte solceller (DSSC) er et potensielt lavprisalternativ til dagens silisiumbaserte solceller. De har ikke det samme behovet for ultra-høy renhet i halvledermaterialet, og de er enkle å produsere. Derimot er et problem med de fargestoffbaserte solcellene at de har vært og til dels er avhengige av kostbare fargestoff som inneholder det dyre og sjeldne edelmetallet ruthenium. Det er i midlertidig mange nye lovende rutheniumfrie fargestoff som er under utvikling. For å kunne utvikle disse fargestoffene videre, er det viktig å ha metoder for å kunne karakterisere de fargestoffbaserte solcellene. En måte å gjøre slik karakterisering, er ved hjelp av foto-elektrokjemiske målinger i kombinasjon med numerisk modellering.

Strøm-spenningskarakteristikker ble målt, og intensitetsmodulert fotostrøm-spektroskopi (IMPS), intensitetsmodulert fotospenning-spektroskopi (IMVS) og elektrokjemisk impedans-spektroskopi ble gjennomført på to forskjellige fargestoff-baserte solceller. De to solcellene var identiske, bortsett fra at den ene ble laget med et godt kjent rutheniumfargestoff (N719), mens den andre ble laget med et nyutviklet ruteniumfritt fargestoff (AFB5-098, forkortet til AFB8). Anta et al. sin numeriske versjon av diffusjonsmodellen[1] ble utvidet til å inkludere lav-amplitude perturbasjon, for så å bli brukt til å tolke eksperimentelle data. Dette utgjorde et fundament som ble brukt til å karakterisere, sammenligne og foreslå måter å optimalisere solcellene på.

Den utvidede numeriske modellen lyktes bra i å gjenskape strøm-spenningskarakteristikker, samt IMPS og IMVS-spektre. Solcellen laget med N719 viste seg å ha utmerket injeksjon- og absorbsjons-virkningsgrad, men hadde stort forbedringspotensial på ladningsoppsamlings-virkningsgraden. Solcellen som ble laget med AFB8 derimot, viste seg å ha utmerket ladningsoppsamlings-virkningsgraden, men hadde sub-optimal injeksjon og/eller absorbsjons-virkningsgrad. Videre, så var det sterke indikasjoner på at solcellen laget med N719 kunne oppnå betydelig økning i virkningsgrad hvis den ble laget med et tynnere titandioksidlag, eller hvis diffusjonshastigheten kunne blitt økt. Det var noen indikasjoner på at solcellen laget med AFB5-098 kunne øke sin virkningsgrad moderat, hvis den ble laget med tykkere titandioksidlag. Begge solcellene vil kunne levere høyere potensial om rekombinasjonen ble tregere, mens N719-solcellen også vil kunne levere økt strømtetthet. Alt i alt lyktes de foto-elektrokjemiske målingene i kombinasjon med den utvidede numeriske modellen i å karakterisere og i å foreslå forbedringer for solcellene.

Table of Contents

List of symbols, terms and abbreviations

Abbreviations and terms	Description
AFB8	A purely organic dye, whose full name is AFB5-098
DSSC	Dye Sensitized Solar Cell
EIS	Electrochemical Impedance Spectroscopy
FTO	Fluoride-doped Tin Oxide
HOMO	Highest Occupied Molecular Orbital
IMVS	Intensity Modulated photoVoltage Spectroscopy
IMPS	Intensity Modulated Photocurrent Spectroscopy
IPCE	Incident Photon-to-electron Conversion Efficiency
IV	Current-Voltage
LUMO	Lowest Unoccupied Molecular Orbital
N719	A Ruthenium based dye
TCO	Transparent Conducting Oxide. This is where the current is collected. The TCO is situated at $x = 0$ in the model.

Symbol	Units	Description
$_0$		Subscript indicating reference state. The reference state chosen in this work is a solar cell with no illumination, i.e. in the dark.
a	-	$(1-\alpha)/\alpha$
b	-	$(\beta-\alpha)/\alpha$
c	$\mathrm{m.s^{-1}}$	Speed of light
C	F	Capacitance
C_0	F	Capacitance at a reference state
d	m	Thickness of the active titanium dioxide layer, ref Figure 2.4.
D_n	$\mathrm{m^2.s^{-1}}$	Density dependent diffusion "constant" for electrons in conduction band of TiO_2
D_{ref}	$\mathrm{m^2.s^{-1}}$	D_n for a given reference state
D_0	$\mathrm{m^2.s^{-1}}$	D_n for the reference state of a DSSC in the dark
D		Dye molecule
D*		Dye molecule with an electron excited into the LUMO
e		Eulers number
E	-	Indicating that the axis shows Energy
f	Hz	Frequency of modulation
$f_{min,IMPS}$	Hz	The frequency at the minimum in an IMPS-spectrum
$f_{min,IMVS}$	Hz	The frequency at the minimum in an IMVS-spectrum
F		$K_D n^a \frac{\partial n}{\partial x}$
F_{Im}		$K_D n_{ss}^a \frac{\partial P_{Im}}{\partial x} + K_D P_{Im} a n_{ss}^{(a-1)} \frac{\partial n_{ss}}{\partial x}$
F_{Re}		$K_D n_{ss}^a \frac{\partial P_{Re}}{\partial x} + K_D P_{Re} a n_{ss}^{(a-1)} \frac{\partial n_{ss}}{\partial x}$

Symbol	Units	Description
h	$\mathrm{m}^2.\mathrm{kg}.\mathrm{s}^{-1}$	Planck Constant
i		Imaginary number
I	$\mathrm{A}.\mathrm{m}^{-2}$	Current density
I_{Im}	$\mathrm{A}.\mathrm{m}^{-2}$	Imaginary part of the current response. Measured in IMPS
I_{sc}	$\mathrm{A}.\mathrm{m}^{-2}$	Short circuit current
J_D	$\mathrm{C}.\mathrm{m}^{-3}.\mathrm{s}^{-1}$	The diffusion term
J_G	$\mathrm{C}.\mathrm{m}^{-3}.\mathrm{s}^{-1}$	The generation term
J_R	$\mathrm{C}.\mathrm{m}^{-3}.\mathrm{s}^{-1}$	The recombination term
k_0	s^{-1}	k_{ref} for the reference state of a DSSC in the dark
k_l	s^{-1}	$k_{ref}\left(\frac{n}{n_{ref}}\right)^b$
k_{ref}	s^{-1}	The recombination rate constant, at a given reference state
k_B	$\mathrm{J}.\mathrm{K}^{-1}$	Boltzmann constant
K_D		D_0/n_0^a
K_G	$\mathrm{A}.\mathrm{W}^{-1}$	Constant stating how many amperes there is in one watt of light with 453 nm wavelength.
K_R		$(\beta k_0)/(\alpha n_0^b)$
n	$\mathrm{mol}.\mathrm{m}^{-3}$	Electron concentration in TiO_2's conduction band
n_0	$\mathrm{mol}.\mathrm{m}^{-3}$	n for the DSSC in the dark.
n_A	$\mathrm{mol}.\mathrm{m}^{-3}$	Amplitude for the time dependent part of *n*
n_{ss}	$\mathrm{mol}.\mathrm{m}^{-3}$	The steady state part of *n*
n_t	$\mathrm{mol}.\mathrm{m}^{-3}$	The time dependent part of n
n_{ref}	$\mathrm{mol}.\mathrm{m}^{-3}$	n for the DSSC at a reference state
p	-	Constant used in describing injection rate
P_{Im}		$n_A \sin(\phi)$
P_{Re}		$n_A \cos(\phi)$
q	C	Elementary charge
R_r	Ω	Recombination resistance
R_{r_0}	Ω	Recombination resistance at a reference state
R_s	Ω	Series resistance
R_{sh}	Ω	Shunt resistance
T	K	Temperature
V	V	Potential
V_{Im}	V	Imaginary part of the potential response. Measured in IMVS
V_{loss}	V	Potential loss
V_{oc}	V	Potential over the DSSC at open circuit
x	m	Variable indicating the distance from the TCO in the titanium dioxide. Can have values from $x = 0$ to $x = d$
Z_{Im}	Ω	Imaginary part of impedance
Z_{Re}	Ω	Real part of impedance
α	-	A parameter related to the energy and distribution of trap states
β	-	A parameter related to the recombination reaction rate order
η_{abs}	-	Absorption efficiency
η_{cc}	-	Charge capture efficiency
η_{inj}	-	Injection efficiency
η_{inj_0}	-	Injection efficiency when the potential in the TiO_2 is zero
η_{pc}	-	Power conversion efficiency. Often called just "efficiency"

Symbol	Units	Description
ϵ	m^{-1}	Absorption coefficient
λ	m	Wavelength
$\Lambda(x)$		$\eta_{\mathrm{inj}} K_G \epsilon \left(e^{-\epsilon x} + \eta_{\mathrm{refl}} e^{\epsilon(x-2d)}\right)$
τ_{rec}	s	Recombination time constant
τ_{trans}	s	Transport time constant
ϕ	-	The phase difference between Φ and n
Φ	$\mathrm{W.m}^{-2}$	Intensity of the light shining on the DSSC.
Φ_A	$\mathrm{W.m}^{-2}$	Amplitude for the time dependent part of Φ
Φ_t	$\mathrm{W.m}^{-2}$	The time dependent part of Φ
Φ_{ss}	$\mathrm{W.m}^{-2}$	The steady state part of Φ
ω	s^{-1}	Angular velocity
ω_{max}	s^{-1}	Angular velocity giving the largest Z_{Im}

1 Introduction

The Paris Agreement was signed in 2015, and one aim of it is "Holding the increase in the global average temperature to well below 2 °C above pre-industrial levels and to pursue efforts to limit the temperature increase to 1.5 °C above pre-industrial levels, recognizing that this would significantly reduce the risks and impacts of climate change;"[2]. The CO_2 emissions needs to be drastically reduced for this goal to be reached, and one way to do so is to replace fossil fuels with renewable energy sources.

The renewable energy source with the largest potential is the sun. The energy received from the it is approximately 10 000 times the worlds energy needs[3, 4]. Currently, traditional silicon solar cells represent the most widely adapted technology for harvesting the radiative power from the sun. These cells are durable and efficient, but they also depend on silicon of ultra-high purity (99.9999%) to work[5]. Vast amounts of energy are required in the production of the very pure silicon, contributing to a relatively high cost.

Dye sensitized solar cells (DSSC's) may represent a low-cost alternative to the traditional silicon solar cells. They consist of a dye, a semiconductor, an electrolyte, and two electrodes. The semiconductor does typically have a bandgap in the UV-range, and does not absorb any light. Instead the dye absorbs the light, and injects electrons into the semiconductor. DSSC's do not contain any p-n junction, and thus do not have the same demands on material purity as the traditional solar cells. They are however very dependent on specialized dyes to capture the light. Not only does a good dye need strong absorption, but it also needs to be tailored to go well along with the electrolyte and the semiconductor.[6]

One of the main obstacles before commercialization of the DSSC's is that there is no dye which is both effective and inexpensive. The best dyes have typically been organo-metallic molecules with ruthenium. They can give efficiencies of ~13%[7], but they are costly both because of a complex synthesis and because ruthenium is an expensive noble metal. Ruthenium-free dyes giving high efficiencies are needed if DSSC's are to become a low-cost alternative. Purely organic dyes present a promising alternative to the ruthenium dyes, and are currently approaching the ruthenium dyes' efficiencies at 13%[8], while 15% has been considered necessary for commercialization of DSSC's[9].

It is important to know how the dyes perform in a DSSC, both so that better dyes can be developed, and so that the DSSC's can be tailored to work as well as possible for a given dye. A common way to investigate this is by using photo-electrochemical methods in combination with numerical models[10]. The models can estimate important parameters like the charge collection efficiency and predict the power conversion efficiency for different thicknesses of the titanium dioxide.

This thesis has three main objectives:
- The first goal is to see whether the diffusion model as presented by Anta et al.[1] can be extended to include small amplitude perturbations. This would enable a model were all the parameters are determined experimentally. The model could be controlled up against experimental results from both small amplitude perturbation techniques and current-potential characteristics.
-The second goal is to see whether this model can give useful information on how two DSSC's made with different dyes work and compare. One of the dyes is a well-known ruthenium dye, namely N719. The other dye is AFB8, a novel purely organic dye made at the department of chemistry at NTNU, which shows similar efficiency as N719.
-The third goal is to see whether the model can be used for optimization of the two cells which were investigated.

The diffusion model by Anta et al[1] was extended and implemented in MATLAB, and fit to experimental data obtained from Intensity modulated photo-current spectroscopy (IMPS), intensity modulated photo-voltage spectroscopy (IMVS), electrochemical impedance spectroscopy (EIS) and current voltage characteristics (IV-characteristics). The model was used to interpret the experimental results, so that information on the charge collection efficiency η_{cc}, the injection efficiency η_{inj}, and the absorption efficiency η_{abs} could be achieved. Finally, the model was used to suggest whether the cells had the optimal thickness, and whether there were transport or recombination limitations. This is summarized in Figure 1.1:

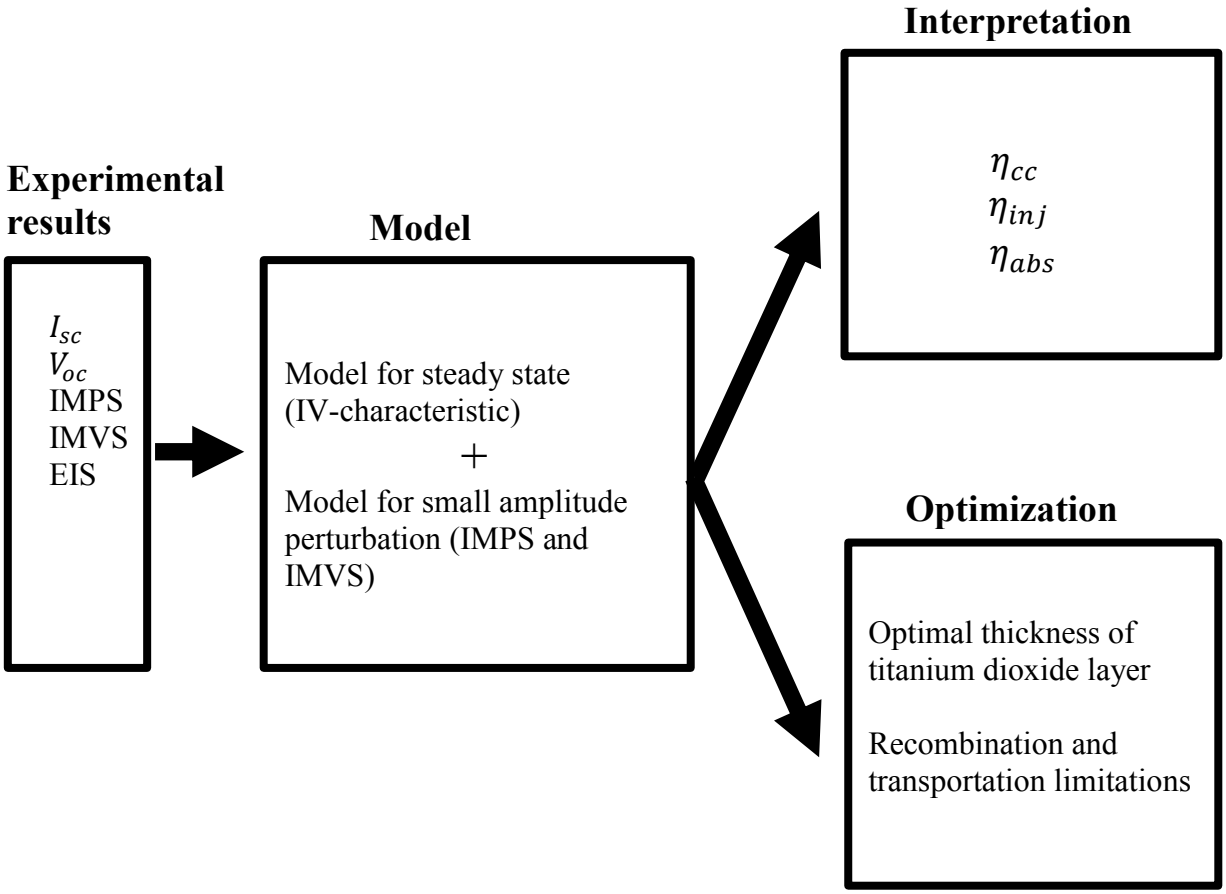

Figure 1.1: A summary of the workflow presented in this thesis. First, the short circuit current I_{sc}, the open circuit potential V_{oc} and IMPS, IMVS and EIS spectra were obtained. A model was used to interpret these experimental results, giving information on the charge collection efficiency η_{cc}, the injection efficiency η_{inj}, and the absorption efficiency η_{abs}. The model was also used to suggest how the DSSC's could be optimized, by giving information on optimal thickness of titanium dioxide layer and recombination and transportation limitations.

2 Theory of dye sensitized solar cells

2.1 Basic working principle

There are different types of DSSC's, but they are most commonly made from four parts: At least one dye, a semiconductor with a bandgap in the ultra violet range, two electrodes made from glass coated with a transparent conducting oxide (TCO), and an electrolyte[6]. The cells treated in this thesis are made with nanoporous titanium dioxide as the semiconductor, an electrolyte based on the redox couple I^-/I_3^-, and a cathode with platinum catalyst. This combination of four parts enables the DSSC's to convert radiative energy to electric work. The way a DSSC does this is best explained in several steps[6, 11], as shown in Figure 2.1. First, a photon is absorbed by a dye molecule. This will cause an electron in the dye to be excited. If the dye molecule is designed properly, the excited electron will be injected into the titanium dioxide, instead of falling back to the ground state. The dye molecule is oxidized in this process, but quickly regains an electron from the electrolyte. The electrolyte will in turn be regenerated at the cathode. The electron which was injected into the titanium dioxide will be transported by diffusion through the titanium dioxide and collected at the TCO anode. However, bear in mind that the working principles presented here are greatly simplified. A more thorough explanation can be found in [6]. Figure 4.2 shows a picture of what an assembled DSSC can look like.

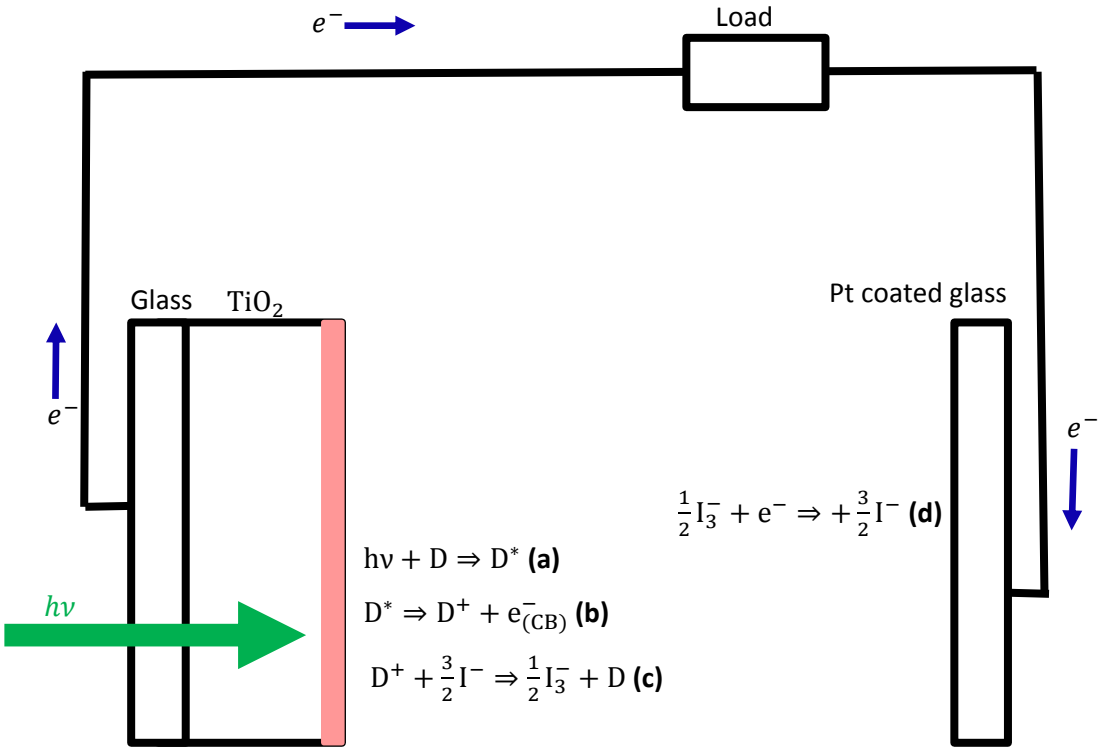

Figure 2.1: The basic principle of a DSSC with TiO_2 semiconductor and I^-/I_3^- based electrolyte. To the left is the anode, composed of dye-coated TiO_2 deposited on glass. Though not shown in the figure, the TiO_2 is typically nanoporous to increase the area which the dye can adsorb on. To the right is the cathode, which consists of glass coated with catalytic platinum. The glass at both sides is coated with a transparent

conducting oxide (TCO), giving it electrical conductivity The arrow coming in from the right illustrates the light shining on the DSSC. Reaction (a) is a dye molecule (D) absorbing a photon (hν), resulting in excitation of the dye molecule (D*). Reaction (b) is the excited dye molecule injecting an electron into the conduction band of the TiO_2. Reaction (c) is the oxidized dye molecule being regenerated by reacting with the electrolyte. Reaction (d) is the regeneration of the electrolyte at the cathode.

Figure 2.2 shows the same as Figure 2.1, just with names for the different processes, and indications of the energy levels.

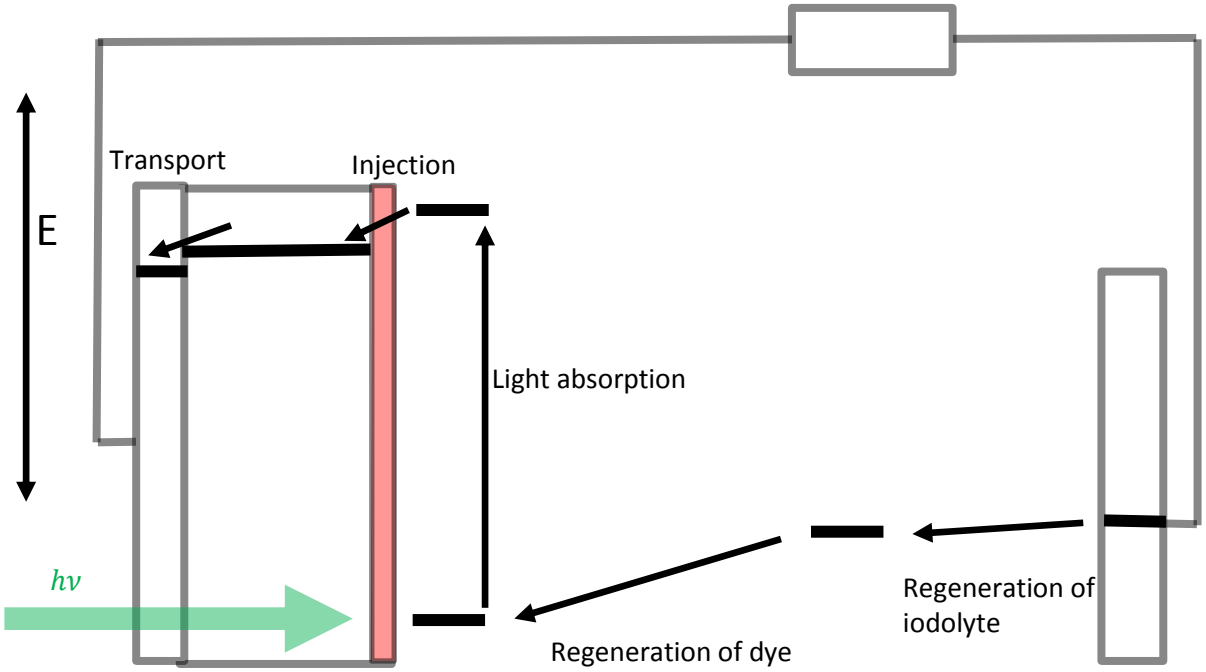

Figure 2.2: The processes in a DSSC labeled with names. The arrows indicate how the electron is transported through the cell. The energy levels are indicated, but are not to scale.

An electron is raised in potential when the dye absorbs a photon. For all other processes in the cell, there will be a potential loss. This results in that the potential which is measured over the cell is lower than the potential which would be expected from the energy of the photon absorbed alone. This is shown in Figure 2.3:

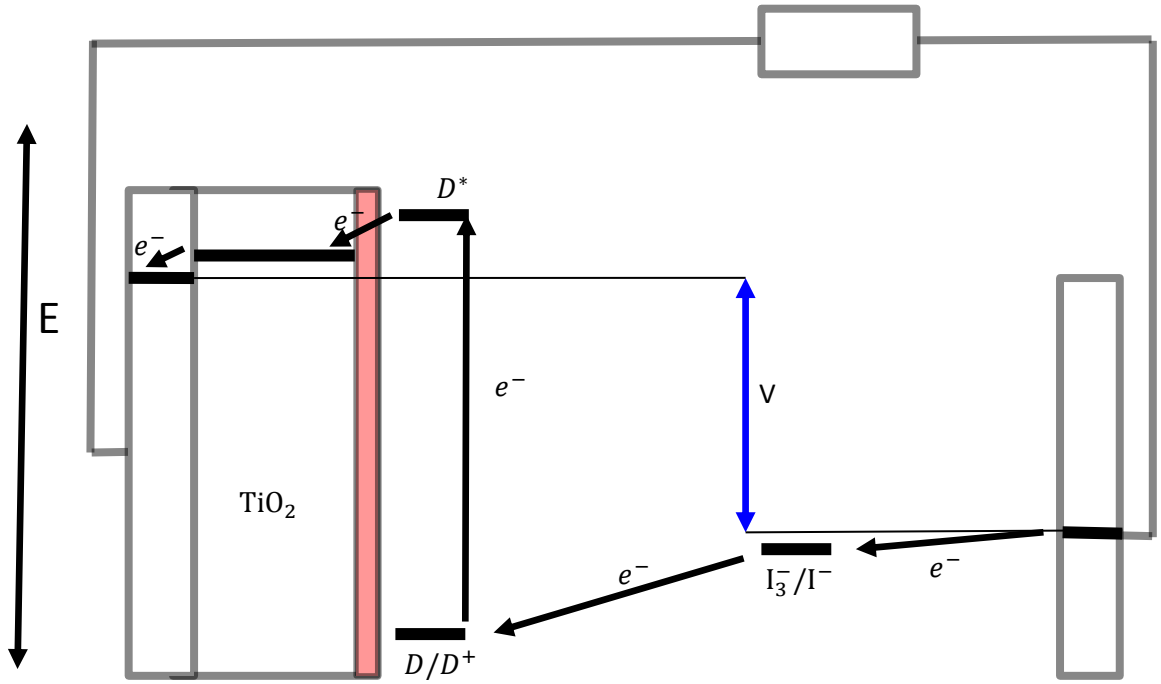

Figure 2.3: The energy levels in a DSSC. The blue arrow is the potential difference which would be measured over an illuminated cell connected to a load. The energy levels are not to scale.

It is the losses in the anode (the titanium dioxide) which is the focus of this work. The other potential losses can often be assumed negligible[1], especially for the moderate light intensities which has been utilized[9, 12].

The anode is greatly simplified in Figure 2.1, Figure 2.2 and Figure 2.3. A more correct description of the anode can be found in Figure 2.4. Figure 2.4 shows that the titanium dioxide layer is nanoporous. This increases the surface area, so that more dye can be adsorbed. This does again enable more light to be absorbed by the DSSC.

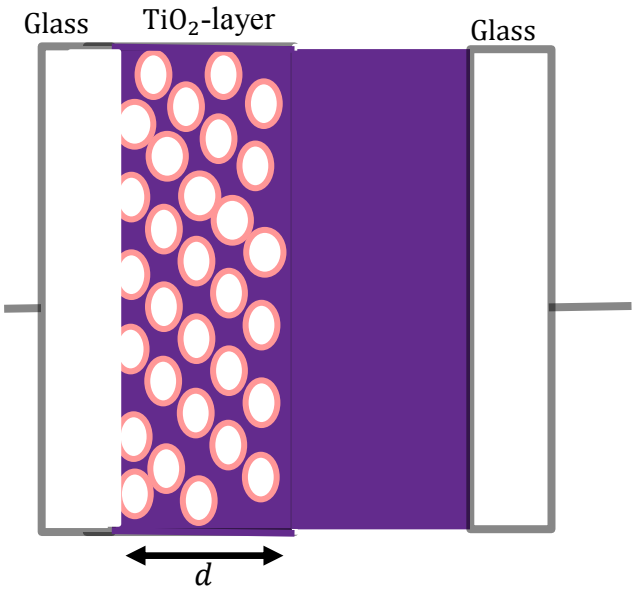

Figure 2.4: The DSSC, illustrated with emphasis on the nanoporous titanium dioxide layer. The white circles are nanoporous titanium dioxide, which is coated with a dye (light red). The purple area illustrates the electrolyte. The glass anode is in contact with both the titanium dioxide and the electrolyte. The thickness of the titanium dioxide layer is denoted with *d*. There is often a porous reflective layer to the right of the titanium dioxide layer, which is not shown in this figure.

2.2 The dye and the electrolyte

A good dye for a DSSC needs to fulfill several requirements. First of all, it needs to be effective at absorbing photons. The thickness of the titanium dioxide layer is limited, and thus is also the amount of the surface area which the dye can adsorb onto. It is therefore important that the limited amount of adsorbed dye can absorb as much of the light as possible. Next, the dye needs to absorb photons with the right energies. An ideal dye for a single dye DSSC would absorb all photons from the near infrared region and up [6]. This combination of both broad and strong absorption is however hard to achieve, since strong absorption typically also means narrow absorption[13]. Though if ideal absorption is achieved, then that would enable a theoretical maximum efficiency slightly above 30% [6]. This is the same theoretical efficiency as of a traditional single junction solar cell, as given by the Shockley-Queisser limit [14]. The cells which are examined in this thesis are made with a single dye, but it can be mentioned that DSSC's can be made with multiple dyes with different absorption as well. This would be analogous to tandem cells, and would allow even higher efficiencies [6].

There are also structural requirements for a good dye. First, it needs an anchoring group[12]. That is, a part of the molecule must be designed to attach to the titanium oxide, ensuring good adsorption. It is useful to introduce the terms HOMO and LUMO to understand the other structural requirements. Highest occupied molecular orbital, abbreviated HOMO, is the orbital in a molecule where the electron highest in energy resides. Lowest unoccupied molecular orbital, abbreviated LUMO, is the orbital with lowest energy that is unoccupied. Simplified, it can be said that an electron is excited from HOMO to LUMO when a photon is absorbed by

the dye [12]. The excited state with an electron in LUMO is not stable, and in a ruthenium-dye the electron will fall back into the HOMO in the timespan of 10^{-8}s[6]. What makes dyes used for DSSC's special, is the spatial position of the HOMO and LUMO. LUMO should preferably be close to or at the anchoring group, while the HOMO should be separate from the LUMO. This is shown in Figure 2.5 for the ruthenium-free dye AFB8. When an electron is excited to the LUMO orbital, it will have a shorter distance to the titanium dioxide than to the HOMO. Thus, it will have a kinetic favoring of going to the titanium dioxide. This kinetic favoring needs to be considerably stronger than the energetic favoring of the electron falling back to HOMO. The electron is said to be "injected" into the titanium dioxide when it goes from LUMO to the titanium dioxide. The fraction of electrons in LUMO that are injected, instead of falling back to HOMO, is called the injection efficiency. For a ruthenium-dye, the injection process happens in the timespan of 10^{-11} to 10^{-13} s[12], considerably faster than de de-excitation. This is contributed to the short distance between the titanium dioxide and the LUMO, and ensures high injection efficiency. The whole process, from a dye absorbing a photon to it injects an electron is illustrated in Figure 2.5. DSSC's can be made with natural dyes. For instance, something as simple as blackberry dye can be used [15, 16]. However, even though natural dyes can have strong absorption, they typically do not meet the structural requirements, and have not achieved efficiencies higher than ~2% as of 2015[17]. This illustrates the importance of the dye's structure.

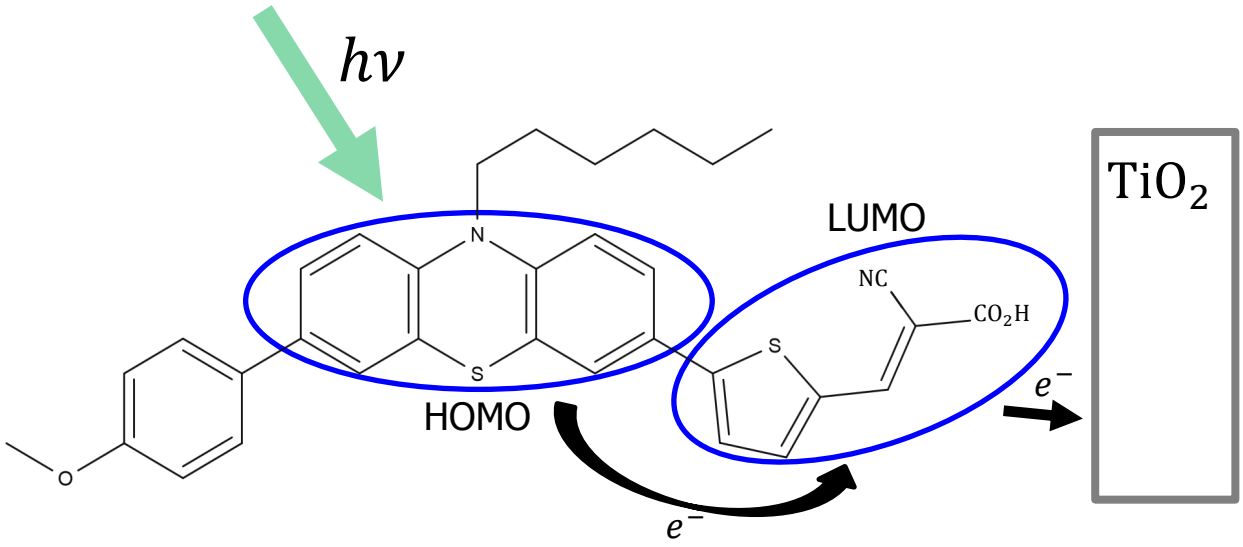

Figure 2.5: The structure of the organic dye AFB8 used in a DSSC in this work. To the right is TiO_2 which the dye is attached to the surface of. The blue circle to the left indicated the position of the HOMO. The blue circle to the right is the position of the LUMO and the anchoring group. To the right is also the titanium dioxide which the anchoring group is attached to. The green arrow symbolizes a photon which is absorbed by the dye. This results in an electron being excited to the LUMO, before being injected into the titanium dioxide. This figure is based on information from Audun Formo Buene at the department of chemistry, NTNU.

The injection efficiency is often treated as independent of the potential in the titanium dioxide [6]. This is only true up to a certain potential however. The energy for electrons in the titanium dioxide needs to be lower than the energy for an electron in LUMO, for injection to occur. It is not enough that the injection process is kinetically favored, it must also be energetically possible. The needed energy difference is indicated in Figure 2.2. However, even at potentials over the DSSC as high as 1070 mV, the decrease in injection efficiency was only found to be from 83% to 76% for a N719-based DSSC [18]. To comparison, the highest potentials measured in this thesis were around 600 mV. This indicates that the potential dependence can be neglected, at least for the moderate light intensities used in this work.

The energy level of HOMO needs to match with the electrolyte, both when the dye molecule is ionized and in its neutral state. This is so that the dye is stable in contact with the electrolyte, and so that the electrolyte will be able to regenerate the dye, as shown in Figure 2.1 c). This can also be looked at the other way around, by saying that the electrolyte needs to have an energy level which matches well with the dye's energy level.[6]

Three criteria for a good electrolyte are high conductivity, quick transportation of I^-/I_3^-, and fast kinetics for reaction c) and d) in Figure 2.1. These criteria need to be fulfilled to avoid potential losses between the cathode and the anode, as shown in Figure 2.3. It is especially for high current densities in DSSC's which are made with thick nanoporous anodes that the

aforementioned criteria are of high importance. The kinetic overpotential at the anode is often minimized by using a platinum catalyst at the cathode. The transport overpotential can be minimized by using a thin titanium dioxide layer, but this will also decrease the absorption. A thick nanoporous anode on the other hand, will be able to absorb much of the light, but have increased transport overpotential due to a longer distance for the I^-/I_3^- to diffuse through the nanoporous titanium dioxide. Thus, there is a tradeoff between potential loss and absorption efficiency. However, for low enough current densities in properly designed cells, both ohmic, kinetic and transport overpotentials are assumed neglectable[1].[6]

2.3 Transport and recombination in the titanium dioxide

An electron which has been injected into the titanium dioxide can either be transported to the TCO and collected, or it can recombine. The transportation in the titanium dioxide is mainly diffusion driven. This is because the electrolyte shields the electrons from electrical fields in the nanoporous titanium dioxide. With negligible electrical fields to cause drift, it is only the concentration gradient which will fuel the transportation. The average time it takes for an electron to diffuse through the titanium dioxide and be collected, is often denoted with a time constant[19]. This characteristic time is in this work labeled τ_{trans}.

Recombination is the process of the injected electron reacting from the titanium dioxide and back into the electrolyte or with the oxidized dye. This is shown in Figure 2.6 The electrons in the conduction band will be at a higher potential than the electrolyte, and it is thus energetically favorable to recombine with the electrolyte or the oxidized dye. A good DSSC is dependent on unfavorable kinetics for this back reaction. In the same way as for transportation, a time constant can be defined for recombination[20]. In this work, it is labeled τ_{rec}. It is a measure of the average time an electron resides in the titanium dioxide before it recombines. The more kinetically unfavorable the recombination, the higher the recombination time constant will be. The recombination with the electrolyte is the dominant reaction for DSSC's with I^-/I_3^--based electrolytes, because the oxidized dye is regenerated by the electrolyte very quickly[6].

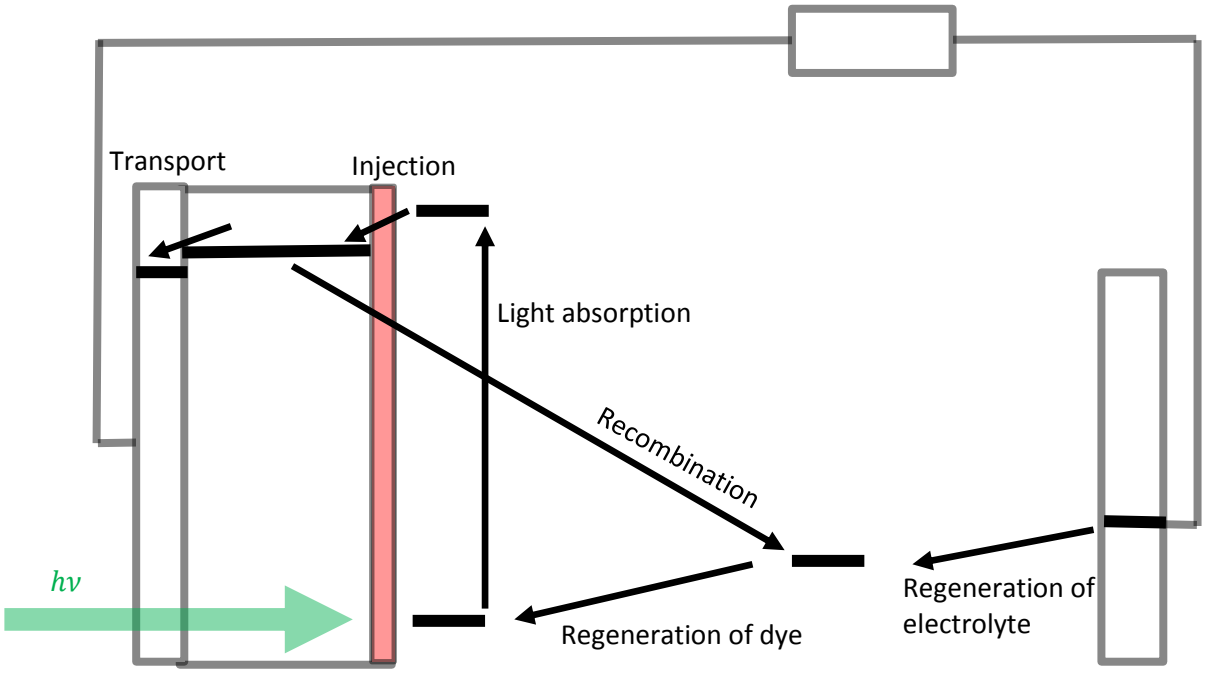

Figure 2.6: The same as Figure 2.2, but with recombination included as well. Electrons in the conduction band can recombine with both the electrolyte and the oxidized dye. It is only shown recombination with the electrolyte in this figure.

The ratio of the recombination time constant and the transportation time constant gives a qualitative indication of how effectively electrons are collected at the anode. A large time constant for recombination and a small time constant for transportation implies that most electrons will be transported before they get time to recombine. The transportation is quicker than the recombination in this case. The ratio between injected electrons and collected electrons is an important parameter in the evaluation of a DSSC. This ratio is called the charge collection efficiency, and will be discussed further in the next section. The charge collection efficiency is however somewhat complicated to calculate, because the recombination and transportation rates are nonlinear with respect to electron concentration[10].[21]

The nonlinearity of both transportation and recombination arises due to trapping of electrons in the titanium dioxide. Once injected into the titanium dioxide, most of the electrons fall into trapped states. There is an equilibrium between the trapped states and the free states in the titanium dioxide. Electrons in trapped states cannot diffuse nor recombine, but the free electrons can. Thus, the state of the equilibrium between free and trapped states greatly influences both recombination and transportation dynamics. This equilibrium is for instance dependent on the illumination of the DSSC.[1, 6]

2.4 Incident photon to electron conversion efficiency

The theory of DSSC's which has been presented so far, can be summarized to a large degree in the "incident photon to electron conversion efficiency", commonly abbreviated IPCE. The IPCE can be expressed as[22]:

$$IPCE = \eta_{abs}\eta_{inj}\eta_{cc} \quad (1)$$

Where η_{abs} is the absorbance efficiency, η_{inj} is the injection efficiency, and η_{cc} is the charge capture efficiency. The absorption efficiency is the amount of photons which are absorbed by the dye, divided by the amount which enters the DSSC. $\eta_{abs} = 1$ would be the case of all the light shining on the DSSC being absorbed by the dye at some point. Thick nanoporous titanium dioxide layers will have much surface area, enabling large amounts of dye to be absorbed by the titanium dioxide. The stronger absorption of the dye molecules, the more of the absorption of photons. Thus, DSSC's with thick nanoporous titanium dioxide layers, stained with dyes with strong absorption, will give high absorption efficiencies.

The injection efficiency is the fraction of absorbed photons which result in an electron being injected into the titanium dioxide. $\eta_{inj} = 1$ corresponds to the case of one electron being injected into the titanium dioxide for every photon which is absorbed. As previously mentioned, a high η_{inj} is dependent on a carefully designed molecular structure. It is also dependent on that the potential is low enough in the titanium dioxide. The structure makes the injection process kinetically favorable, while the potential needs to be low enough so that the injection process is energetically possible.

The charge capture efficiency, η_{cc}, is the fraction of injected electrons which are successfully transported through the titanium dioxide and collected at the TCO. η_{cc}=1 is the case when every injected electron ends up being collected at the TCO. Quick transportation and slow recombination promotes high charge capture efficiency.

The IPCE can be measured experimentally by using the relation:

$$I = IPCE * \Phi * K_G \quad (2)$$

Where I is the current, Φ is the light intensity shining on the cell, and K_G is a constant. These are explained in more detail in section 3. From equation (2) it can be seen that the IPCE has to be zero for the case of open circuit. This will typically be because the recombination limits the build-up of electrons in the titanium dioxide, and thus the potential. For an ideal DSSC however, the recombination would be zero. The IPCE would still have to be zero at open circuit. This would then be due to the injection efficiency going towards zero as the energy difference between LUMO in the dye and the potential in the titanium dioxide goes toward zero. For all other potentials, the IPCE would be 100% for the case of ideality.

3 Mathematical models

Modelling of DSSC's stretches back to the 90's. One of the first publications on the topic was Sødergrens paper "Theoretical Models for the Action Spectrum and the Current-Voltage Characteristics of Microporous Semiconductor Films in Photoelectrochemical Cells"[23] from 1994. Here it was established that an analytical model for the IV-characteristics of DSSC's could be developed by considering the electron transport in the semiconductor as purely diffusion driven. This model is hereafter described as the "diffusion model". The original diffusion model treated diffusion and recombination as linear processes in the DSSC's. However, it is now known that neither transportation nor diffusion behaves linearly, due to trapping and de-trapping, as mentioned in section 2.3. The diffusion model has been expanded and adjusted several times [24-26], to account for these non-linearities.

A numerical variant of the diffusion model was presented by Anta et al. in the paper "A continuity equation for the simulation of the current–voltage curve and the time-dependent properties of dye-sensitized solar cells"[1]. Being numerical, the model can consider both non-linear diffusion and non-linear recombination, and also predict the transient in the cell when the light intensity is switched from one steady illumination to another. It can however not predict the small amplitude perturbation behavior for a DSSC. This behavior is of great interest for the common characterization techniques IMPS and IMVS, as will be explained in subsection 3.3. The goal with this section, is to show how Anta et al.'s variant of the diffusion model can be expanded to include small amplitude perturbation in the form of IMPS- and IMVS-spectra.

An analytical model for the IMPS-spectra has been presented by Dloczik [27], and an analytical model for IMVS-spectra has been presented by Kern [20]. A numerical model that treats the non-linear recombination and calculates the EIS-spectra of a DSSC has been presented by Cappellutti [28]. But a variant of the diffusion model which considers the non-linear behavior of both recombination and diffusion, and also predicts IMPS- and IMVS-spectra, has as far as the author knows not been presented before.

3.1 The diffusion model as presented by Anta et al. [1]

Anta et al.'s variant of the diffusion model rests on mainly eight assumptions and approximations which are given in Table 3.1:

Table 3.1: Assumptions and approximations as written in Anta et al.'s model.

Approximation 1	-Charge transport occurs only by diffusion
Approximation 2	-Electron density and Fermi level are related by Boltzmann statistics
Approximation 3	-The I–V curve is determined by the electronic part only
Approximation 4	-A quasi-static equilibrium holds between free and trapped electrons
Assumption 1	-Electron traps exist in the nanostructured semiconductor
Assumption 2	-Traps in the semiconductor fit to an exponential distribution of energies
Assumption 3	-Electron transport occurs according to the multiple-trapping model
Assumption 4	-Effective diffusion coefficient, pseudo-first order recombination constant, and electron diffusion length correspond to quantities measured by small-perturbations techniques

Based on these approximations, the following equations are presented by Anta for describing the electron concentration in a DSSC. The model treats the DSSC as one dimensional, since the thickness of the cell is in the micrometer range and is a lot smaller than the length and height which is in the mm range or more. The first equation presented below, equation (3), states that the change in electron concentration at a given point will equal the sum of three different terms. This equation is called the continuity equation, and makes the fundament for the diffusion model. It is by solving it numerically for steady state condition that Anta et al calculates the current voltage characteristics.

$$\frac{\partial n(x,t)}{\partial t} = J_D + J_G - J_R \tag{3}$$

Where n is the total electron concentration at a given point in the cell. The total electron concentration is the sum of both free electrons and trapped electrons. t is the time, x is the position in the cell, where $x = 0$ is defined as the boundary between the TCO anode and the titanium dioxide. J_D is a term describing the net diffusion of electrons, J_G is a term describing how many electrons which are generated/injected, and J_R is a term describing how many electrons which recombine. J_D, J_G and J_R are all functions of x, and can also be functions of t.

The diffusion term in equation (3) is expressed as [1]:

$$J_D = \frac{\partial}{\partial x}\left(D_n(n)\frac{\partial n}{\partial x}\right) \tag{4}$$

Where D_n is a diffusion "constant" which depends on the total electron concentration. This dependency is expressed as [1]:

$$D_n = D_{ref}\left(\frac{n}{n_{ref}}\right)^{\frac{1-\alpha}{\alpha}} \tag{5}$$

Where D_{ref} is the diffusion constant at a reference state, n_{ref} is the electron concentration at the same reference state, and α is an experimentally accessible parameter, reflecting the average energy of the trap states below the conduction band.

The recombination rate is expressed as quasi first order [1]:

$$J_R = \frac{\beta}{\alpha} k_l(n) n \tag{6}$$

Where β is an experimentally accessible parameter, and $k_l(n)$ is the recombination reaction rate "constant" which depends on the electron concentration in the following way [1]:

$$k_l(n) = k_{ref}\left(\frac{n}{n_{ref}}\right)^{\frac{\beta-\alpha}{\alpha}} \tag{7}$$

Where k_{ref} is the reaction rate constant at a given reference state. This reference state should be the same as the reference state for D_{ref} and n_{ref}. It is set to be the DSSC when it is in the dark, in both this work and in the work by Anta et al. This state with no illumination, is denoted with the subscript $_0$. D_{ref}, k_{ref} and n_{ref} is therefore replaced with D_0, k_0 and n_0 for the rest of this thesis.

The time constant for recombination τ_{rec}, i.e. the average lifetime for electrons in the conduction band of the titanium dioxide, can according to Anta et al. be expressed as [1]:

$$\tau_{rec} = k_l^{-1} = \left(k_0\left(\frac{n}{n_0}\right)^{\frac{\beta-\alpha}{\alpha}}\right)^{-1} \tag{8}$$

The time constant for transportation τ_{trans}, i.e. the average time it takes from an electron is injected into the titanium dioxide until it is collected at the anode, can according to Anta et al. be expressed as [1]:

$$\tau_{trans} = \frac{d^2}{2.77 D_n} \tag{9}$$

The potential in the anode can be expressed as [1]:

$$V(x) = \frac{k_B T}{\alpha q} \ln\left(\frac{n(x)}{n_0}\right) \tag{10}$$

Where V is the potential, k_B is the Boltzmann constant, T is the temperature, and q is the elementary charge.

The generation term is given as [1]:

$$J_G = \int_{\lambda_{min}}^{\lambda_{max}} \eta_{inj} I_0(\lambda) \epsilon_{Anta}(\lambda)(1 - \exp[-\epsilon_{Anta}(\lambda)d]) \exp[-\epsilon_{Anta}(\lambda)x]\, d\lambda \quad (11)$$

Where η_{inj} is the injection efficiency, $I_0(\lambda)$ is the solar spectrum, and ϵ_{Anta} is the absorption coefficient used in Anta et al.s work for a given dye in the DSSC. The injection efficiency is treated in two different ways. It is either set to 1, or it is calculated from [1]:

$$\eta_{inj} = \frac{\eta_{inj_0}}{1 - p(n/n_0)} \quad (12)$$

Where p is a constant, and η_{inj_0} is the injection rate in the dark.

Equation (3) is solved numerically for n, with the help from equation (4), (5), (6), (7) and (11). The current voltage characteristic can be calculated if n is known for several different potentials over the DSSC. Anta et al. does this by using equation (10) to calculate the potential in the titanium dioxide. The potential used in the IV-characteristic will then be the potential at the contact between the titanium dioxide and the TCO (at $x = 0$), minus potential loss due to series resistance. It is assumed that Anta et al. used resistive potential loss of the form:

$$V_{loss,R_s} = IR_s \quad (13)$$

Where V_{loss,R_s} is the resistive potential loss, I is the current generated by the DSSC and going through the circuit, and R_s is the series resistance, resulting from resistive losses in the TCO, the electrolyte, and in wires and leads. The current going through the circuit is calculated from the gradient in the electron concentration n at the contact (x=0).

Anta et al. needs to determine several parameters to solve equation (3) and obtain the current voltage characteristic. These parameters are α, β, k_0, D_0, n_0, R_s, η_{inj}, p and ϵ_{Anta}. To determine α and β, Anta et al. used the following expressions [1]:

$$C(V) = C_0 \exp\left(\frac{\alpha V}{k_B T}\right) \quad (14)$$

$$R_r(V) = R_{r_0} \exp\left(-\frac{\beta V}{k_B T}\right) \quad (15)$$

Where C is the capacitance, C_0 is the capacitance at a reference state, R_r is the recombination resistance and R_{r_0} is the recombination resistance at a reference state. The capacitance and recombination resistance were measured as functions of the potential, by using electrochemical impedance spectroscopy on the DSSC's in the dark. They were then plotted semi logarithmically to give a straight line, and α and β was determined from linear regression. This is explained in more detail in section 3.4.2.1.

It was somewhat unclear how Anta et al. determined D_0, but it seemed that an analytical model in [27] was used together with IMPS-measurements at different potentials. k_0 was estimated by adjusting k_0 so that the open circuit potential, V_{oc}, matched with experimental

results. ϵ_{Anta} was estimated from the short circuit current, I_{sc}, by assuming that there were no recombination losses at short circuit conditions. R_s was estimated from the point on the IV-characteristic giving the largest power. p was determined in the same way as R_s. Anta et al. neglected R_s when calculating p, and vice versa. How n_0 was determined, was never stated in the article, nor in the supplementary material for the article. This is strange, since n_0 influences the IV-characteristic greatly, and there is no straight forward way to determine it experimentally that the author is aware of.

3.2 Numerical solution of the steady state equations

This section proposes how a set of two first order differential equations describing the steady state behavior of a DSSC can be achieved, by using the equations in section 3.1 with some minor modifications. The two differential equations which are obtained can be solved to find the electron density in the titanium dioxide as a function of both position and for the potential applied over the DSSC. This makes the basis for modeling the IV-characteristics of a DSSC.

The starting point is the same as in section 3.1, namely equation (3), which for steady state is written:

$$J_D + J_G - J_R = 0 \tag{16}$$

Next, equation (6) and (7) are combined, the notation $\frac{\beta-\alpha}{\alpha} = b$ is introduced and the reference state is set to be the DSSC with no illumination. The recombination can then be written:

$$J_R = \frac{\beta}{\alpha} k_0 \left(\frac{n}{n_0}\right)^b n \tag{17}$$

By combining equation (4) and (5), and defining $\frac{1-\alpha}{\alpha} = a$, the following expression is achieved for the diffusion term:

$$J_D = \frac{\partial}{\partial x}\left(D_0 \left(\frac{n}{n_0}\right)^a \frac{\partial n}{\partial x}\right) \tag{18}$$

The current being collected at the TCO can be found from:

$$I = D_0 \left(\frac{n}{n_0}\right)^a \frac{\partial n(x=0)}{\partial x} \tag{19}$$

The generation term, J_G, in this thesis differs from the generation term used in Anta et al.'s work. There are two reasons for this. The first is that monochromatic light was used in all the measurements in this work, and thus there is no need for wavelength dependent absorption coefficient. Next, the DSSC's which were tested in this work were equipped with a backscatter layer. That is, a layer designed to reflect the light which is not absorbed back though the solar cell. This increases the absorption efficiency, or alternatively permits a thinner titanium dioxide layer to be used in the cell. If Beer-Lambert profile for the light absorbance is assumed, then the generation term can be expressed as:

$$\mathrm{J_G} = \eta_{\mathrm{inj}}\Phi_{\mathrm{ss}}\mathrm{K_G}\epsilon\left(\mathrm{e}^{-\epsilon \mathrm{x}} + \eta_{\mathrm{refl}}\mathrm{e}^{\epsilon(\mathrm{x}-2\mathrm{d})}\right) \tag{20}$$

Where Φ_{ss} is the steady state intensity of the light shining on the cell, ϵ is the absorption coefficient, η_{refl} is the reflection efficiency of the reflective backscatter layer, and d is the thickness of the nanoporous titanium dioxide layer. For the above equation to be valid, all the light shining on the cell must have an equal absorption, which will be the case for monochromatic light. K_G is a constant defined $K_G = \frac{\lambda q}{hc}$, where λ is the wavelength of the monochromatic light shining on the cell, q is the elementary charge, h is Planck's constant, and c is the speed of light. K_G has unit $\mathrm{C.j^{-1}}$ and is introduced so that the unit for the generation term becomes $\mathrm{C.m^{-3}.s^{-1}}$.

Next, the following abbreviations are introduced:

$$\eta_{inj}K_G\epsilon\left(e^{-\epsilon x} + \eta_{refl}e^{\epsilon(x-2d)}\right) = \Lambda(x) \tag{21}$$

$$\frac{\beta}{\alpha}\frac{k_0}{n_0^b} = K_R \tag{22}$$

$$\frac{D_0}{n_0^a} = K_D \tag{23}$$

The generation term, recombination term and diffusion term can then be written

$$J_G = \Phi_{ss}\Lambda(x) \tag{24}$$

$$J_R = K_R n^{(b+1)} \tag{25}$$

$$J_D = \frac{\partial}{\partial x}\left(K_D n^a \frac{\partial n}{\partial x}\right) \tag{26}$$

By combining equation (16), (24), (25) and (26) the following expression is achieved:

$$0 = \frac{\partial}{\partial x}\left(K_D n^a \frac{\partial n}{\partial x}\right) + \Phi_{ss}\Lambda(x) - K_R n^{(b+1)} \tag{27}$$

Equation (27) is split into two first order differential equations by defining a variable F as:

$$F = K_D n^a \frac{\partial n}{\partial x} \tag{28}$$

Giving the set consisting of

$$\boldsymbol{\frac{\partial n}{\partial x} = \frac{F}{K_D n^a}} \tag{29}$$

$$\boldsymbol{\frac{\partial F}{\partial x} = -\Phi_{ss}\Lambda(x) + K_R n^{(b+1)}} \tag{30}$$

This system of two first order differential equations needs two boundary conditions to be solved. One comes from the fact that there cannot be any current flowing at the right side boundary of the titanium dioxide, regardless of the potential over the cell. This implies that the right-side boundary condition must be:

$$\frac{dn(x=d,t)}{dx}=0 \tag{31}$$

The left-side boundary condition will depend on what potential is applied to the cell. It is assumed that the electron concentration at the boundary between the TCO and the titanium dioxide is given by equation (10). This leads to the right side boundary condition being expressed as:

$$\frac{n(x=0,t)}{n_0}=\exp\left(\frac{V\alpha e}{k_B T}\right) \tag{32}$$

For the special case of open circuit, the boundary condition at the left side can be expressed as:

$$\frac{dn(x=0,t)}{dx}=0 \tag{33}$$

for the same reasons as to why the right-side boundary condition is based on the derivative. For the special case of short circuit equation (32) becomes:

$$\frac{n(x=0,t)}{n_0}=1 \tag{34}$$

3.3 Extension to a model for small amplitude perturbations

Two common small amplitude perturbation techniques used for characterizing dye sensitized solar cells are IMPS (intensity modulated photocurrent spectroscopy) and IMVS (intensity modulated photovoltage spectroscopy). These techniques are based on illuminating the DSSC's with modulated light on the form:

$$\Phi=\Phi_{ss}+\Phi_t=\Phi_{ss}+\Phi_A e^{i\omega t} \tag{35}$$

Were Φ_A is a constant giving the amplitude to the modulation of the light, ω is the angular velocity and i is the imaginary number. Φ_A is typically between 1-10% of Φ_{ss}, hence why it is called small amplitude perturbations. IMPS is based on measuring the current response for different frequencies/angular velocities. IMVS is based on measuring the potential response for different frequencies/angular velocities. IMVS is typically performed at open circuit while IMPS is typically performed at short circuit. The IMPS/IMVS response will to a varying degree be out a phase with the modulated light, dependent on the angular velocity. A practical way of presenting this effect, is to divide the response into a real part which is completely in phase, and an imaginary part which is completely out of phase. The frequency which gives the largest imaginary response is often of interest, and it is common to plot the imaginary

response as a function of frequencies (Bode plot). These plots are called the IMVS and IMPS spectra in this thesis.

This section proposes how a set of four first order differential equations can be developed from Anta et al.'s equations in section 3.1, to describe small amplitude perturbation. These four equations can be solved numerically to obtain $n(x,t)$, which can give either the potential response or the current response for a DSSC for different angular velocities/frequencies. In other words, IMVS and IMPS spectra can be produced from this extended model. The motivation for doing this is to gain more information from experimental IMPS and IMVS spectra.

This model is based on solving the time dependent case of the continuity equation, equation (3), in contrast to the steady state model shown in section 3.2.

First it is assumed that the electron concentration can be written on the same form as Φ, just with a phase difference:

$$n = n_{ss} + n_t = n_{ss} + n_A e^{i(\omega t+\phi)} \tag{36}$$

Were ϕ is the phase difference, n_{ss} is the steady state part of the electron concentration, n_t is the time dependent part, and n_A is the amplitude of the time dependent part. The generation term, diffusion term, and recombination term is then rewritten with the help of equation (35) and (36), giving:

$$J_G = (\Phi_{ss} + \Phi_t)\Lambda(x) \tag{37}$$

$$J_R = K_R(n_{ss} + n_t)^{(b+1)} \tag{38}$$

$$J_D = \frac{\partial}{\partial x}\left(K_D(n_{ss} + n_t)^a \frac{\partial n}{\partial x}\right) \tag{39}$$

Next, $(n_{ss} + n_t)^{(b+1)}$ and $(n_{ss} + n_t)^a$ are Taylor expanded and truncated after the two first terms, giving:

$$n^{b+1} \cong n_{ss}^{b+1} + n_t(b+1)n_{ss}^b \tag{40}$$

$$n^a \cong n_{ss}^a + n_t a n_{ss}^{(a-1)} \tag{41}$$

The recombination and diffusion term can then be approximated to:

$$J_R \cong K_R(n_{ss}^{b+1} + n_t(b+1)n_{ss}^{b}) \tag{42}$$

$$J_D \cong \frac{\partial}{\partial x}\left(K_D(n_{ss}^{a} + n_t a n_{ss}^{(a-1)})\frac{\partial n}{\partial x}\right) \tag{43}$$

By rewriting the recombination and diffusion term the following expressions are achieved:

$$J_R \cong K_R(n_{ss}^{(b+1)} + n_{ss}^{b} n_t + n_t b n_{ss}^{b}) \tag{44}$$

$$J_D \cong K_D \frac{\partial}{\partial x}\left(n_{ss}^{a}\frac{\partial n_{ss}}{\partial x} + n_{ss}^{a}\frac{\partial n_t}{\partial x} + n_t a n_{ss}^{(a-1)}\frac{\partial n_{ss}}{\partial x} + n_t a n_{ss}^{(a-1)}\frac{\partial n_t}{\partial x}\right) \tag{45}$$

The last term in equation (45) is of higher order than the other terms, and if the amplitude of the light is small enough, giving a small enough n_t, then it is assumed safe to approximate it equal to zero, giving:

$$J_D \cong K_D \frac{\partial}{\partial x}\left(n_{ss}^{a}\frac{\partial n_{ss}}{\partial x} + n_{ss}^{a}\frac{\partial n_t}{\partial x} + n_t a n_{ss}^{(a-1)}\frac{\partial n_{ss}}{\partial x}\right) \tag{46}$$

The equation describing the steady state solution to the system, Equation (27), enables the steady state terms of equations (37), (44) and (46) to be removed. This is because the sum of the steady state parts cancel each other out. Combining equations (37), (44) and (46) and removing the steady state terms yield:

$$\frac{\partial n}{\partial t} = K_D \frac{\partial}{\partial x}\left(n_{ss}^{a}\frac{\partial n_t}{\partial x} + n_t a n_{ss}^{(a-1)}\frac{\partial n_{ss}}{\partial x}\right) + \Phi_t \Lambda(x) - K_R n_{ss}^{b} n_t (1+b) \tag{47}$$

The term to the very left can be written:

$$\frac{\partial n}{\partial t} = \frac{\partial(n_{ss} + n_A e^{i\omega t} e^{i\phi})}{\partial t} = i\omega n_A e^{i\phi} \tag{48}$$

by applying the relationship $n_t = n_A e^{i\omega t} e^{i\phi}$ from equation (36). Applying the same relationship to equation (47) and rearranging gives:

$$\begin{aligned} i\omega n_A e^{i\phi} = K_D \frac{\partial}{\partial x}\left(n_{ss}^{a}\frac{\partial(n_A e^{i\phi})}{\partial x} + n_A e^{i\phi} a n_{ss}^{(a-1)}\frac{\partial(n_{ss})}{\partial x}\right) + \\ \Lambda(x)\Phi_A - K_R n_{ss}^{b} n_A e^{i\phi}(1+b) \end{aligned} \tag{49}$$

Equation (49) is relatively simple to solve, because all the time dependent terms cancelled out during the rearrangement. This could be done because every term had the same dependence on the time, namely $e^{i\omega t}$. Next, the following notation is introduced:

$$n_A e^{i\phi} = n_A \cos(\phi) + i n_A \sin(\phi) = P_{Re} + iP_{Im} \tag{50}$$

This allows equation (49) to be split into a real part:

$$\begin{aligned} -\omega P_{Im} = K_D \frac{\partial}{\partial x}\left(n_{ss}^a \frac{\partial P_{Re}}{\partial x} + P_{Re} a n_{ss}^{(a-1)} \frac{\partial n_{ss}}{\partial x}\right) \\ + \Lambda(x)\Phi_A - K_R n_{ss}^b P_{Re}(1+b) \end{aligned} \tag{51}$$

And an imaginary part:

$$i\omega P_{Re} = iK_D \frac{\partial}{\partial x}\left(n_{ss}^a \frac{\partial P_{Im}}{\partial x} + P_{Im} a n_{ss}^{(a-1)} \frac{\partial n_{ss}}{\partial x}\right) - iK_R n_{ss}^b P_{Im}(1+b) \tag{52}$$

Next, the notation F_{Re} and F_{Im} is introduced:

$$F_{Re} = K_D n_{ss}^a \frac{\partial P_{Re}}{\partial x} + K_D P_{Re} a n_{ss}^{(a-1)} \frac{\partial n_{ss}}{\partial x} \tag{53}$$

$$F_{Im} = K_D n_{ss}^a \frac{\partial P_{Im}}{\partial x} + K_D P_{Im} a n_{ss}^{(a-1)} \frac{\partial n_{ss}}{\partial x} \tag{54}$$

Equation (51) and (52) is then split into four first order differential equations which can be solved by Matlab:

$$\boldsymbol{\frac{\partial P_{Re}}{\partial x} = -P_{Re} a n_{ss}^{-1} \frac{\partial n_{ss}}{\partial x} + \frac{F_{Re}}{n_{ss}^a}} \tag{55}$$

$$\boldsymbol{\frac{\partial F_{Re}}{\partial x} = -\Lambda(x)\Phi_A + \mathrm{K_R}\ n_{ss}^b P_{Re}(1+b) - \omega P_{Im}} \tag{56}$$

$$\boldsymbol{\frac{\partial P_{Im}}{\partial x} = \frac{F_{Im}}{n_{ss}^a} - P_{Im} a n_{ss}^{-1} \frac{\partial n_{ss}}{\partial x}} \tag{57}$$

$$\boldsymbol{\frac{\partial F_{Im}}{\partial x} = \mathrm{K_R}\ n_{ss}^b P_{Im}(1+b) + \omega P_{Re}} \tag{58}$$

Four boundary conditions are needed to solve this system of first order differential equations. For the right boundary, the conditions are the following regardless of the potential over the cell:

$$\frac{dP_{Re}(x=d,t)}{dx} = \frac{dP_{Im}(x=d,t)}{dx} = 0 \tag{59}$$

For open circuit, the left-side boundary is the same as the right-side boundary:

$$\frac{dP_{Re}(x=0,t)}{dx} = \frac{dP_{Im}(x=0,t)}{dx} = 0 \tag{60}$$

For all potentials except for circuit, the left-side boundary condition is given by:

$$P_{Re}(x=0,t) = P_{Im}(x=0,t) = 0 \tag{61}$$

Equations **(55)** to **(58)** must be solved with the right boundary conditions for all desired values of ω, before the IMVS spectra be calculated from equation (10):

$$V_{Im}(\omega) = \frac{k_B T}{\alpha q} \ln\left(\frac{P_{Im}(x=0,\omega) + n_{ss}}{n_{ss}}\right) \tag{62}$$

Where $V_{Im}(\omega)$ is the imaginary part of the potential response. Similarly, by noticing that F_{Im} is the imaginary part of the diffusion term in equation (49), can the IMPS spectra be calculated from:

$$I_{Im}(\omega) = F_{Im}(x=0,\omega) \tag{63}$$

Where $I_{Im}(\omega)$ is the imaginary part of the current response.

3.4 Implementation in Matlab

3.4.1 The basics

The equations in section 3.2 and 3.3 were solved in Matlab. The built-in solver bvp4c was used. The thickness of the titanium dioxide layer was discretized into 100 points. The points were generated in such a way that the distance between them increased quadratically. This ensured that the density of grid points increased towards the boundary between the TCO and the titanium dioxide. This was because the numerical solution had a large gradient at the boundary between the titanium dioxide and the TCO, and the grid needed to be extra fine close to the boundary for bvp4c to be able to solve the equations. The error tolerance was 0.1%, meaning that the error in the numerical solution was less than 0.1% from the true solution for every grid point.

The steady state solution was calculated before the small perturbations solution. The steady state solution was calculated for open circuit, short circuit, and at 98 potentials spread evenly between open circuit and short circuit. These 100 solutions were used to generate the IV-characteristic. The initial guess had to be good for bvp4c to find the right solution. The steady

state solution for open circuit proved to be the simplest one to guess, and was therefore calculated first. Then, the solution for open circuit was used to guess the solution for the potential just below open circuit, and so on. It was thus avoided having to guess directly what all other solutions except the open circuit looked like. The open circuit solution was guessed by assuming that the diffusion was so quick that the concentration profile would be flat, so that $J_R = J_G$ could be solved for n. This value for n proved sufficient for bvp4c to find the true non-flat concentration profile.

The solution for small amplitude perturbations can only be calculated after the steady state solution is known. The initial guess does once again have to be good if bvp4c was to succeed. Equation (55), (56), (57) and (58) in section 3.3 were first solved for the smallest angular velocities. For small enough angular velocities, the phase difference between the current and potential response and the light source will be negligible. This ensures that the imaginary part of the response will be negligible, and the initial guess for both F_{Im} and P_{Im} will thus be zero at every grid point. For P_{Re} the initial guess was estimated based on two separate steady state solutions. One solved for the case of $\Phi = \Phi_{ss}$, the other one for $\Phi = \Phi_{\mathrm{ss}} + \Phi_A$. The initial guess was set equal to the solution for $\Phi_{\mathrm{ss}} + \Phi_A$minus the solution for Φ_{ss}. The initial guess for P_{Re} was set to zero, in lack of any better method. This combination of initial guesses proved sufficient for bvp4c to find the solution. Setting all the initial guesses to zero was however not sufficient.

3.4.2 Determination of parameters

This section describes how the parameters α, β, k_0, D_0, n_0 and ϵ were determined. α and β were determined in the same way as in Anta et al.'s work, namely from EIS measurements of the cells in the dark. k_0 and D_0 were determined from IMVS and IMPS respectively. n_0 and ϵ were determined from V_{oc} and I_{sc} respectively. k_0, D_0, n_0 and ϵ had to be iterated on, because they could not be determined independently from each other. A summary of all the parameters and their values can be found in Table 3.2, and a flowchart showing how k_0, D_0, n_0 and ϵ were determined can be found in Figure 3.1.

3.4.2.1 Determination of α and β

Equation (14) and (15) were rewritten to:

$$\ln(C) = \frac{\alpha V}{k_B T} + \ln(C_0) \tag{64}$$

$$\ln(R_r) = \frac{-\beta V}{k_B T} + \ln(R_{r_0}) \tag{65}$$

It can now be seen that plotting $\ln(C)$ as a function of V/k_BT should give a straight line with a slope equal to α. In the same way will a plot of $\ln(R)$ as a function of V/k_BT give a straight line with slope equal to $-\beta$. Both R_r and C was found from data obtained with EIS of the DSSC in the dark for different potentials. This data is shown in Figure 5.4. R was found as the

radius of the half circle Figure 5.4 [29], estimated to be the same as the height of the half circle. C was found from the relation $C = (R\omega_{max})^{-1}$ [29], where ω_{max} is the angular velocity giving the top of the half circle in Figure 5.4. $\ln(C)$ and $\ln(R_r)$ were plotted versus V/k_BT as shown in Figure 5.5 and Figure 5.6, and linear regression was performed to give α and β.

3.4.2.2 Determination of initial guesses for k_0, D_0, ϵ and n_0

The first step in the iterative scheme for determining of k_0, D_0, ϵ and n_0, was to get initial guesses. The guess for k_0 was estimated from the experimental IMVS spectrum and simplified equations. The value Anta et al. used for D_0 was used as the initial guess for D_0 in this work. The guess for ϵ was estimated from the short circuit current, and n_0 was simply set to 1 in lack of any way to estimate it.

A common approximation was used to obtain the initial guess for k_o. This approximation is that the time constant for recombination can be expressed as [20]:

$$\tau_{rec} = \frac{1}{2\pi f_{min,IMVS}} \tag{66}$$

Where $f_{min,IMVS}$ is the frequency which give the largest imaginary potential response during an IMVS measurement. Next, equation (8), (10) and (66) are combined to obtain:

$$k_0 = 2\pi f_{min,IMVS}\left(\exp\left(\frac{\alpha V_{oc} e}{k_B T}\right)\right)^{-b} \tag{67}$$

By inserting $f_{min,IMVS}$ from the experimental IMVS spectrum and V_{oc} from the experimental IV-characteristic an initial value for k_0 is obtained. As previously mentioned, the initial value for D_0 was obtained by using the value that Anta et al. used for D_0, namely 10^{-14} $\mathrm{m^2.s^{-1}}$.

The initial guess for ϵ was made by assuming that there is no recombination during short circuit and that $\eta_{refl} = 0$. No recombination implies that all the injected electrons will contribute to the short circuit current. This results in the following expression:

$$I_{sc} = \int_{x=0}^{x=d} \Phi K_G \epsilon e^{-\epsilon x}\, dx = K_G \Phi (1 - e^{-\epsilon d}) \tag{68}$$

Which can be solved for ϵ:

$$\epsilon = -d^{-1} ln\left(1 - \frac{I_{sc}}{\Phi K_G}\right) \tag{69}$$

3.4.2.3 Iteration to find consistent values for k_0, D_0, ϵ and n_0

This subsection describes how the parameters were adjusted during the iteration to ensure that the model agreed with the experimental IMPS and IMVS spectra and the IV-characteristic. As explained in the previous section, initial guesses for k_0, D_0, ϵ and n_0 were chosen, and the other parameters were set to the values indicated in Table 3.2. After this, k_0, D_0, ϵ and n_0 was iterated on, as shown in Figure 3.1.

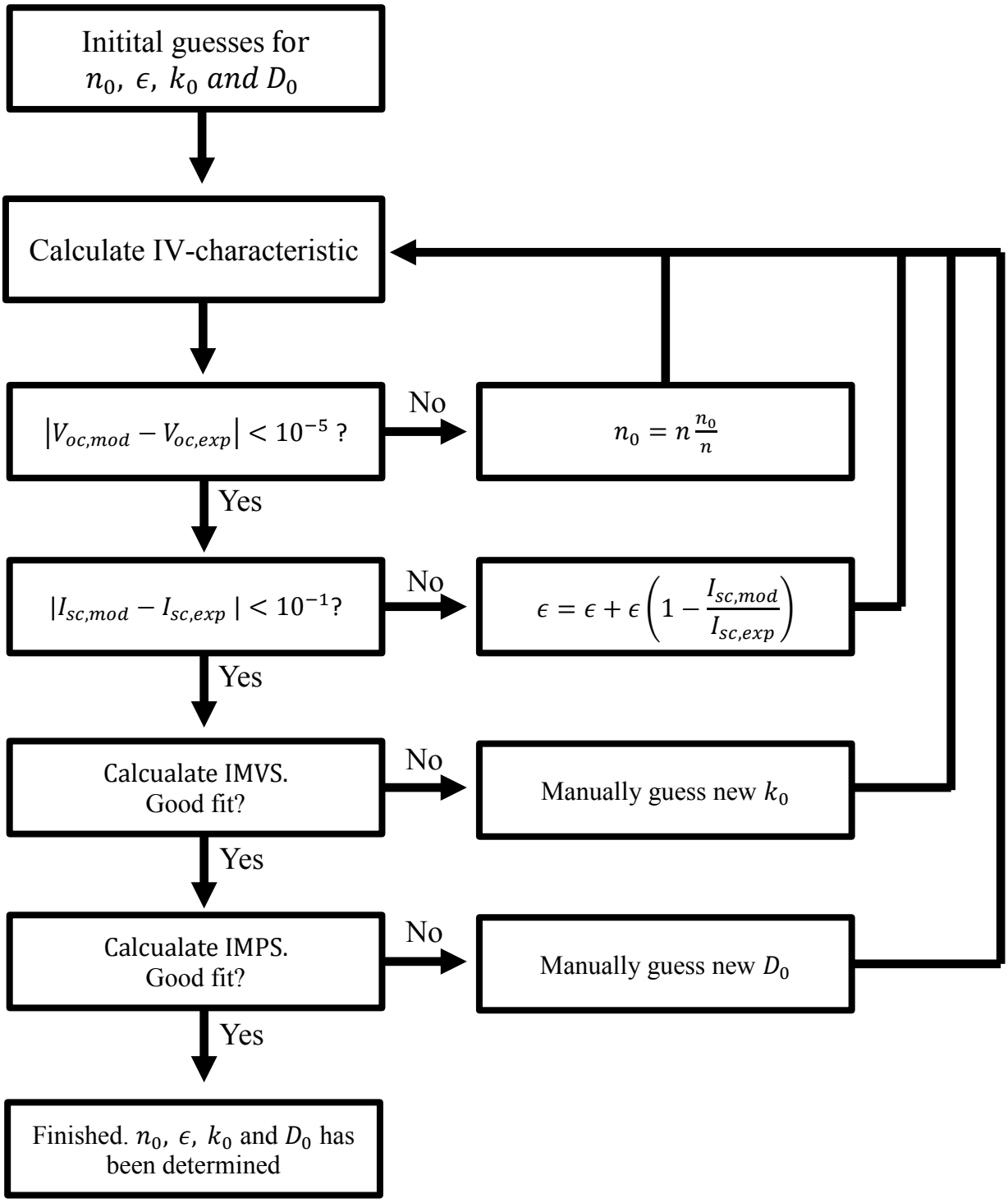

Figure 3.1: Flowchart illustrating how the parameters k_0, D_0, ϵ and n_0 were determined through iteration. Notice that each parameter is fitted based on a unique experimental value or figure.

First, the IV-characteristic is calculated based on the initial guesses, as shown in Figure 3.1. This includes the steady state solution for $n(x)$ at open circuit. Then a new value for n_0 was calculated by utilizing equation (10) and the calculated $n(x=0)$:

$$n_{0,i+1} = n\frac{n_{0,i}}{n} = n(x=0)exp\left(\frac{\alpha V_{oc} e}{k_B T}\right) \tag{70}$$

This new value for n_0 was used to calculate a new $n(x)$, which again was used to calculate a new n_0. This continued, until the iterations converged. The criteria for sufficient convergence was based on the potential which the steady state solution gave:

$$|V_{oc,mod} - V_{oc,exp}| < 10^{-5} \tag{71}$$

Where $V_{oc,mod}$ is the potential calculated by the model from equation (10) with $n(x=0)$, and $V_{oc,exp}$ is the potential which was measured experimentally over the DSSC.

ϵ was iterated on once n_0 was determined. This was done by:

$$\epsilon_{i+1} = \epsilon_i + \epsilon_i\left(1 - \frac{I_{sc,mod}}{I_{sc,exp}}\right) \tag{72}$$

With the criteria of convergence set to:

$$\left|I_{sc,mod} - I_{sc,exp}\right| < 0.1 \tag{73}$$

Where ϵ_{i+1} and ϵ_i is the next and current calculated absorbance coefficient respectively. $I_{sc,mod}$ and $I_{sc,exp}$ is the short circuit current provided by the model and from experimental data. This iteration is needed, since it was shown that the recombination was significant at short circuit, and that equation (69) thus was invalid. It was iterated on n_0 again for every time a new ϵ was calculated. Thus, the IV-characteristic had to be calculated anew several times for each iteration of ϵ.

Both n_0 and ϵ converged such that I_{sc} and V_{oc} were the same for the experimental IV-characteristic and the modelled IV-characteristic. The iteration on n_0 and ϵ was performed automatically within the script. Next, k_0 was adjusted such that the minima in the modelled IMVS spectrum matched the experimental IMVS spectrum. This was done "manually", and took some time, because n_0 and ϵ had to be iterated on again for every value of k_0 that was tried. The IMPS spectrum was calculated once the experimental and modelled IMVS spectra were considered to match as good as possible. D_0 was adjusted manually as well, until a good fit was obtained. This last step was the most time consuming, since all the three previous parameters had to be iterated on again. This can be seen in Figure 3.1.

3.4.2.4 η_{inj} and η_{refl}

The injection efficiency, η_{inj}, assumed to be independent of the potential over the DSSC, as described in section 2.2. The equipment at the lab did not permit higher intensities than 190 $\mathrm{W.m^{-2}}$. This is a relatively low intensity compared to the often-used standard of one sun, which equals about 1000 $\mathrm{W.m^{-2}}$. The potential over the cells depends on the light intensity, and was never more than ~0.6 V. It was thus assumed that the assumption of the injection efficiency being constant was good. The injection efficiency was also set equal to 1, due to lack of any good way to determine it. This assumption is discussed in section 6.2. A lower limit for the η_{inj} can however be calculated by rearranging equation (1) into:

$$\eta_{abs}\eta_{inj} = IPCE/\eta_{cc} \tag{74}$$

By inserting values for IPCE from Table 5.1 and using the common assumption that $\eta_{cc} = 1$ at short circuit, it is achieved that the product of the absorption and injection efficiency is 55% and 70% for the N719 and AFB8 cell respectively. It follows that this is the lower limit for the injection efficiency since the absorption efficiency cannot be more than 100%. It was however not managed to determine which of η_{abs} and η_{inj} that result in the loss in the IPCE, and it was chosen to assume that it was only η_{abs}. The assumption of $\eta_{cc} = 1$ was however tested, and found to be invalid for the 719-DSSC, ref section 6.2.

A way for estimating η_{refl} was not known. It was therefore tried mainly with the values of $\eta_{refl} = 0$ and $\eta_{refl} = 0.5$.

Table 3.2 shows a summary of all the parameters and their values. Notice that the initial guess values are quite far from the final values.

Table 3.2: The parameters used to simulate the IV-characteristic for a DSSC based on N719-dye and a DSSC based on AFB8-dye

Parameter	Initial guess	Final value N719	Final value AFB8	Unit
D_0	10^{-14}	$2.8 * 10^{-15}$	$2.1 * 10^{-11}$	$\mathrm{m^2.s^{-1}}$
k_0	0.87	0.14	0.24	$\mathrm{s^{-1}}$
ϵ	$5.4 * 10^4$	$3.0 * 10^5$	$8.9 * 10^4$	$\mathrm{m^{-1}}$
n_0	1	17	5.3	$\mathrm{C.m^{-3}}$
d	-	15	10	µm
α	-	0.43	0.43	-
β	-	0.63	0.63	-
ϕ_{ss}	-	190	190	$\mathrm{W.m^2}$
Φ_A	-	$0.05\Phi_{ss}$	$0.05\Phi_{ss}$	$\mathrm{W.m^2}$
η_{inj}	-	1	1	-
η_{refl}	-	0	0.5	-
λ	-	453	453	nm

3.5 Limitations and adjustments of the model

The presented model has some limitations. One is that it does not include potential losses from processes at the cathode, nor potential losses in the electrolyte. These potential losses are assumed, as described previously, to be small because for the relatively low intensity of the light used. However, they can be treated to some extent by introducing a series resistance, R_s, as mentioned in section 3.1. This resistance is a simple way to describe all potential losses, by assuming that they are on the form [1]:

$$V_{loss,R_s} = IR_s \tag{75}$$

Where V_{R_s} is the potential loss due to various mechanisms that are not included in the model, such as losses in the electrolyte and at the cathode. The IV-characteristic calculated from the model can be adjusted by subtracting V_{loss,R_s}. R_s can be adjusted so that experiemental IV-characateristic and modelled IV-characteristic match as good as possible.

The model does not include current losses apart from those included in the IPCE. Experimental data will however often fit better if a shunt resistance, R_{sh}, with accompanying leakage currents is introduced [6]:

$$I_{loss,R_{sh}} = \frac{V}{R_{sh}} \tag{76}$$

Where $I_{loss,R_{sh}}$ is the current lost to leakage due to non-infinite shunt resistance. The IV-characteristic can then be modified to better fit experimental data, by subtracting the $I_{loss,R_{sh}}$ from the I predicted by the model. The physical meaning behind the shunt resistance would be that the current collected at the TCO has an alternate way to go to the cathode. This alternate way is characterized by a resistance, which ideally should be infinite. This alternate way could be that the current goes from the TCO and into the electrolyte.

3.6 Comparison to work by Anta et al.

There are some differences from the diffusion model presented by Anta et al, and the diffusion model used in this work. These are summarized in Table 3.3. The main difference would be that the model in this thesis includes both steady state behavior and the small amplitude perturbation behavior. This enables calculation of the IMVS and IMPS spectra, in addition to the IV-characteristic. Anta et al.'s model calculates the IV-characteristic, and stepped light transients (not of interest in this thesis). A major advantage with calculating the IMVS and IMPS spectra, is that they can be used to determine k_0 and D_0.

Anta et al. states that IMPS is used to calculate D_0, and that k_0 is calculated from V_{oc}. Anta et al. does not explain how D_0 is calculated from IMPS, except for referring to [27]. In [27], several approaches to determine the diffusion constant are discussed and demonstrated. It is not possible to know which one that was used by Anta et al., but all the approaches were analytical and treated the recombination, transportation and electron concentration simpler than in the work of Anta et al.

The perhaps most striking difference lies in the treatment of n_0 (the electron concentration in the titanium dioxide in the dark). Anta et al. does not state how n_0 is calculated, while in this thesis n_0 is calculated from V_{oc}. Anta et al. cannot have calculated n_0 from V_{oc}, since they used V_{oc} to determine k_0. It thus seems that n_0 was a free variable in Anta et Al's work. It is considered strange that the value used for n_0 was not even mentioned, while values for the other parameters were both given and explained. This was done even though n_0 significantly affects the IV-characteristic. Being able to determine every parameter from experimental data was considered a significant advantage with this work.

Table 3.3: How the parameters were determined in this work and in the work by Anta et al.

Parameter	**Way of determination in this work**	**Way of determination Anta et al.**
D_0	IMPS	IMPS and an analytical model [27]
k_0	IMVS	V_{oc}
ϵ	I_{sc}	I_{sc}
n_0	V_{oc}	Unknown
α	EIS in dark	EIS in dark
β	EIS in dark	EIS in dark

4 Experimental

4.1 Manufacture of the dye sensitized solar cells

The DSSC's were manufactured by PhD-candidate Audun Formo Buene at the department of organic chemistry at NTNU. The first step in making a DSSC is to make the anode and the cathode. The cathode is made by depositing a catalyst on a piece of TCO-coated glass. This catalyst is typically a layer of platinum that is so thin that it cannot be seen by the human eye. It can also be based on graphite if state of the art efficiency is not needed[15]. The anode is prepared by depositing a nanoporous titanium dioxide layer with at thickness in the micrometer range. The anode is then sintered. The anode is then submerged in a staining solution, typically for several hours. The solution contains the dye(s) and possibly some additives. The additives are for increasing the performance of the cell, for example by reducing recombination. The anode is ready for being connected to the cathode once the staining is done. The dyes which were used for staining can be seen in Figure 4.3 and Figure 4.4.

The anode is connected to the cathode by melting a plastic gasket between them. This is done as shown in Figure 4.1. The electrolyte is then injected into the compartment made between the electrodes and the gasket. The electrolyte is typically injected through a small predrilled hole in the cathode, which is not shown in Figure 4.1. The cell is sealed afterwards, and is then ready for use. Audun Formo Buene's own detailed description of the manufacturing process can be found in Appendix A.

The cells were made with five active layers of titanium dioxide. Audun Formo Buene measured one of the layers with a profilometer, and based on this assumed a thickness of all the layers to be 15 μm. However, Audun Formo Buene stated that it was a rough estimate, and a lower bound for the thickness was given at 10 μm.

It is standard to equip DSSC's with masks, to ensure that the area of the cell is as exact as possible. It was extra important to mask Audun Formo Buene's DSSC's since the size of the titanium dioxide was somewhat uneven, as can be seen in Figure 4.2. Therefore, all the cells were equipped with a circular mask with diameter of 3.5 mm. This ensured that all the DSSC's had the same active area of 9.62 mm^2. This was done by drilling holes into black electrical tape. The tape was adhered to cardboard for mechanical support when the drilling was performed. Care was taken to ensure that the holes in the black electrical tape were drilled as similarly as possible. A masked cell can be seen fastened in the apparatus in Figure 4.5.

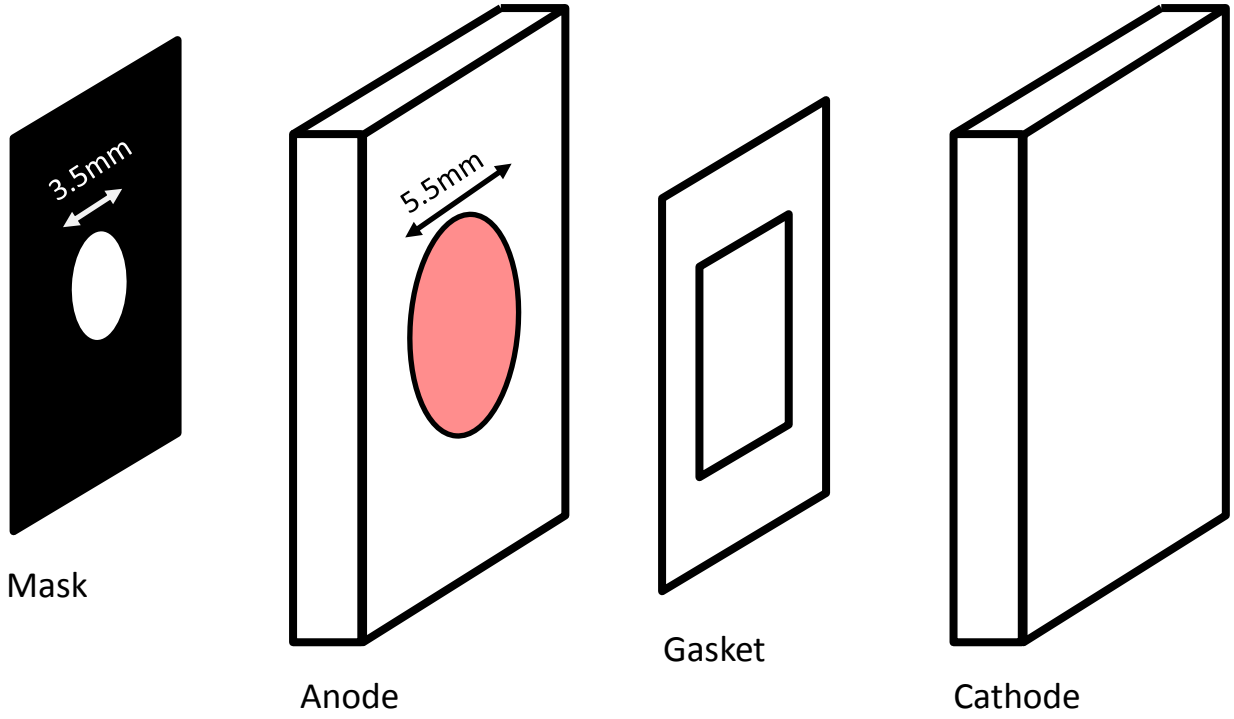

Figure 4.1: The main parts of a DSSC. First from the left: The mask which has a diameter of 3.5 mm. Second from the left: The anode which consists of a glass plate coated with TCO. The TCO is again coated with titanium dioxide which has been stained with a dye. The stained titanium dioxide layer is the red circular area with a diameter of 5.5 mm. Third from the left: The gasket, used to separate and connect the electrodes. To the very right is the cathode, which also consists of a glass plate coated with TCO and a catalyst. Neither the catalyst nor the TCO can be seen by the eye, and are therefore omitted from the figure. Figure 4.2 shows what a DSSC looks like when assembled.

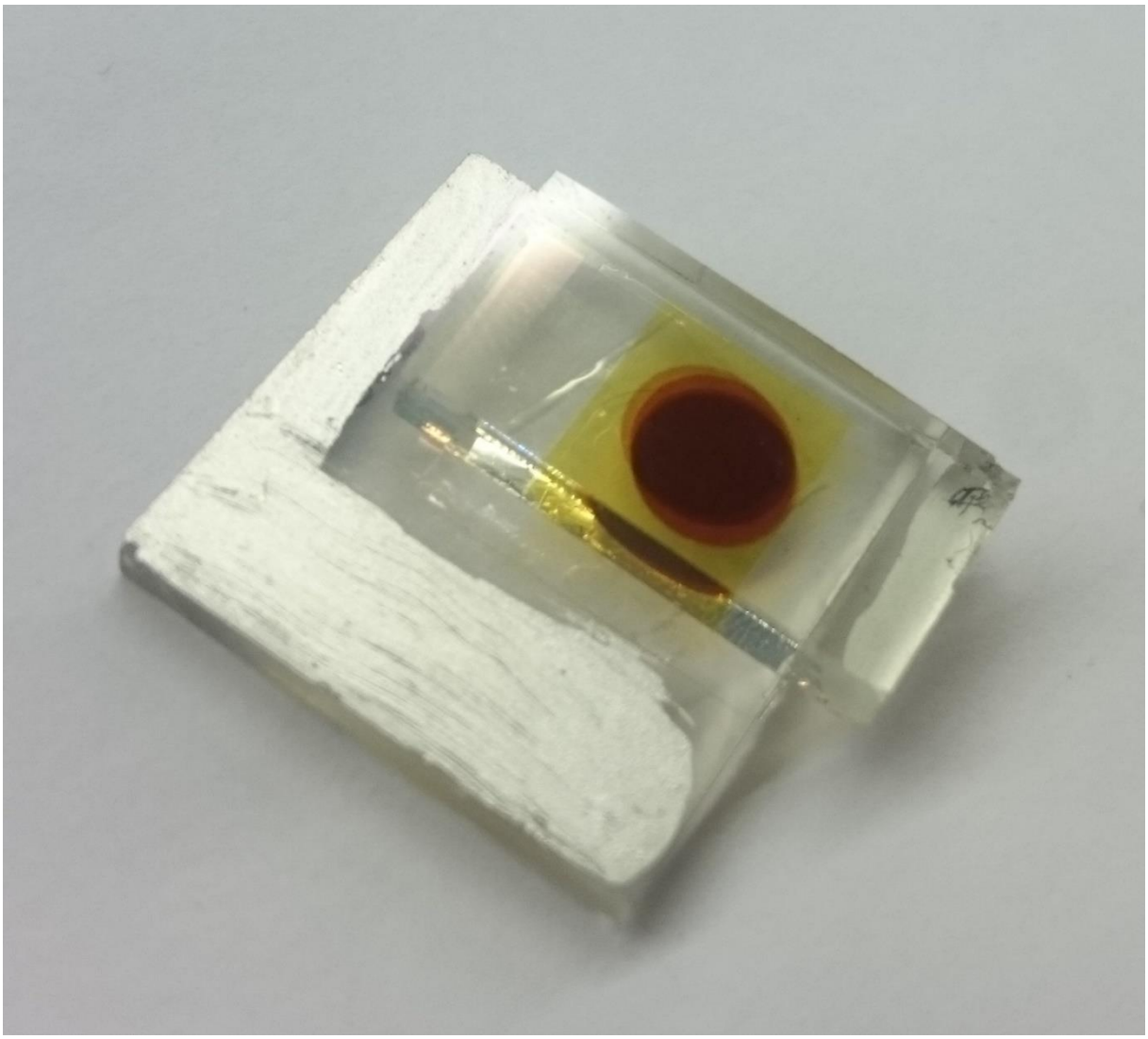

Figure 4.2: A DSSC fabricated by the methods detailed in the text. The anode is the smaller glass plate at the top. The cathode is the larger glass plate at the bottom. The dark red area is the stained titanium dioxide. The yellow area is excess electrolyte. The gasket can only be seen indirectly, as the border where the yellow area ends. The cathode and anode are both painted with metallic paint to increase conductivity.

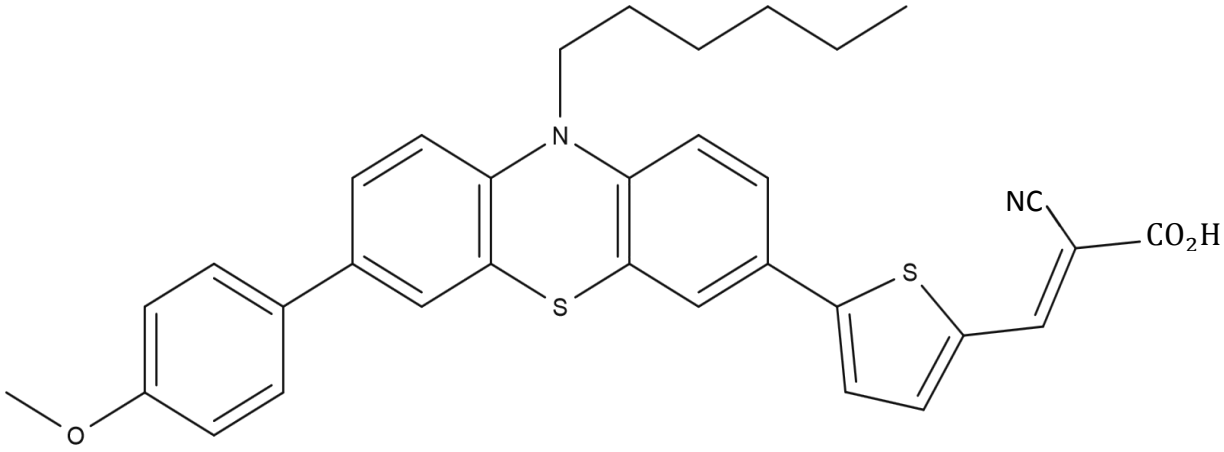

Figure 4.3: The purely organic dye AFB5-098, abbreviated AFB8. Notice that it is purely organic, with no metals.

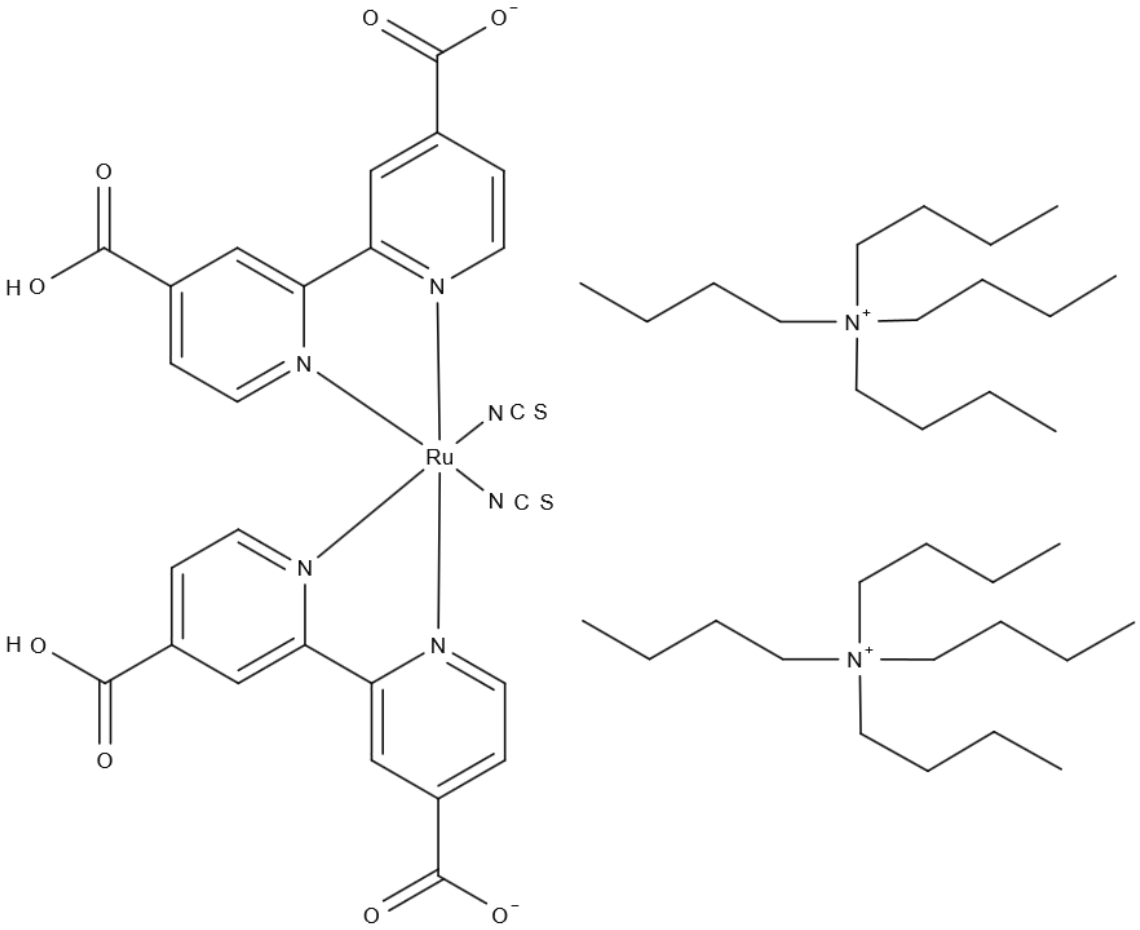

Figure 4.4: The ruthenium dye N719. Notice that it contains a ruthenium atom in the center of the anion.

4.2 Experimental setup and characterization

The experimental setup for the photo-electrochemical measurements consisted of the DSSC connected to a potentiostat, while a light source illuminated the DSSC. The light source used in the photo-electrochemical setup was a Zahner TLS03 tunable light source. The light source was connected to a Zahner XPOT which again was attached to a Zahner IM6ex potentiostat. The Zahner IM6ex was used to measure and control current and potential over the DSSC. A special setup for fastening the DSSC was put together, allowing careful adjustment in both x, y and z-direction, and adjusting the inclination of the cell to the light source. Some of this setup can be seen in Figure 4.5. The setup was used to place the DSSC at only 1 mm distance from the light source during the measurements. This was a condition for the light intensity reading from the TLS03 to be correct. The whole setup was placed inside a box which was painted black and could be closed to prevent unwanted light from entering.

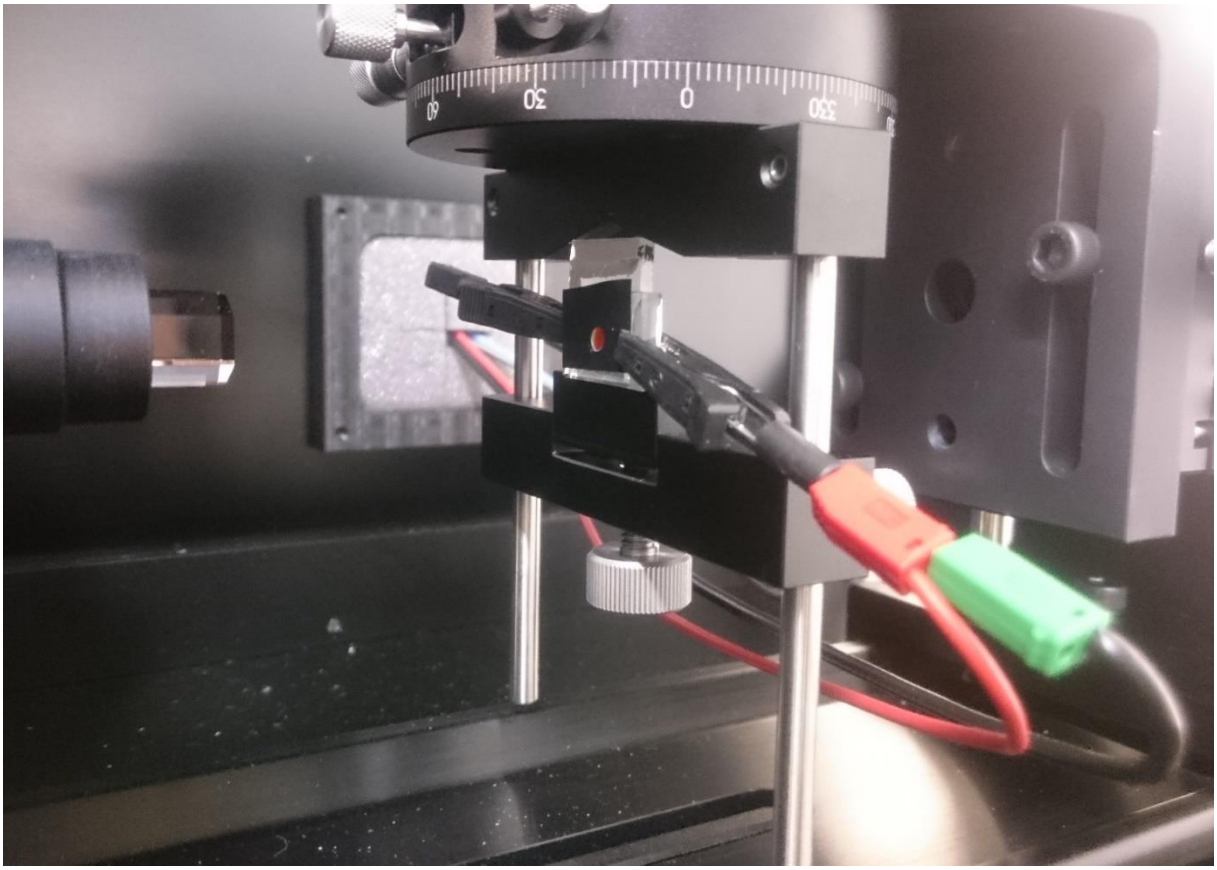

Figure 4.5: The experimental setup for doing photo-electrochemical measurements on DSSC's. To the left is the light source, seen as a short glass rod. In the middle is a masked DSSC, with two crocodile clips attached to it. The DSSC is attached to rails and levers which enable the careful adjustment of positioning, so that it can be moved very close to the light source. Notice that the distance from the DSSC and the light source is much larger than during measurements.

The IV-curves were recorded from open circuit to zero potential and back to open circuit potential. This was done to control that there was negligible hysteresis. The light illuminating the DSSC was monochromatic with a wavelength at 453 nm and an intensity of 190 $\mathrm{W.m^{-2}}$. The sweep rate was set to 10 $\mathrm{mV.s^{-1}}$.

The Incident photon to electron conversion efficiency (IPCE) was recorded from 300 nm to 700 nm. Built in software in the Zahner TLS03 setup was used to perform the measurement automatically. The only output was the IPCE for every wavelength, and thus the intensity of the light used was not known. It is suspected that it was considerably lower than 190 $\mathrm{Wm^{-2}}$, and that it varied considerably at different wavelengths. This was suspected from visual inspection of the light source while it operated. The resolution was given to be 10 nm by the software. A built-in monochromator was used in the range of 410 to 700 nm. From 300-410 nm there were no monochromator, and the wavelength was selected by switching between different diodes. This resulted in a somewhat lower resolution for the wavelengths from 300 nm to 410 nm, but it was not possible to know how much lower.

The absorbance measurements were performed by Audun Formo Buene. They were performed with $2 * 10^{-5}$ M solutions. AFB8 was solved in dichloromethane and N719 was solved in ethanol. The solutions were measured in a U-1900 spectrophotometer.

Three different spectroscopic methods were used: Electrochemical impedance spectroscopy(EIS), Intensity modulated photocurrent spectroscopy (IMPS) and intensity modulated photovoltage spectroscopy (IMVS)[14]. EIS was performed with 5 mV amplitude on the potential over the DSSC. IMPS and IMVS was performed with 10 mA amplitude over the light source. There was however ambiguity in the Zahner documentation, as to whether the amplitude indeed was 10 mA. EIS was performed with no illumination. IMPS and IMVS was performed with monochromatic with a wavelength at 453 nm and an intensity of 190 $\mathrm{W.m^{-2}}$. The current going through the lightsource was ~200 mA for this intensity.

5 Results

In this section, both results from experimental measurements and from the modelling are presented.

5.1 Experimental characterization

5.1.1 Comparison of the dyes

Figure 5.1 shows the absorbance of the dyes AFB8 and N719, plotted as a function of the wavelength of the light. Notice how the AFB8 dye performs twice as good as N719 at 453 nm.

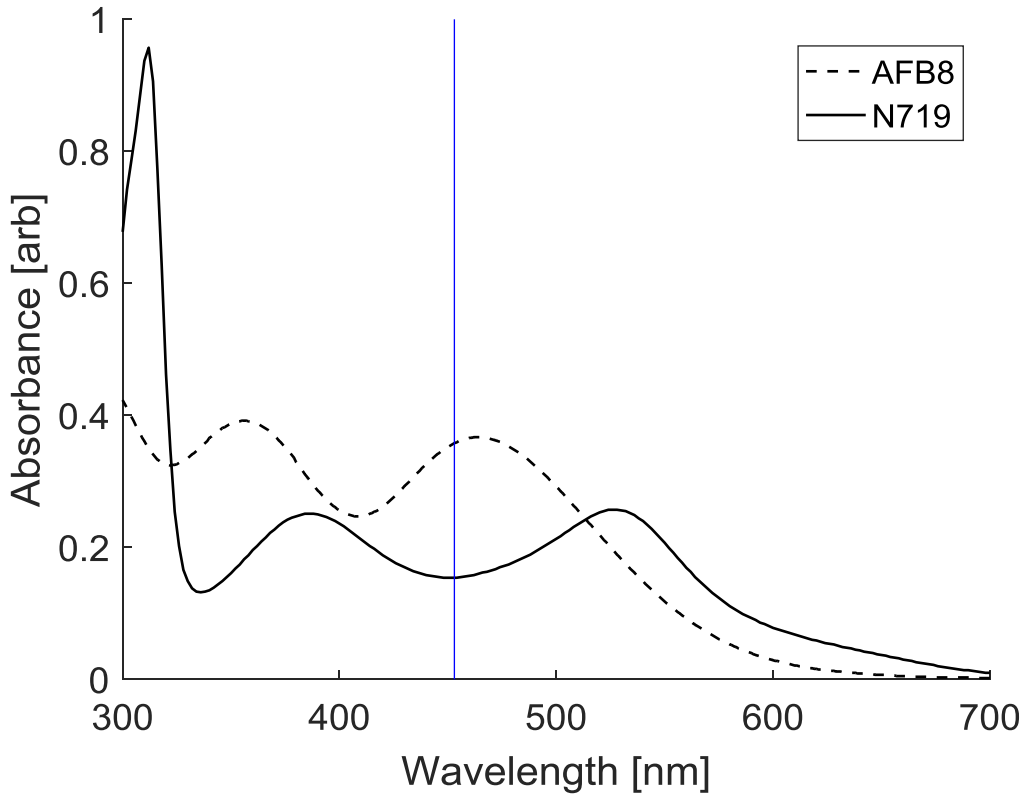

Figure 5.1: Plot showing the absorbance of the dyes AFB8 and N719 plotted as a function of the wavelength. The blue vertical line indicates light with a wavelength of 453 nm.

Figure 5.2 shows the incident photon to electron injection efficiency (IPCE) as a function of wavelength. Notice how the AFB8-dye perform considerably better than the N719 dye. Also notice how the profiles of the dyes in Figure 5.1 are considerably different from the profiles in Figure 5.2.

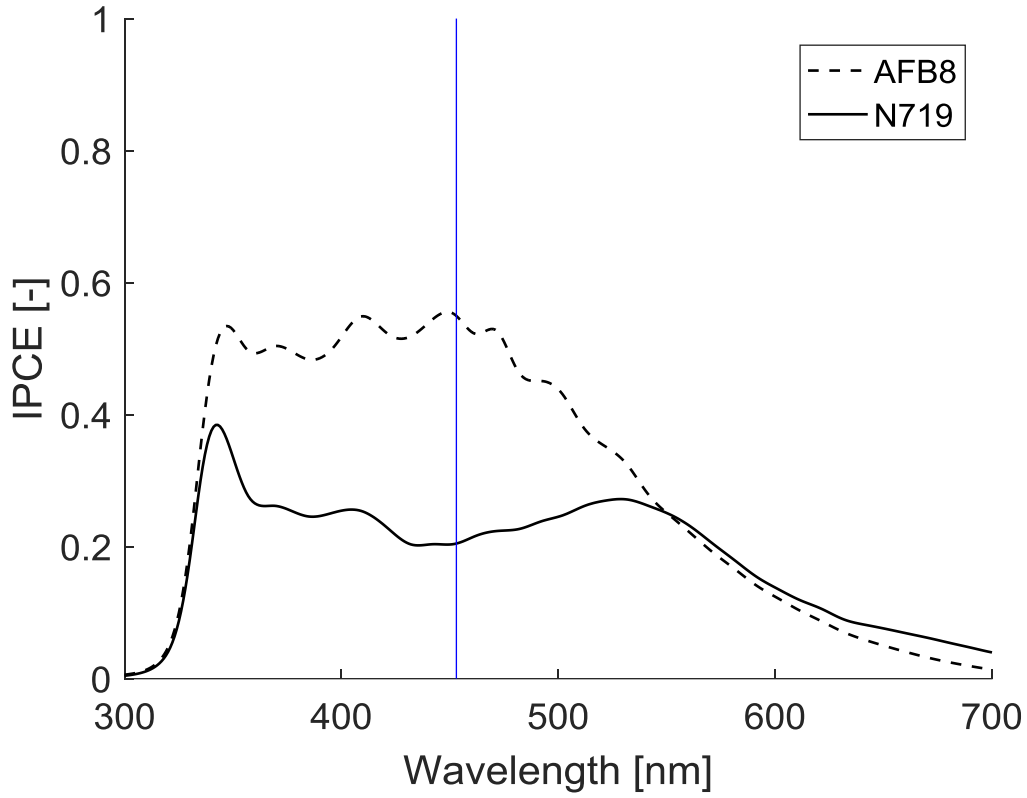

Figure 5.2: Plot showing the IPCE of the AFB8-DSSC and the N719-DSSC plotted as a function of the wavelength. The blue vertical line indicates light with a wavelength of 453 nm.

Figure 5.3 shows the current-potential characteristic for the AFB8-DSSC and the N719-DSSC. The AFB8-cell performs best, especially with respect to the current. It does however appear to have a somewhat lower fill factor.

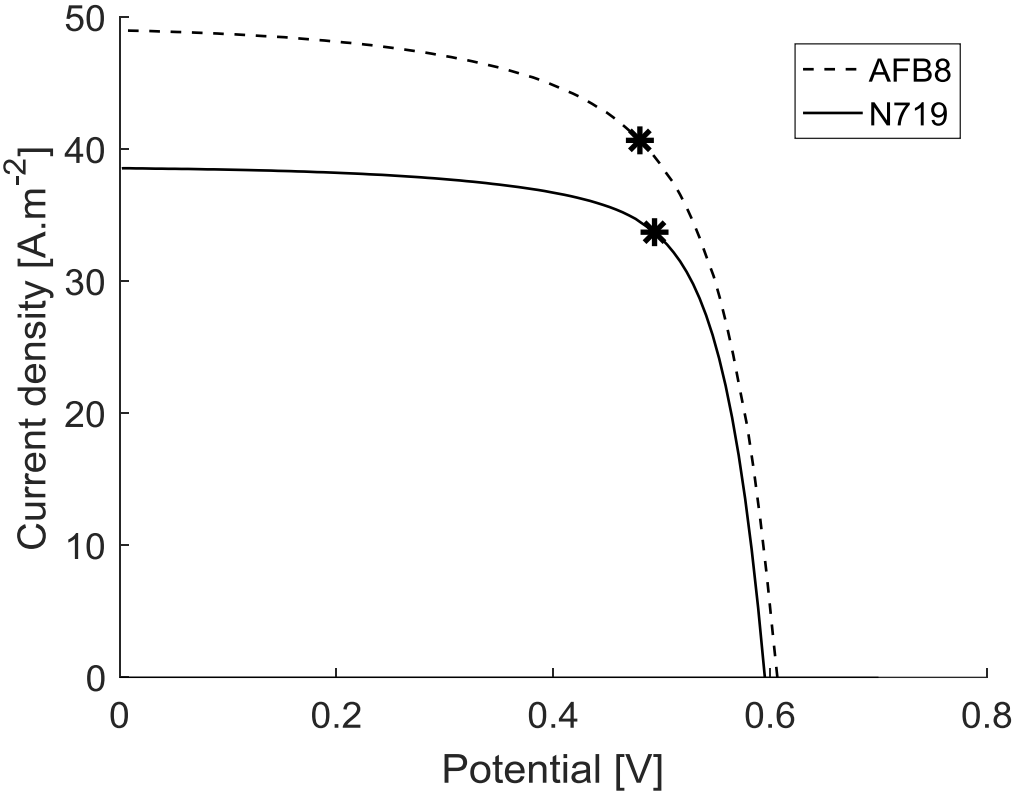

Figure 5.3: Plot showing the current density for two different DSSC's plotted as a function of the potential. This is often called current-potential characteristics, or the IV-characteristic. The DSSC's were made the same way, except for the dye. The dyes which were used for the cells are indicated. The stars represent the potential giving the maximum power for each cell. The characteristics were recorded under 190 $\mathbf{W.m^{-2}}$ 453 nm light.

Table 5.1 presents the most important experimental results. AFB8 performs better than N719 at every parameter except $f_{min,IMVS}$ and the fill factor (FF). Also notice that the IPCE calculated from the short circuit current and the IPCE obtained from Figure 5.2 differ greatly, especially for the N719-cell. It is also remarkable that the $f_{min,IMPS}$ is a factor 28 larger for AFB8 compared to N719. The complete IMVS and IMPS spectra are presented in section 5.2.1, while only the frequencies giving the minimum imaginary response is given in Table 5.1.

Table 5.1: Key experimental results for the two DSSC's which were modelled. V_{oc} is the open circuit potential. I_{sc} is the short circuit current. $f_{min,IMVS}$ is the frequency giving the minimum in the IMVS spectrum, and $f_{min,IMPS}$ is the frequency giving the minimum in the IMPS spectrum. Abs_{blue} is the absorbance at 453 nm measured for solutions of the dyes, ref Figure 5.1. $IPCE_{blue,IV}$ is the IPCE for 453 nm illumination calculated from the I_{sc} in the IV-characteristics. $IPCE_{blue}$ is the IPCE for 453 nm illumination as automatically generated by the Zahner setup, ref Figure 5.2. FF is the fill factor. η_{pc} is the power conversion efficiency.

Parameter	Value N719	Value AFB8	Unit
V_{oc}	0.595	0.607	V
I_{sc}	38.5	49	A
$f_{min,IMVS}$	5.9	7.2	Hz
$f_{min,IMPS}$	18.5	513	Hz
Abs_{blue}	16%	36%	-
$IPCE_{blue,IV}$	55%	70%	-
$IPCE_{blue}$	20%	55%	-
FF	73%	66%	-
η_{pc}	8.7%	10.3%	-

5.1.2 Spectroscopic methods

Figure 5.4 shows the imaginary part of the impedance as a function of the real part of the impedance, for the cell made with N719-dye. The data is shown for four different potentials applied to the cell in the dark. It can be worth noticing that the data points are rather sparse, and that the half-circles have a rather elliptical shape.

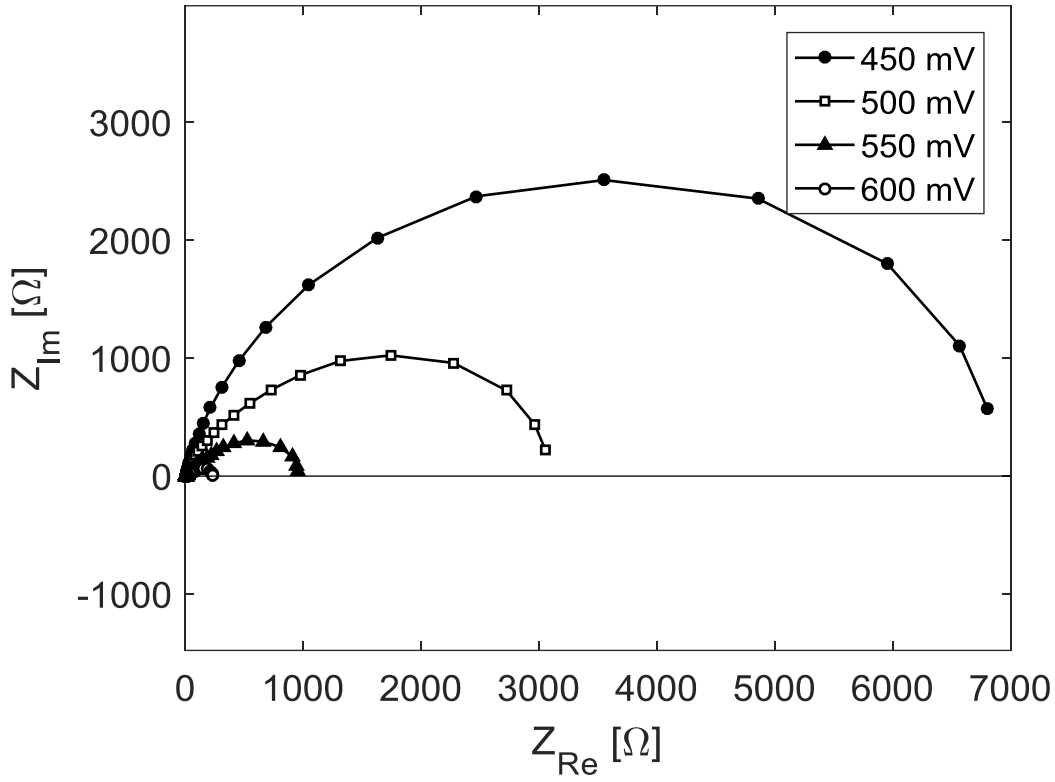

Figure 5.4: Plot showing the imaginary impedance as a function of the real impedance, at four different potentials. The data is from a DSSC made with N719 dye. There was no illumination of the cell during the measurement.

Figure 5.5 and Figure 5.6 shows the recombination resistance and the capacitance, respectively, plotted against the potential of the cell made with N719. The potential was divided by a factor Tk_B. Notice that there are only four data points, and that they are spread close to linearly, but not quite. The same measurements were done for AFB8, and yielded the same slope at two decimals precision for both capacitance and recombination resistance plots. The plots for AFB8 are thus not included, due to practically being identical.

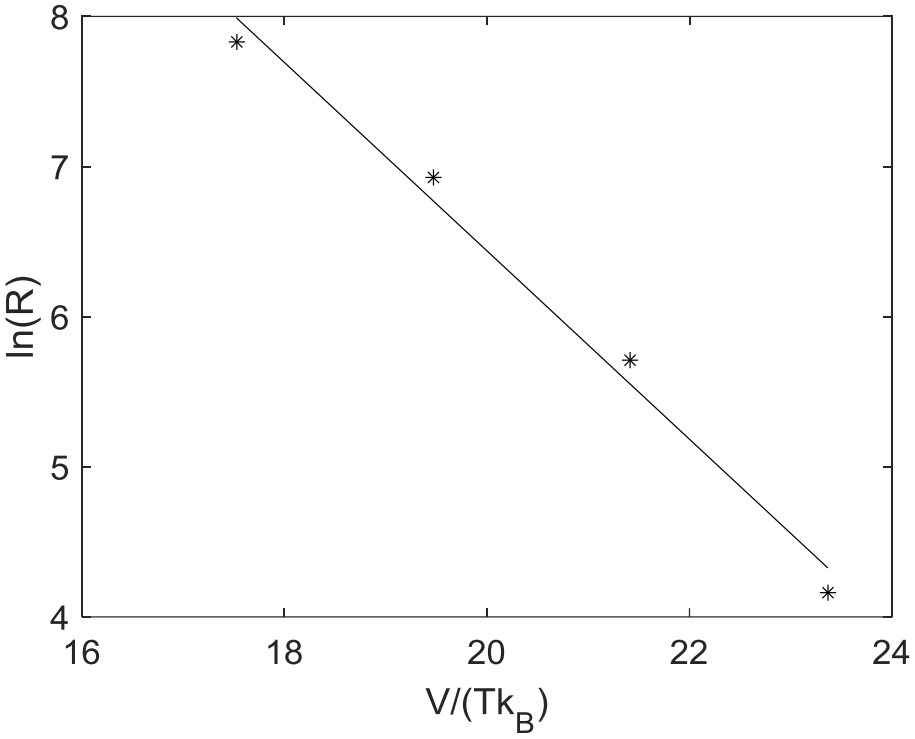

Figure 5.5: Plot showing the natural logarithm of the recombination resistance as a function of $V/(T * K)$, where V is the potential, T is the temperature in kelvin, and k_B is the Boltzmann constant.

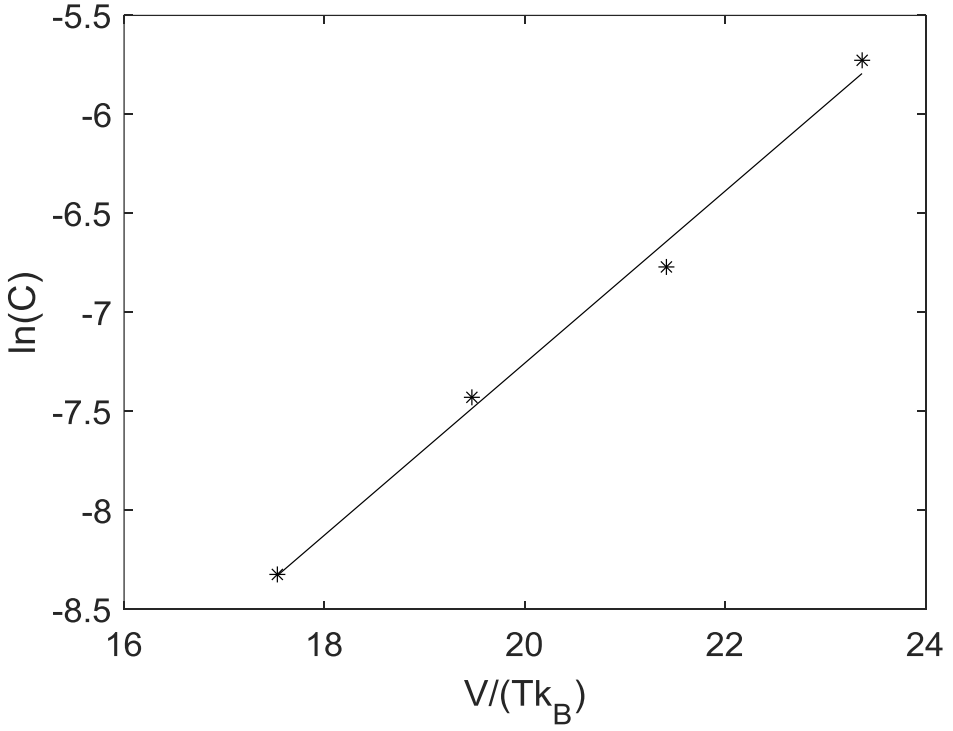

Figure 5.6: Plot showing the natural logarithm of the capacitance as a function of $V/(T * K)$, where V is the potential, T is the temperature in kelvin, and k_B is the Boltzmann constant.

5.2 Results from the model

In this section, results obtained from the model (described in section 3) are presented. The parameters in Table 5.2 were used for the modelling unless stated otherwise. Both the cell made with AFB8 and the cell with N719 was modelled. The cells were made identical, except for the dye. The thickness parameter d should have been identical, since the cells were made with the same thickness of the titanium dioxide layers. However, the parameter was set to 10 µm for the cell with AFB8, and 15 µm for the cell with N719. The reason for this is explained in section 5.2.1.

The parameters k_0, D_0, ϵ and n_0 can give information on how the cells compare. Notice that D_0 is almost a factor 10^4 larger for the AFB8-cell than for the N719-cell. Also notice that the absorption coefficient, ϵ, and the electron concentration the dark, n_0, is largest for N719. k_0 is somewhat larger for the AFB8-cell than for the N719-cell. The differences in the parameters in Table 5.2 are larger than what might be expected from the small difference in power conversion efficiency, ref Table 5.1.

Table 5.2: The default parameters used to model the N719 and AFB8 cell.

Parameter	N719	AFB8	Unit
D_0	$2.8 * 10^{-15}$	$2.1 * 10^{-11}$	$\mathrm{m}^2.\mathrm{s}^{-1}$
k_0	0.14	0.24	s^{-1}
ϵ	$3.0 * 10^5$	$8.9 * 10^4$	m^{-1}
n_0	17	5.3	$\mathrm{C}.\mathrm{m}^{-3}$
d	15	10	µm
α	0.43	0.43	-
β	0.63	0.63	-
ϕ_{ss}	190	190	$\mathrm{W}.\mathrm{m}^2$
Φ_A	$0.05\Phi_{ss}$	$0.05\Phi_{ss}$	$\mathrm{W}.\mathrm{m}^2$
η_{inj}	1	1	-
η_{refl}	0	0.5	-
λ	453	453	nm

It has been reported earlier that the recombination rate is dependent on the dye which is used [6], and it was as expected that k_0 was somewhat different for the two different dyes. However, it has also been reported that the transportation in the semiconductor is independent of the dye [6]. Therefore, it was unexpected to see the vast difference in the D_0 for the two dyes. Another cell with a very similar dye to AFB8 was tested to see whether the high D_0 could be reproduced, and yielded roughly the same large value for D_0. This is a very interesting result. There is no clear consensus on the theory of the transportation and the trap states in the titanium dioxide, nor is there theory that can explain how the transportation is so dependent on the dye which is adsorbed as far as the author knows. This thesis does however not seek to try to explain the differences in the parameters, and this difference in D_0 will thus largely be untouched. Never the less should this striking difference be noticed as an interesting finding.

5.2.1 Modelling of small amplitude perturbations

In this section, experimental and modelled IMPS and IMVS spectra are presented for the cell made with N719. The experimental results were multiplied by a factor ranging from 1-15 to facilitate the comparison between modelled and experimental data. The need for this was attributed to ambiguity in the Zahner documentation.

5.2.1.1 IMPS

Figure 5.7 shows the experimental and modelled IMPS spectrum for the N719-based DSSC. Notice that the experimental spectrum is broader than the modelled one, and that it does not flatten out for frequencies of above 1 kHz. Also notice that there is a "dent" in the lowest part of the experimental IMPS-spectrum where the broadening occurs, and that the slope is slightly steeper at the left than to the right. The experimental results are similar to what has been reported earlier [30], except for the way that the current response does not flatten out, and the dent. It is however hard to tell for sure that there is absolutely no dent in the figure reported by [30]. The modelled IMPS-spectrum looks similar to previous analytically modelled IMPS-spectra [27].

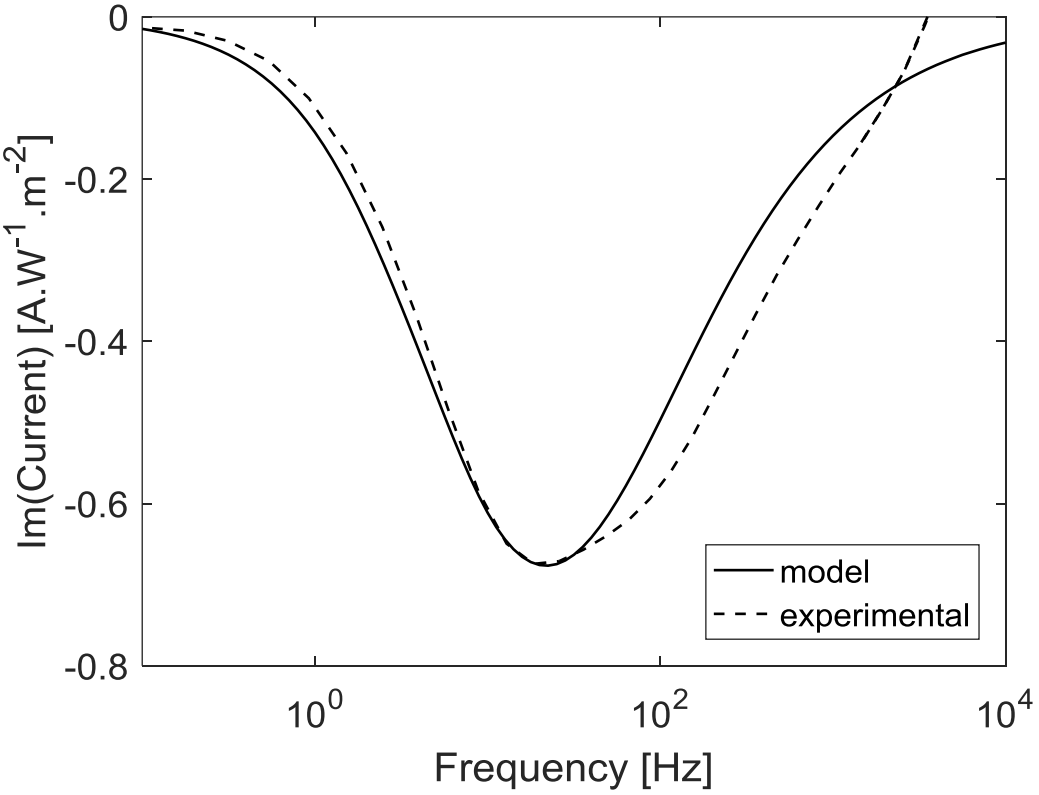

Figure 5.7: Plot showing the experimental and modelled IMPS spectrum for the DSSC made with N719. The parameter *d* is set to 15 µm in the model.

Figure 5.8 shows the experimental and modelled IMPS spectrum for the cell based on N719, when the thickness is set to 10 µm. D_0, k_0, ϵ and n_0 was adjusted anew for this thickness with the procedure described in section 3.4.2.3. The model has a pronounced dent in its lowest part, and the width of the two spectra is more similar than in Figure 5.7. However, the experimental data still deviates from the model at the highest frequencies, and the fit is not excellent at the lowest part.

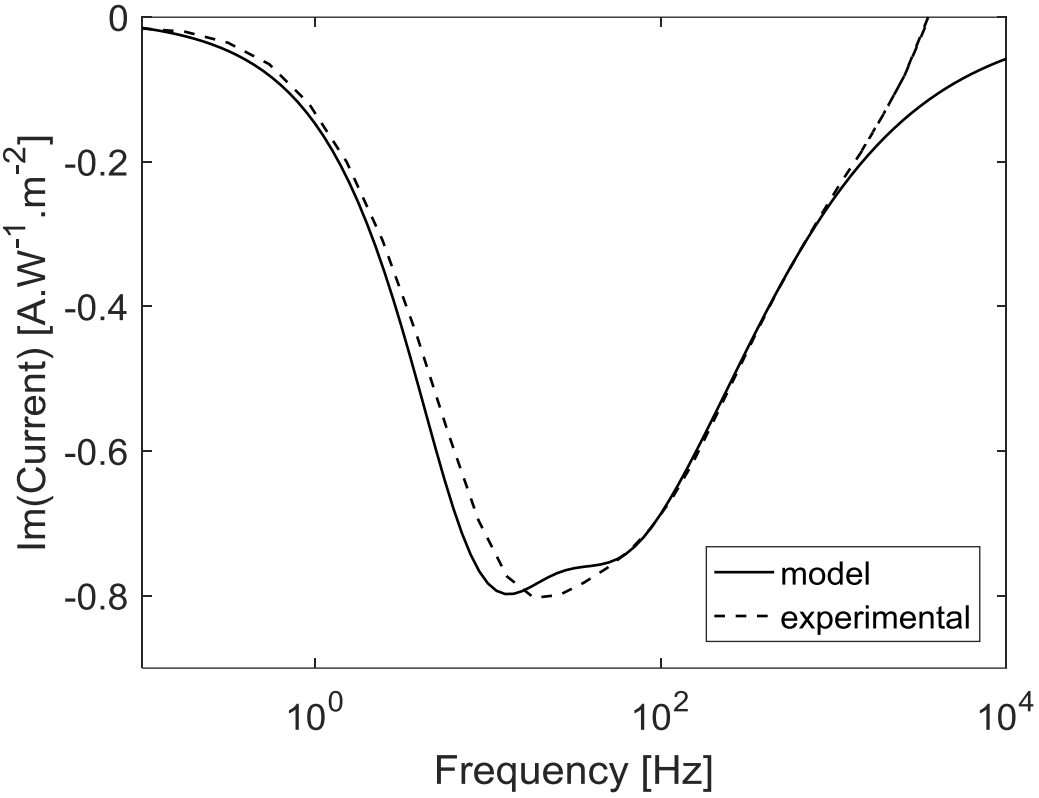

Figure 5.8: Plot showing the experimental and modelled IMPS spectrum for the DSSC made with N719. The parameter d is set to 10 μm in the model.

Figure 5.9 shows the modelled IMPS spectra for the cases of $d = 9$, $d = 10$ and $d = 11$ µm. The same D_0, k_0, ϵ and n_0 as used for Figure 5.8 were used for each thickness. The plots vary greatly at the bottom part. The smaller the thickness, the flatter the profile becomes. It can also be noticed that the plot for $d = 9$ is not completely flat, but has a small bump in the middle. This dependency on d has not been reported previously as far as the author knows.

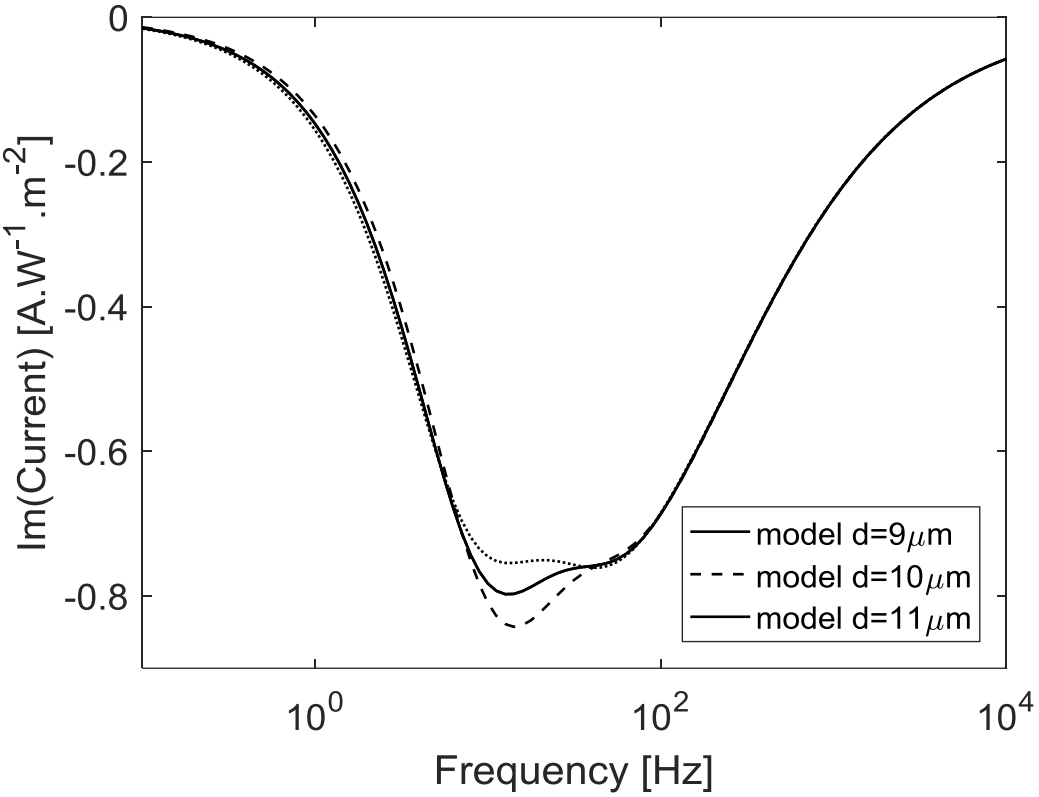

Figure 5.9: Plot showing modelled IMPS spectra for the DSSC made with N719. The parameter d is varied from 9 to 11 µm.

5.2.1.2 IMVS

Figure 5.10 shows the experimental and modelled IMVS spectrum for the cell based on N719-dye. The fit is good, with only a relatively small deviation in width. The shapes of the experimental and modelled curve are more similar than in the case of IMPS in Figure 5.7. The experimental curve matches well with what has been reported before [20, 30], and the modelled curve matches with previous analytical models [20].

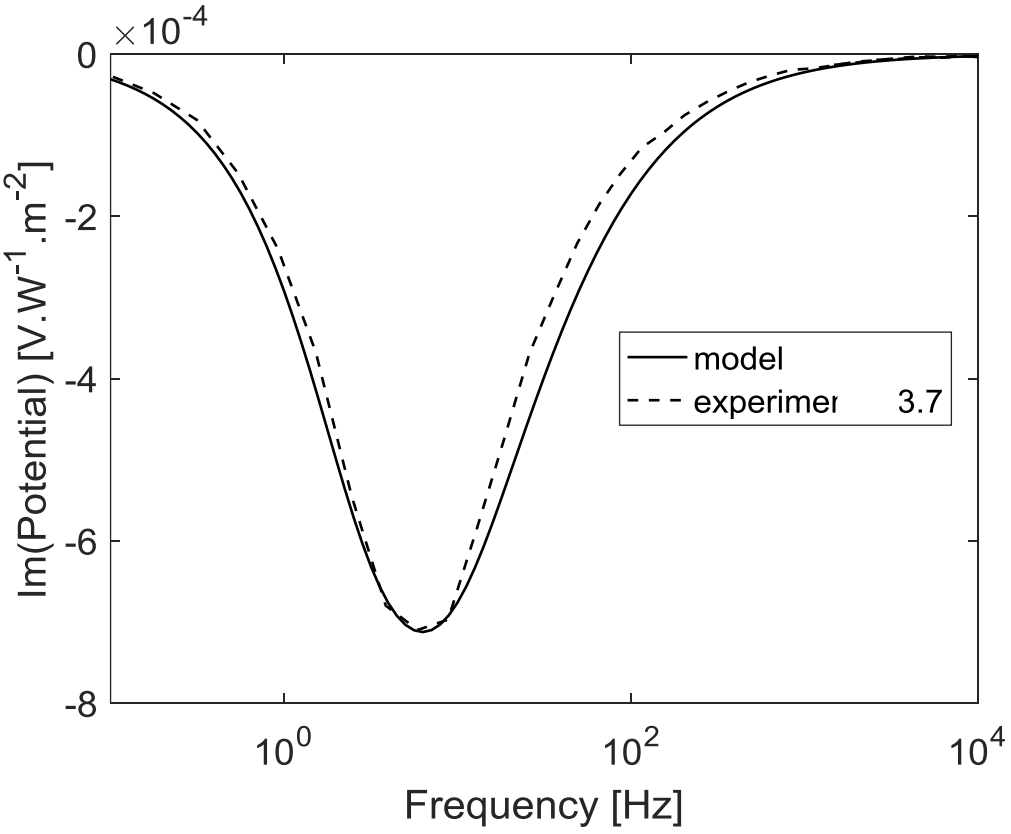

Figure 5.10: Plot showing the experimental and modelled IMVS spectrum for the DSSC made with N719. The parameter *d* is set to 15 µm in the model.

Figure 5.11 shows the experimental and modelled IMVS spectrum for the cell based on N719. The thickness was set to 10 μm in the model, and D_0, k_0, ϵ and n_0 were the same newly adjusted values as used in Figure 5.8 and Figure 5.9. Notice that there is no significant change in the shape of the modelled IMVS spectrum, when comparing Figure 5.10 and Figure 5.11. This contrasts to the case of modelled IMPS spectra, which have varying shape with varying d, as seen in Figure 5.7 and Figure 5.8.

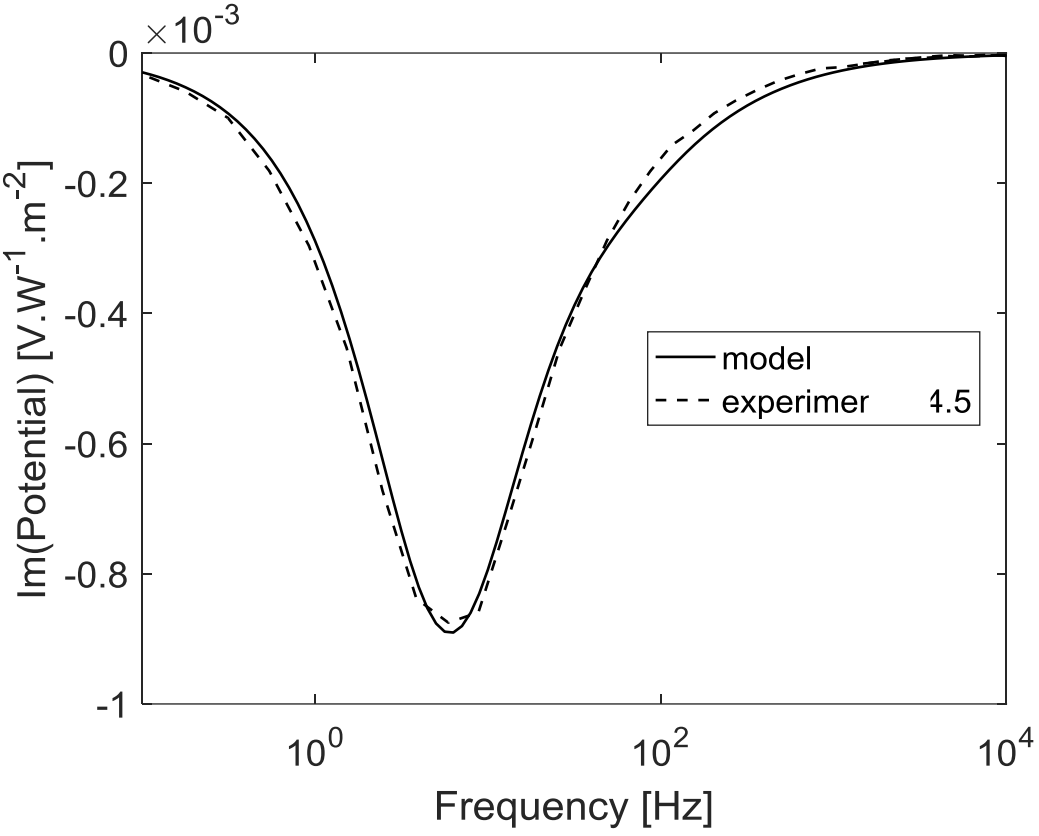

Figure 5.11: Plot showing the experimental and modelled IMVS spectrum for the DSSC made with N719. The parameter d is set to 10 μm in the model.

Varying η_{refl} for both IMPS and IMVS spectra was also studied. It gave practically no difference in neither shape nor amplitude for the N719-cell, and is therefore omitted.

The modelled and experimental IMPS and IMVS spectra for the AFB8-cell are omitted from this thesis, due to time limitations. They were however similar to that of the N719-cell. The IMVS had a good fit, while the IMPS had a somewhat poorer fit for the AFB8-cell. The shape of the IMPS-spectrum was dependent on the thickness parameter d. One dissimilarity between the AFB9-cell and the N719-cell was however that the modelled IMPS spectra to the AFB8-cell was dependent on the reflection parameter η_{refl}.ix This dependency was however only on the frequency giving the IMPS minima, and not on the shape of the spectrum.

5.2.2 Details on a cell made with N719-dye

In this section, details on the cell made with N719 are presented. The details are extracted from the model for two different cases. One case for the measured thickness of 15 μm, and one case for the calculated optimum thickness of 4 micrometer.

5.2.2.1 Details on a 15 μm thick cell made with N719-dye

Figure 5.12 shows the experimental and modelled IV-characteristics of the DSSC made with N719. The parameters used are given in Table 5.2. Notice that the experimental curve has a somewhat lower fill factor than the modelled curve. Figure 5.12 resembles the results reported by Anta et al [1]. The modelled IV-characteristic is the result of the numerical solution of the steady state equations as described in section 3.2.

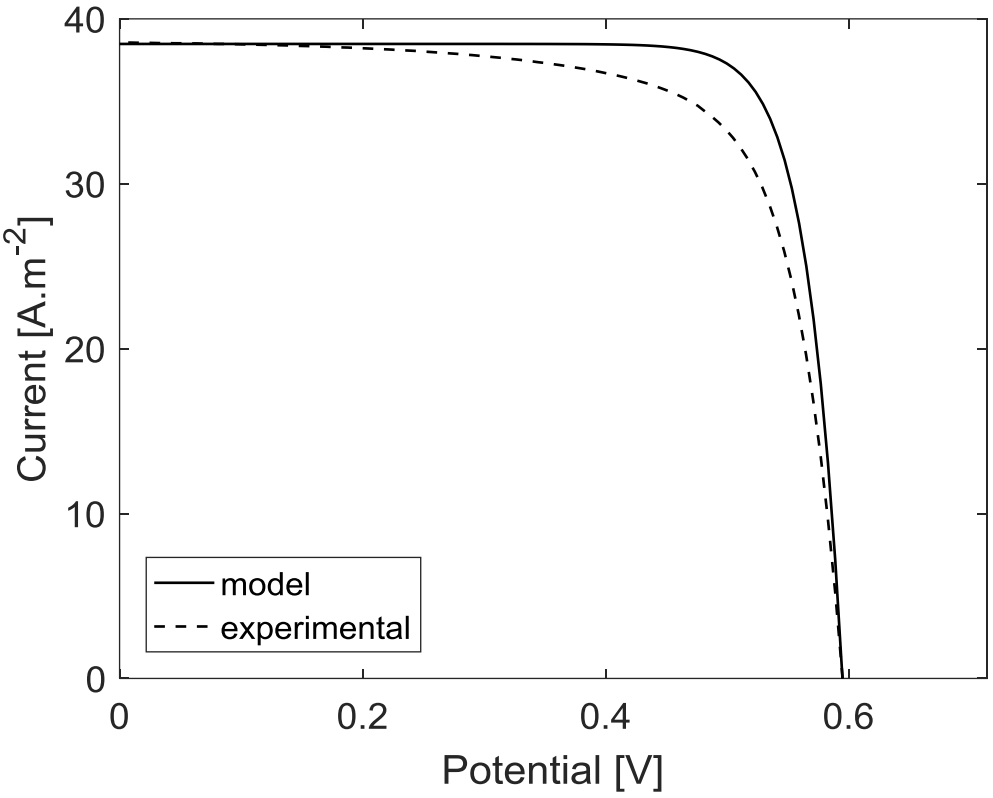

Figure 5.12: Plot showing the modelled and experimental current-potential characteristic of the DSSC made with N719.

Figure 5.13 shows the experimental IV-characteristic and two versions of the modelled IV-characteristics. One of the models is the default model, and the other is the default model which has been adjusted by introduction of shunt resistance and series resistance. Notice that the adjusted model fits the experimental results better than the default model.

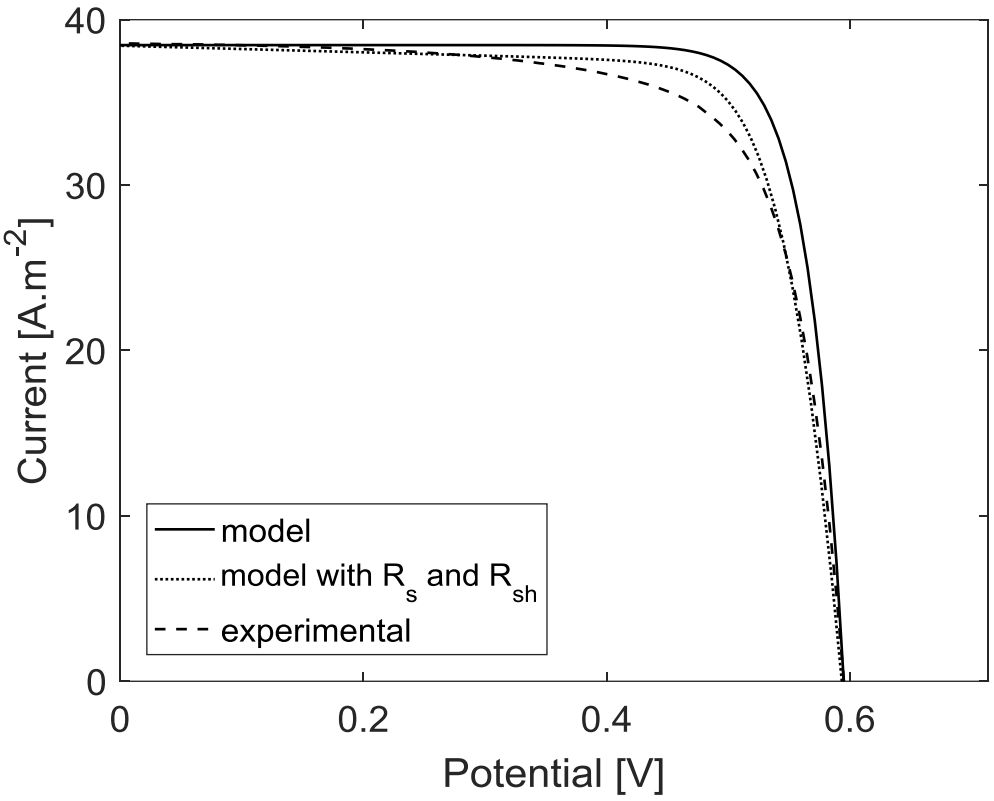

Figure 5.13: Plot showing the experimental IV-characteristic of the DSSC made with N719, the modelled IV-characteristic, and the modelled IV-characteristic with series resistance and shunt resistance included.

Figure 5.14 shows IV-characteristics from experimental results and the (default) model, for 4 different light intensities. The model fits best at 190 $\mathrm{W.m^{-2}}$, as expected. This is because the parameters for the model were calculated from experimental data obtained with 190 $\mathrm{W.m^{-2}}$. The I_{sc} is underestimated by the model at 136 and 74 $\mathrm{W.m^{-2}}$. On the other hand, the V_{oc} fits very well for these intensities. The model which is applied at 9 $\mathrm{W.m^{-2}}$ however, fits good with I_{sc}, but has a large difference in V_{oc}. The fill factor is systematically larger for the model than for the experimental results.

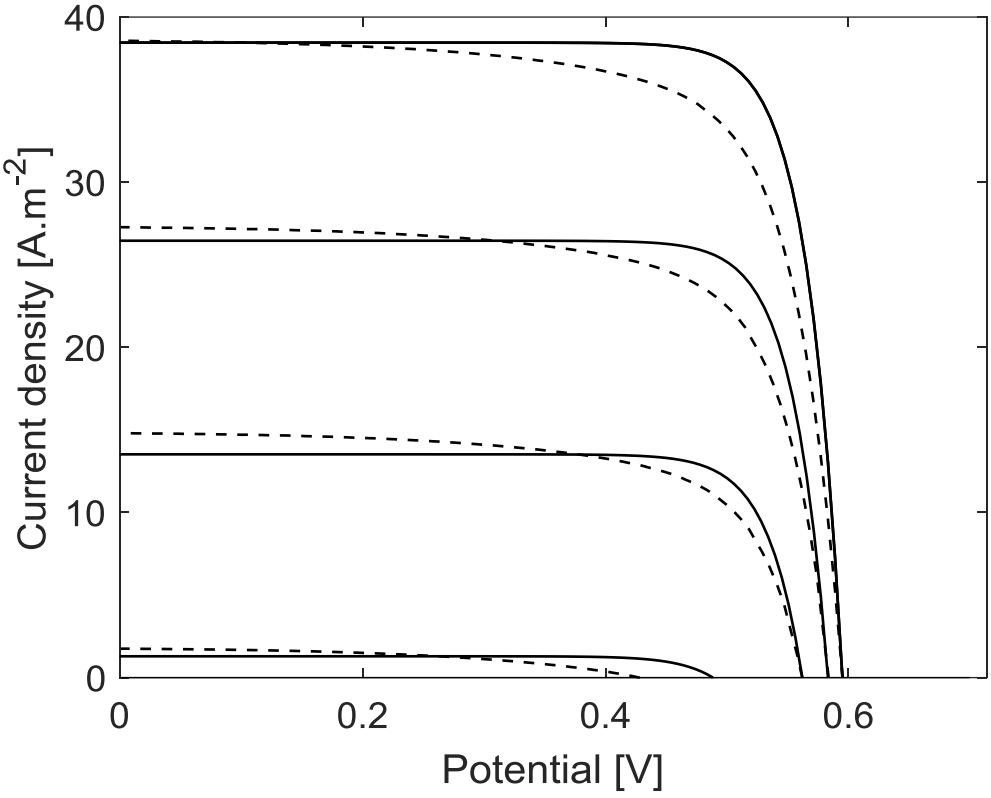

Figure 5.14: Plot showing the experimental and modelled IV-characteristic of the DSSC made with N719 for different light intensities. The Intensities of the light are respectively 190, 136, 74 and 9 $\mathrm{W.m^{-2}}$, from outermost curve and inwards. The dotted line is the experimental IV-characteristic and the whole drawn line is the model.

Figure 5.15 shows the relative electron concentration as a function of x, for potentials ranging from short circuit to open circuit. As previously mentioned, $x = 0$ is the contact between the titanium dioxide and the TCO. As expected, Figure 5.15 shows that the electron concentration increases with increasing potential over the cell. The increased steepness of the slope at $x = 0$ is as expected and explains that the current increases as the potential is lowered. An interesting feature, is that the concentration profile for open circuit is substantially higher at $x = 0$ than at $x = d$. This is not as expected, since it is commonly assumed that the concentration profile is flat at open circuit. Lastly, it can be noticed that the concentration gradient changes sign at around 4 µm for most potentials, implying that the electrons residing deeper than 4 µm will diffuse *away* from the TCO. Figure 5.15 is strikingly different from the much flatter profiles reported by Anta et al. [1]. It should however be kept in mind that the cell modelled in [1] was 9 µm and with a different ruthenium dye.

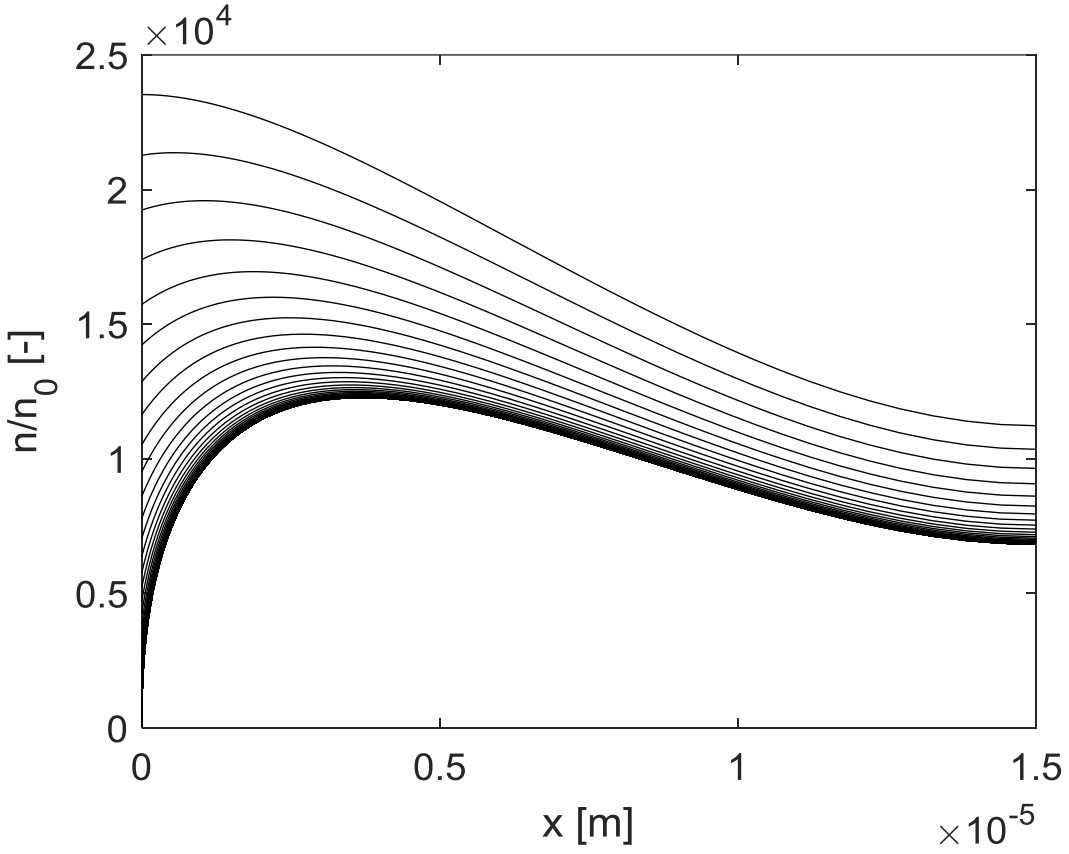

Figure 5.15: Plot showing the modelled relative electron concentration, n/n_0, as a function of x, for different potentials. The curve at the top is n/n_0 during open circuit, while the curve closest to the x-axis is n/n_0 during short circuit. The other curves are n/n_0 for potentials spread evenly from open circuit to short circuit. The figure is calculated for the N719-cell, with $d = 15$ µm.

Figure 5.16 shows the amount of electrons which are injected into the titanium dioxide, as a function of x. The amount is divided into two parts, one part which is the electrons that are injected when the light travels through the cell from left to right. The other term, labeled "$J_G$extra", is the electrons which are injected if the light is reflected from right to left by a reflective layer at the very right of the titanium dioxide. However, in Figure 5.16 the term $J_G$extra can barely be seen, because it is so small. This is because almost all the light is absorbed during its travel from left to right, and there is therefore practically no light which can be reflected.

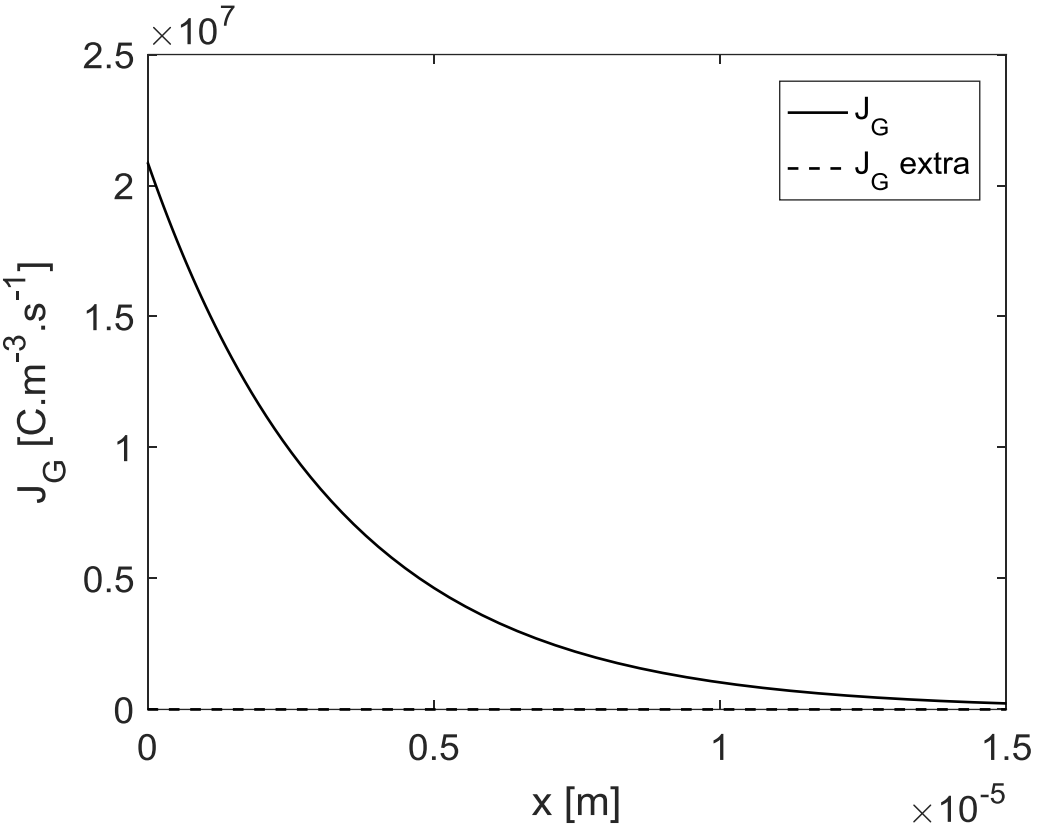

Figure 5.16: Plot showing the modelled generation term, J_G, as a function of x. J_G extra is the extra gain in J_G that results if η_{refl} is 0.75. It is so small that it cannot be seen. The figure is calculated for the N719-cell, with $d = 15$ µm.

Figure 5.17 shows the three main terms of the continuity equation, namely the generation term J_G, the recombination term J_R, and the diffusion term J_D, plotted as functions of x for the case of short circuit. Notice that it is the negative of the diffusion term that is plotted, and that all the terms add up to zero as expected from equation (16). The recombination term is larger than the injection term for $x > 7$ µm. The diffusion term changes sign at about the same place, indicating that the net diffusion into a grid point for $x > 7$ µm is positive. The recombination term resembles the concentration profile in Figure 5.15 just flattened out.

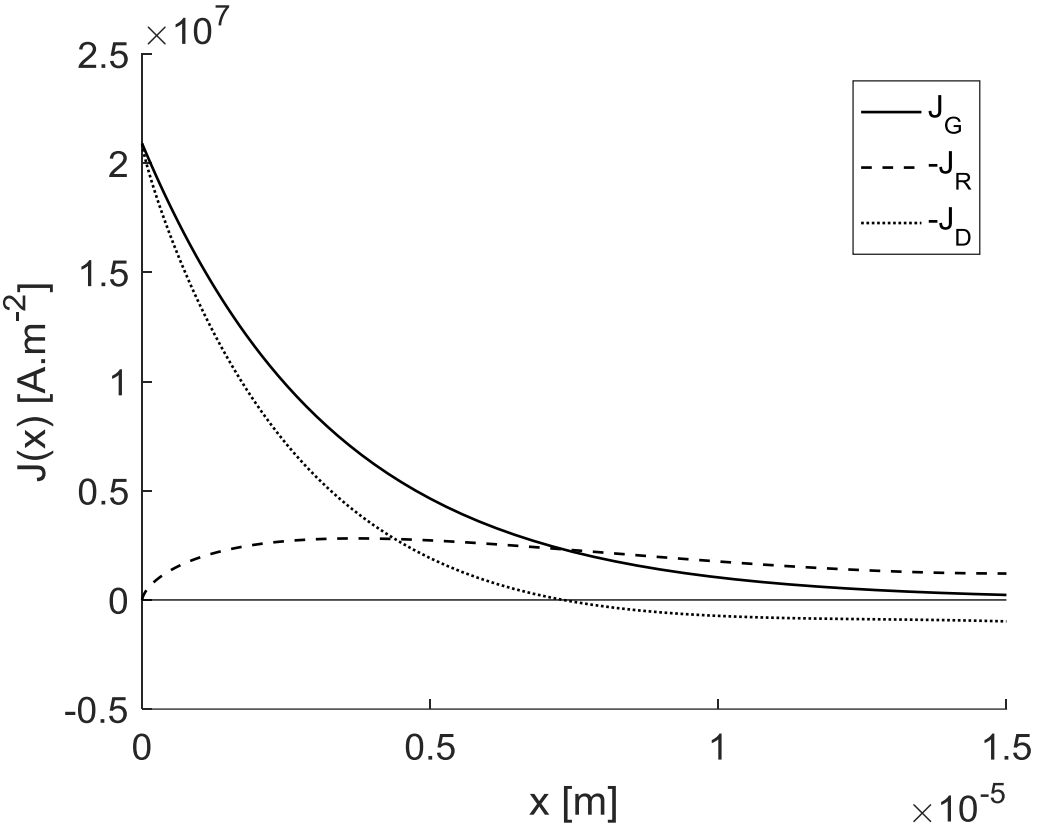

Figure 5.17: Plot showing the modelled generation term (J_G), recombination term (J_R) and diffusion term (J_G), as a function of x. The terms are modelled for short circuit. The figure is calculated for the N719-cell, with $d = 15$ µm.

Figure 5.18 shows the generation term J_G, the recombination term J_R, and the diffusion term J_D, plotted as functions of x for the case of open circuit. Notice that both the diffusion term and recombination term have significantly different profiles than in Figure 5.17.

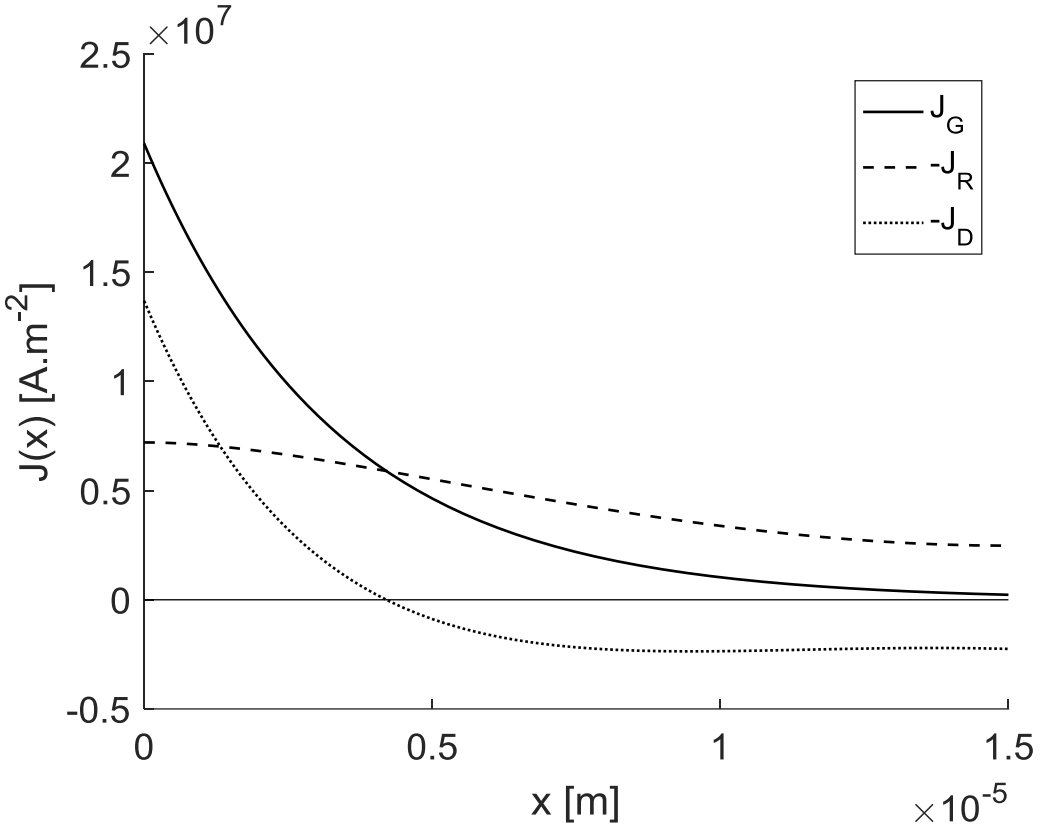

Figure 5.18: Plot showing the modelled generation term (J_G), recombination term (J_R) and diffusion term (J_G), as a function of x. The terms are modelled for the case of open circuit. The figure is calculated for the N719-cell, with $d = 15$ µm.

Figure 5.19 shows how many percent of the incident light which has been absorbed and injected into the titanium dioxide for a given x. The figure shows that the amount of absorbed light increases only slightly from 10 µm to 15 µm.

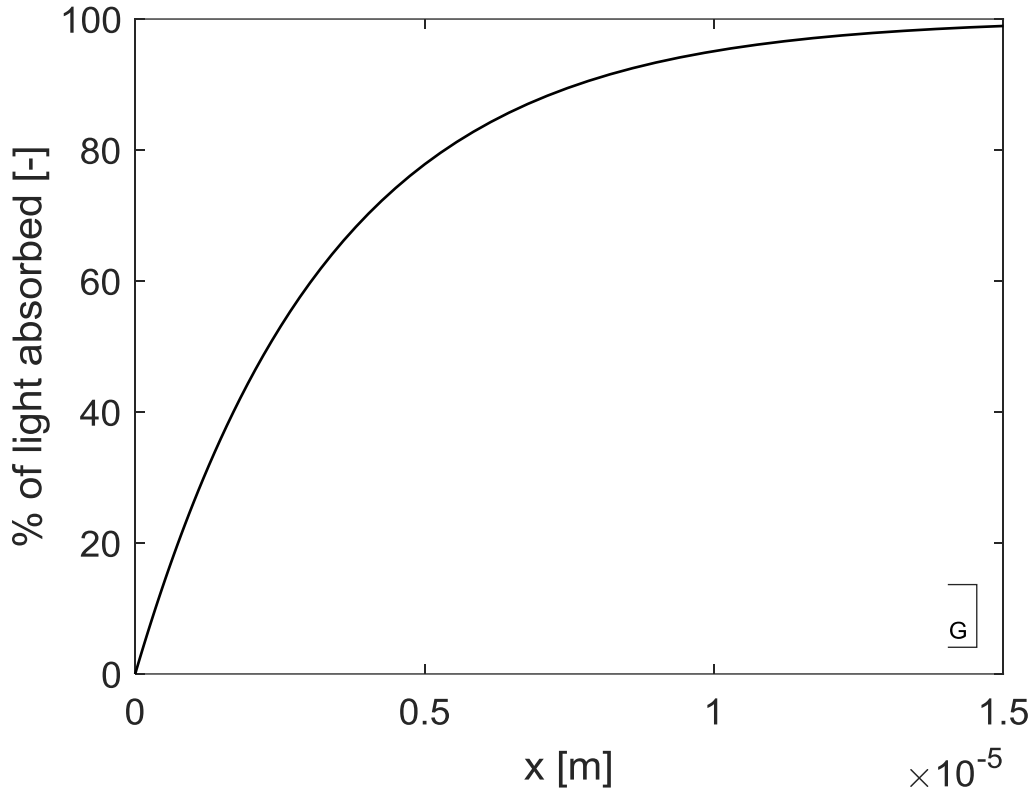

Figure 5.19: Plot showing how many percent of the incident light which has been absorbed at a given depth in the cell, given by x. The figure is calculated for the N719-cell, with $d = 15$ µm.

Figure 5.20 shows the area for each term in Figure 5.17 and Figure 5.18 for different potentials. Another way to describe Figure 5.20 is that it shows the total amount of electrons that recombine, the total amount of electrons that is injected, and the current. The sum of the recombination and the current equals the injection, as expected from the continuity equation for steady state, ref equation (16). The current plot in Figure 5.20 is the same as the modelled IV-characteristic in Figure 5.12. What is perhaps most important to notice in Figure 5.20 is that as much as ~40% of the injected electrons recombine at short circuit.

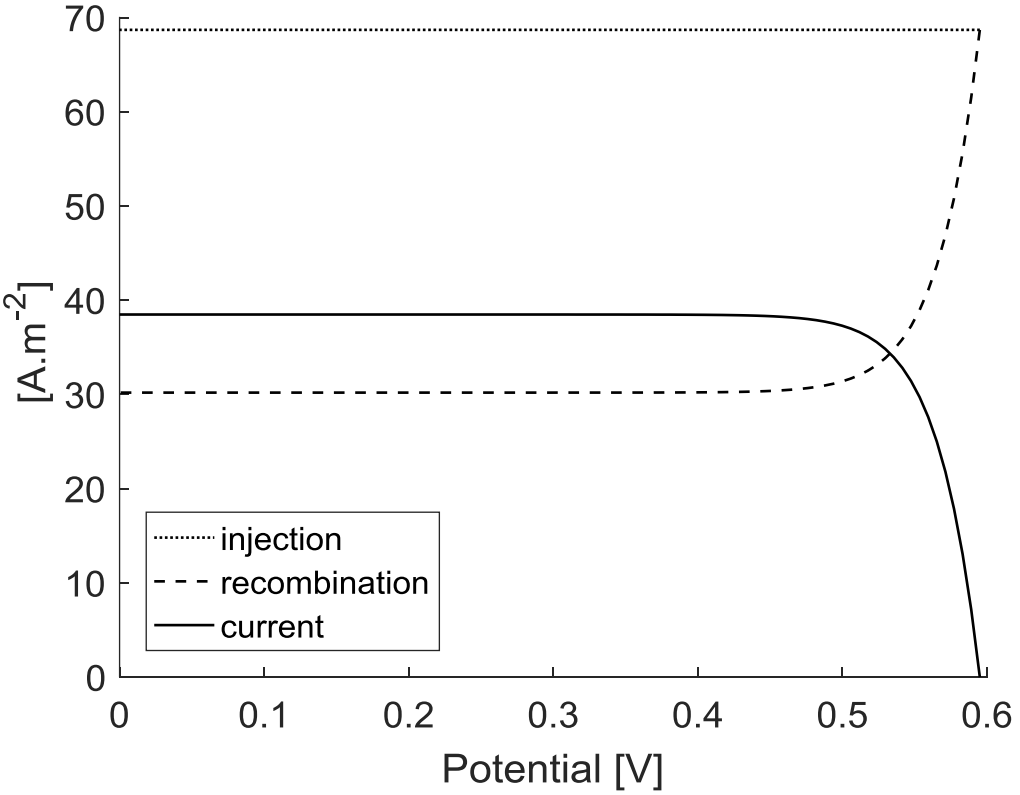

Figure 5.20: Plot showing how many electrons that are injected into the cell, how many which result in a current going out from the cell and how many which recombine as a function of the potential over the cell. The figure is calculated for the N719-cell, with $d = 15$ µm.

Figure 5.21 shows the modelled power conversion efficiency as a function of d, for two different cases. One case is that the cell is made without a reflective layer. The other case is that there is a reflective layer reflecting 75% of the light which is not absorbed on its first time passing though the DSSC. The DSSC will have an improved efficiency by reducing the thickness of the titanium dioxide for both cases. The gain in efficiency is larger for the cell with a reflective layer, and the optimum thickness is also thinner.

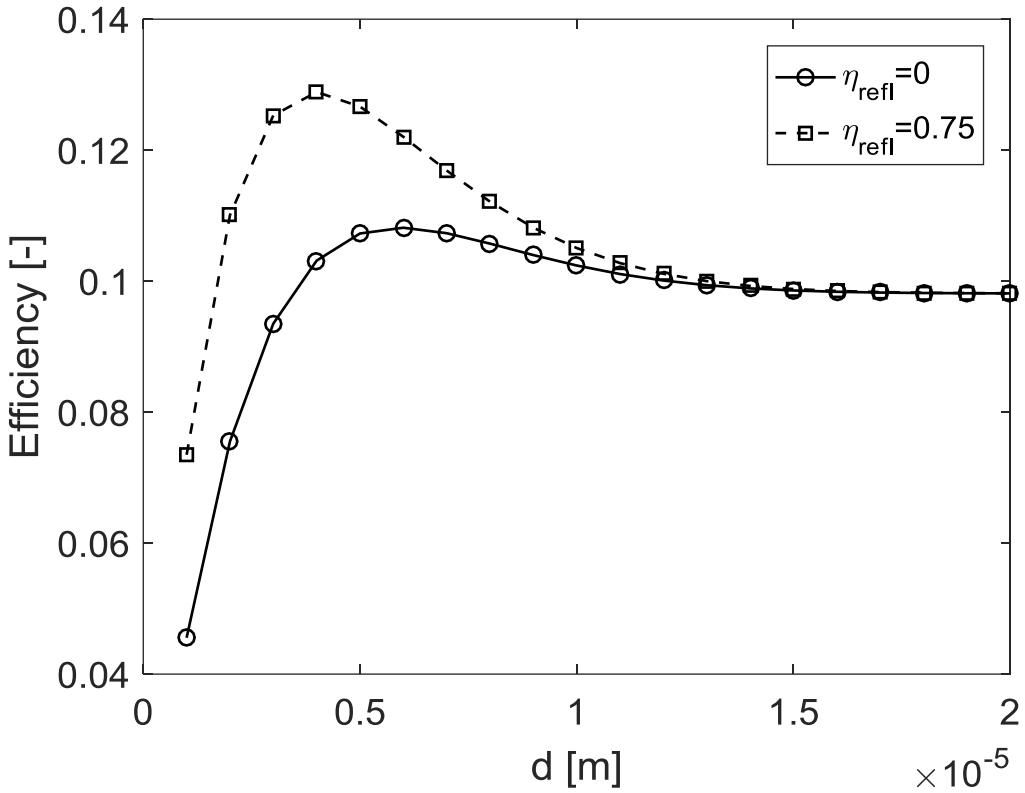

Figure 5.21: Plot showing the predicted power conversion efficiency as a function of the titanium dioxide layer thickness, d. The figure is calculated for the N719-cell, for the cases of $\eta_{refl} = 0$ and $\eta_{refl} = 0.75$.

5.2.2.2 Non-default thickness and reflection

This section presents the same figures as the previous section, apart from that they are calculated from the model with d set to 4 µm, and η_{refl} to 75%. All other parameters are as in the previous section, and given in Table 5.2. It is the same dye as in the previous section, namely N719.

Figure 5.22 shows the modelled IV-characteristic for a N719-cell which is 4 µm thick and with a reflective layer, and the experimental IV-characteristic. The model predicts that the DSSC will perform considerably better if the thickness is reduced from 15 to 4 µm. Both the potential and the current is higher.

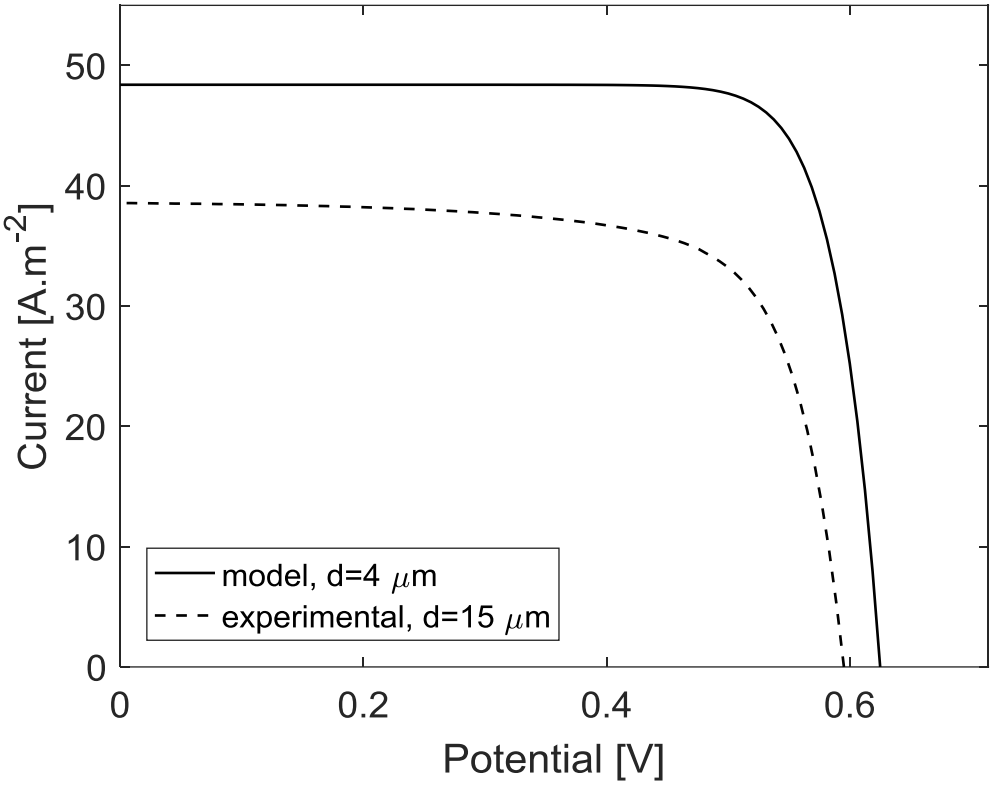

Figure 5.22: Plot showing the experimental IV-characteristic of the cell based on N719, and the modelled IV-characteristic if the cell had been made with a thickness of 4 µm and a reflective layer with $\eta_{refl} = 0.75$.

Figure 5.23 shows the relative electron concentration as a function of x, for potentials ranging from short circuit to open circuit. The electron concentration is considerably higher and the profiles much flatter in Figure 5.23 compared to Figure 5.15. It is also worth noticing that the gradient in Figure 5.23 never changes sign for almost all the potentials except for the highest ones. The slope in Figure 5.23 favors diffusion towards the TCO to a much larger extent than in Figure 5.15. Figure 5.23 shows similar profiles to those reported by Anta et al. [1].

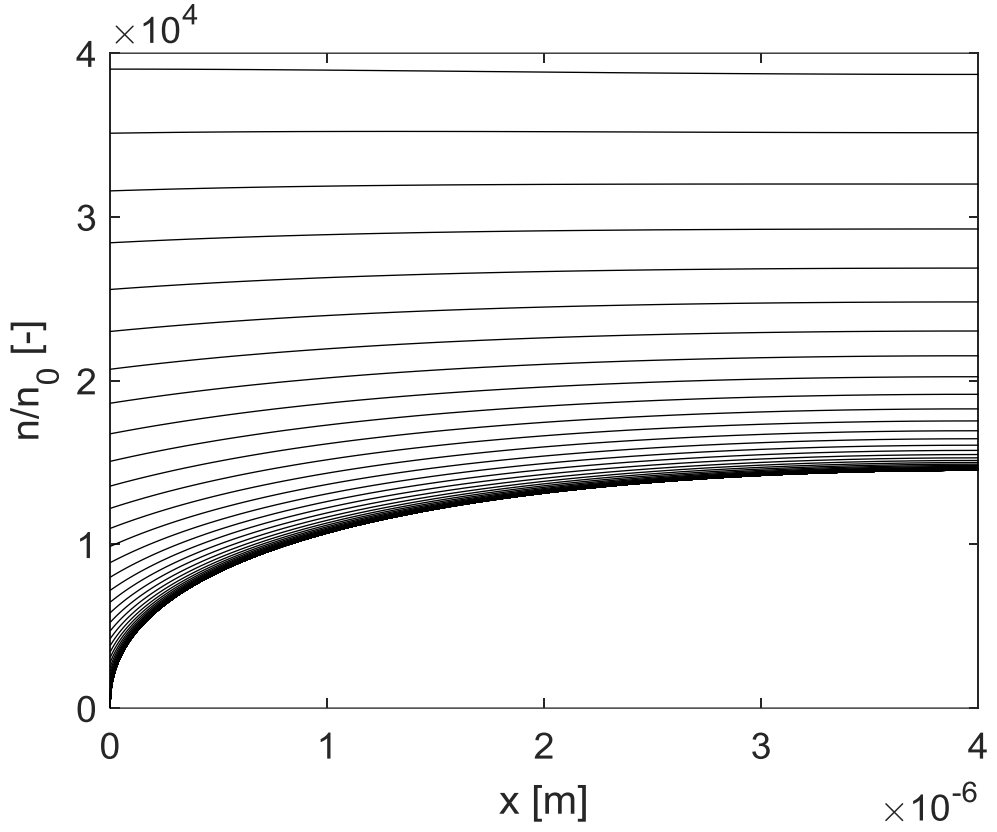

Figure 5.23: Plot showing the modelled relative electron concentration, n/n_0, as a function of x, for different potentials. The curve at the top equals n/n_0 during open circuit, while the curve closest to the x-axis equals n/n_0 during short circuit. The other curves are n/n_0 for potentials spread evenly from open circuit to short circuit. The figure is calculated for the N719-cell, with $d = 4$ µm.

Figure 5.24 shows the amount of electrons which are injected into the titanium dioxide, as a function of x. The amount is divided into two terms. One term is the electrons which are injected when the light travels through the cell from left to right. The other term, labeled $J_G$extra, is the electrons which are injected if the light is reflected from right to left by a reflective layer at the very right of the titanium dioxide. The J_G term is the largest one, but the $J_G$extra does still contribute significantly. Especially when compared to Figure 5.15 and the cell which is 15 µm thick.

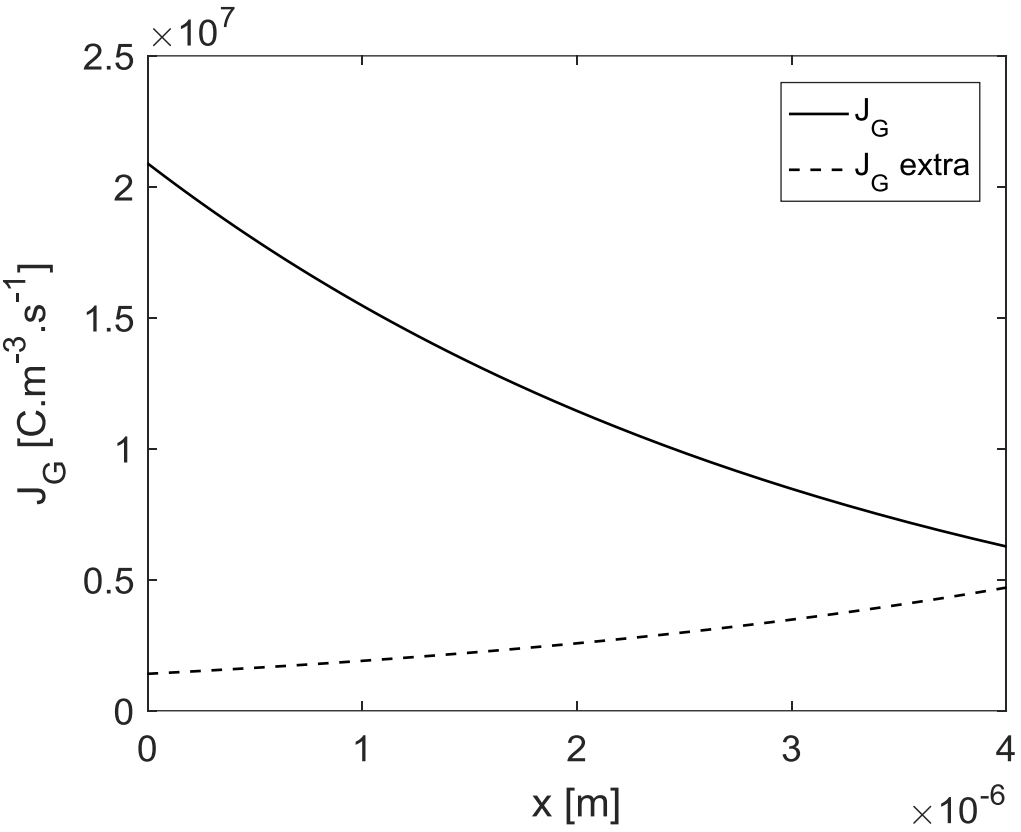

Figure 5.24: Plot showing the modelled generation term, J_G, as a function of x. J_G extra is the extra gain in J_G that results if η_{refl} is 0.75. The figure is calculated for the N719-cell, with $d = 4$ µm.

Figure 5.25 shows the three main terms of the continuity equation, namely the generation term J_G, the recombination term J_R, and the diffusion term J_D, plotted as functions of x for the case of short circuit. The diffusion term is always positive, indicating that net diffusion from every grid point is negative. This contrasts with Figure 5.16, where the sign of the diffusion term changes. The diffusion term is considerably larger than the recombination term for all values of x.

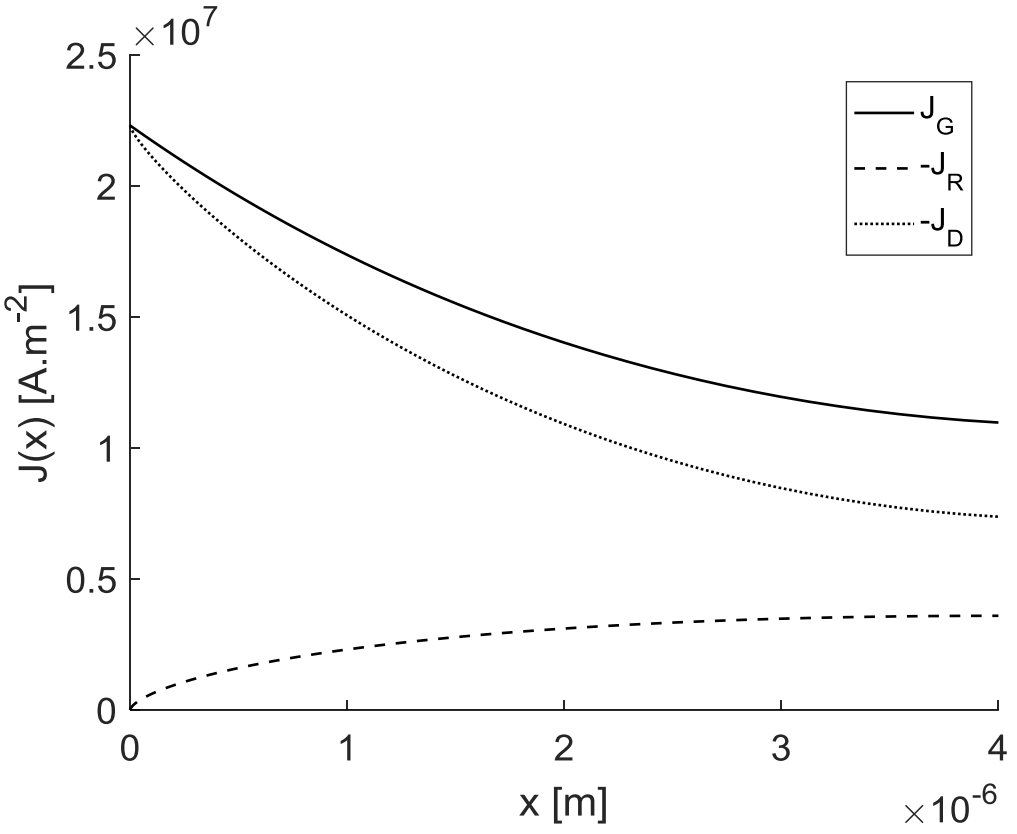

Figure 5.25: Plot showing the modelled generation term (J_G), recombination term (J_R) and diffusion term (J_G), as functions of x. The terms are modelled for short circuit. The figure is calculated for the N719-cell, with $d = 4$ µm.

Figure 5.26 shows the generation term J_G, the recombination term J_R, and the diffusion term J_D, plotted as functions of x for the case of open circuit. The recombination term is as expected flat. This expectation is because the concentration profile is flat as shown in Figure 5.23. The diffusion term has a shape that is very similar to the generation term, explaining the flat concentration profile for open circuit.

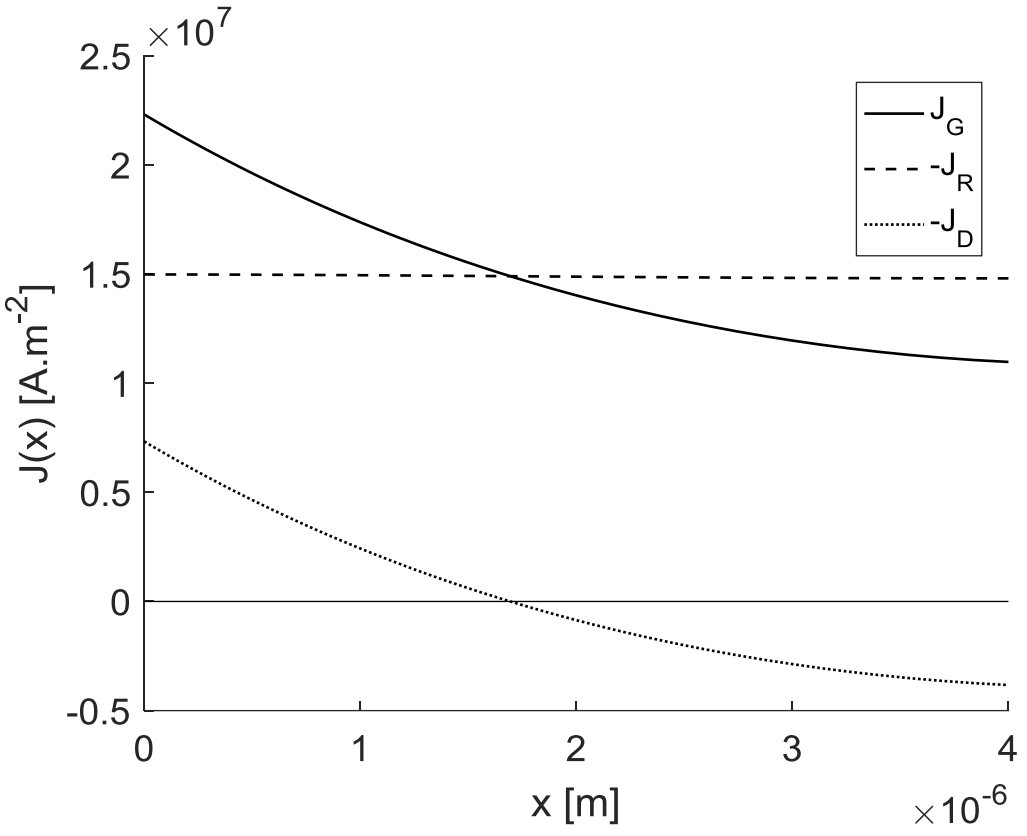

Figure 5.26: Plot showing the modelled generation term (J_G), recombination term (J_R) and diffusion term (J_G), as functions of x. The terms are modelled for the case of open circuit. The figure is calculated for the N719-cell, with $d = 4$ µm.

Figure 5.27 shows how much of the incident light which has been absorbed and injected into the titanium dioxide for a given x. The profile is almost linear compared to Figure 5.18. Slightly more than 80% of the light is captured, which is lower than the almost 100% capture efficiency in Figure 5.18. However, the thickness of the titanium dioxide is only a third of that in Figure 5.18.

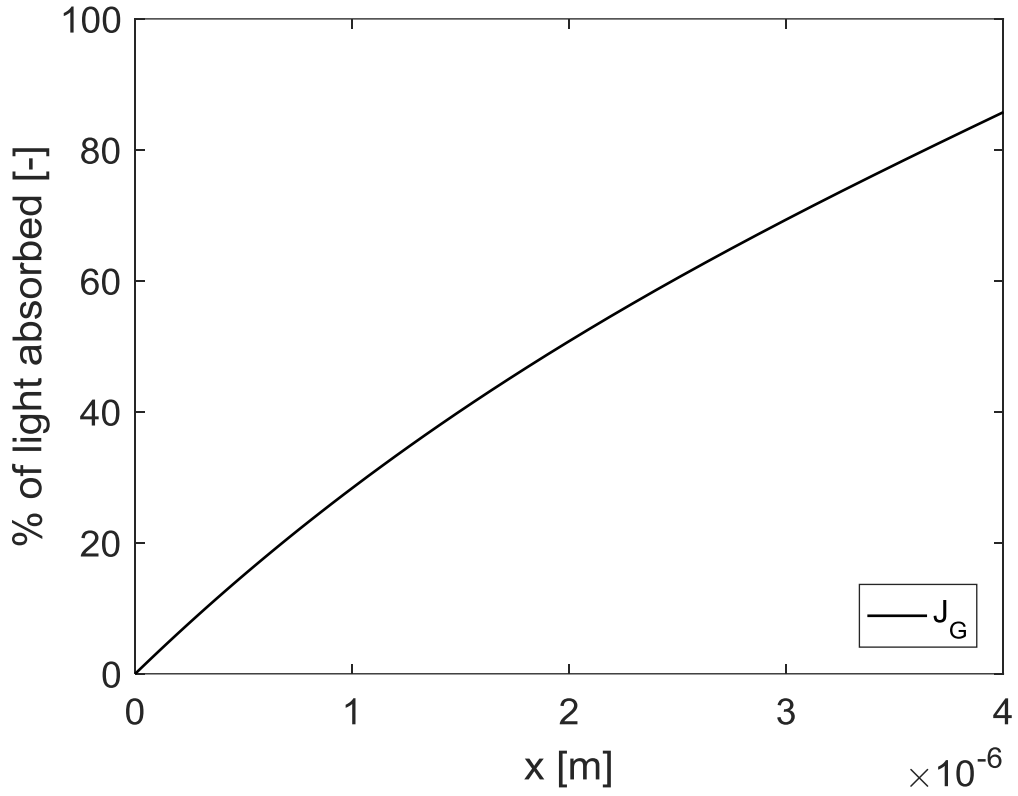

Figure 5.27: Plot showing how many percent of the incident light which has been absorbed at a given depth in the cell, given by x. The plot is extracted from the model. The figure is calculated for the N719-cell, with $d = 4$ µm.

Figure 5.28 shows the total amount of electrons that recombine, are injected, and the current from the DSSC. The recombination term is considerably lower than in Figure 5.19, but still significant, even at short circuit. The current term is considerably higher, and the injection term is somewhat lower compared to Figure 5.19. The increase in the current term is larger than the decrease in the injection term.

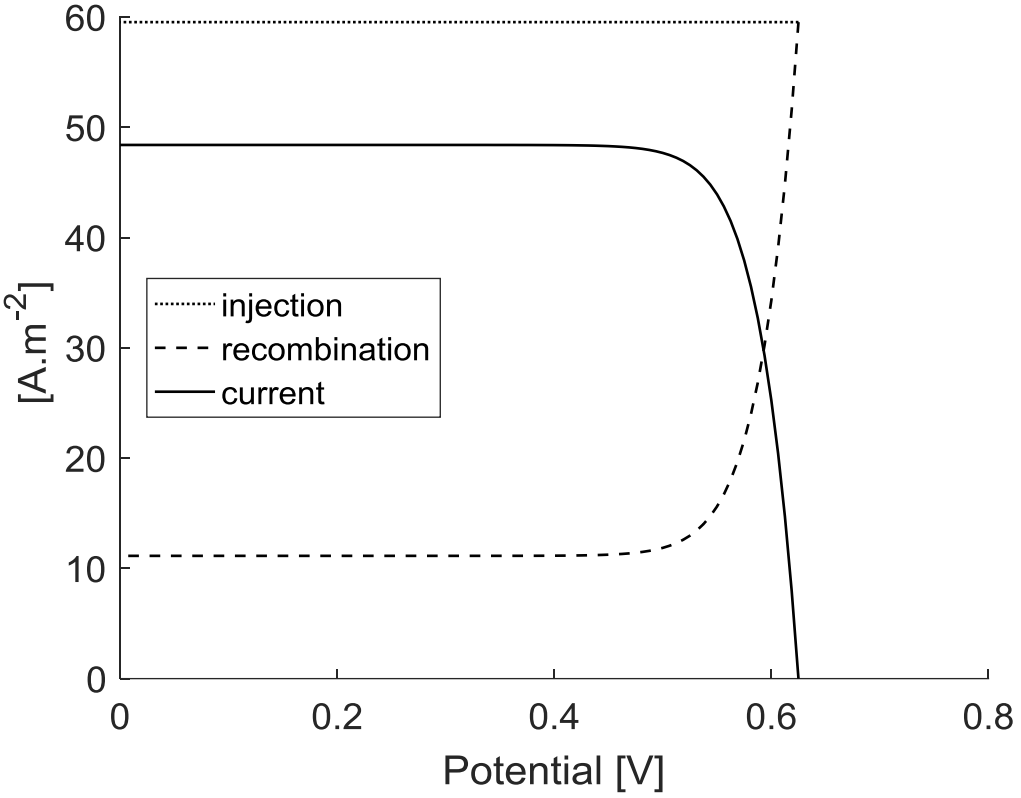

Figure 5.28: Plot showing how many electrons that are injected into the cell, how many which result in a current going out from the cell and how many which recombine, as a function of the potential over the cell. The figure is calculated for the N719-cell, with $d = 4$ µm.

5.2.3 Details on a cell made with AFB8-dye

All the figures in this section are calculated from the model, with the parameters for the AFB8-dye. These parameters are given in Table 5.2. Notice that the thickness parameter d is set to 10 µm. This is because of the IMPS-measurements in section 5.2.1 had a better fit for 10 µm, and because of the high uncertainty in the profilometer measurement of the thickness.

Figure 5.29 shows the modelled IV-characteristic for a AFB8-based DSSC which is 10 µm thick and with a reflective layer, and the experimental IV-characteristic. The modelled IV-characteristic has a higher fill factor than the experimental one, as was the case for the N719 based cell in Figure 5.12.

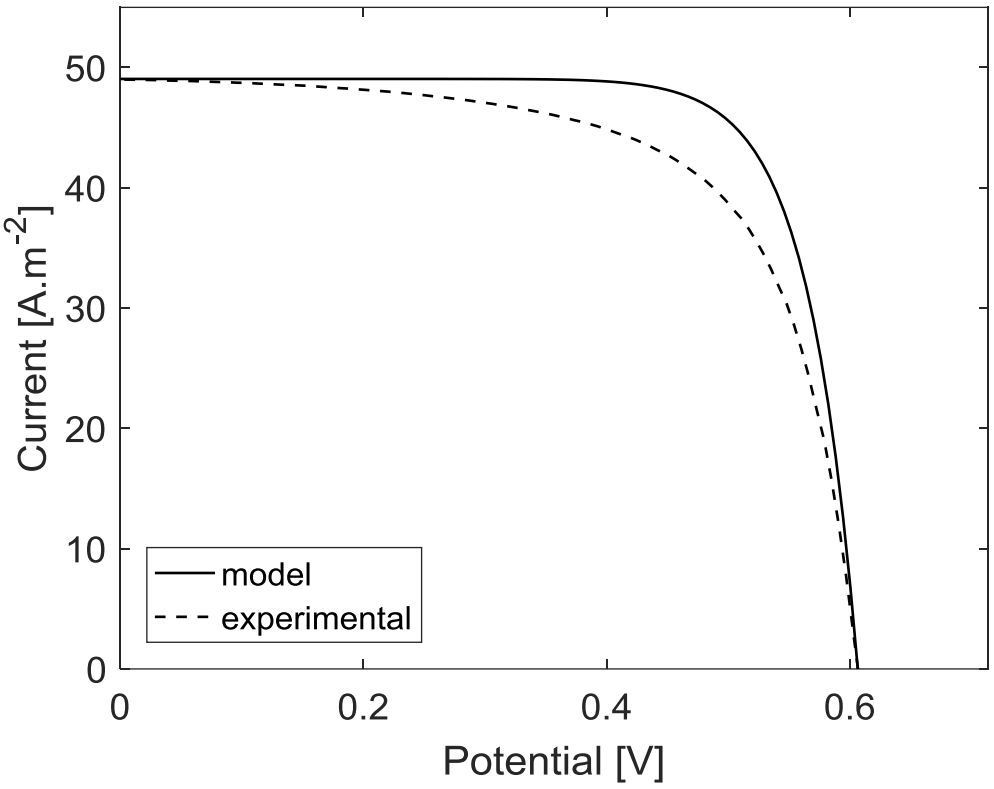

Figure 5.29: Plot showing the modelled and experimental current-potential characteristic of the DSSC made with AFB8.

Figure 5.30 shows the relative electron concentration as a function of x, for potentials ranging from short circuit to open circuit. The concentration profiles are significantly flatter than for the cases with the N719 based DSSC's, ref Figure 5.15 and Figure 5.23. It is only for the very lowest potentials that a gradient in the concentration profiles can be seen.

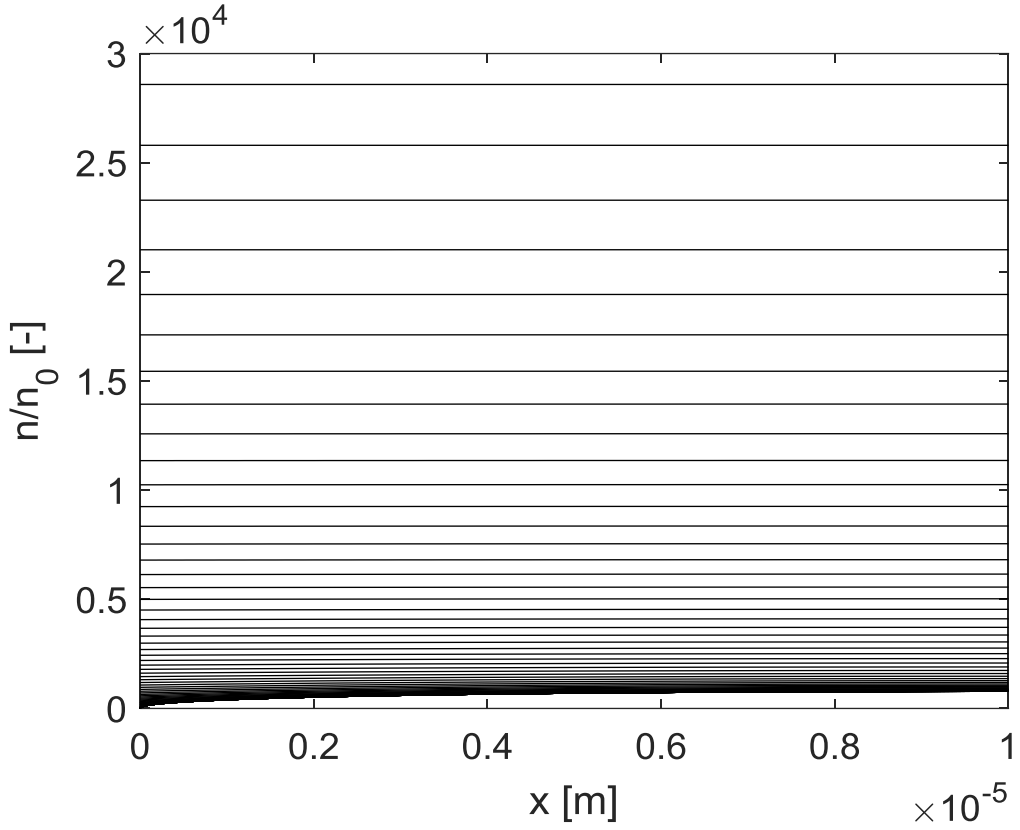

Figure 5.30: Plot showing the modelled relative electron concentration, n/n_0, as a function of x, for different potentials. The curve at the top equals n/n_0 during open circuit, while the curve closest to the x-axis equals n/n_0 during short circuit. The other curves are n/n_0 for potentials spread evenly from open circuit to short circuit. The figure is calculated for the DSSC made with AFB8-dye.

Figure 5.31 shows the amount of electrons which are injected into the titanium dioxide, as a function of x. The J_G term is the largest one, but the $J_G$extra also contributes. It is possible to see that the reflection efficiency is 50%, and that an increase in reflection efficiency could generate significantly more injected electrons.

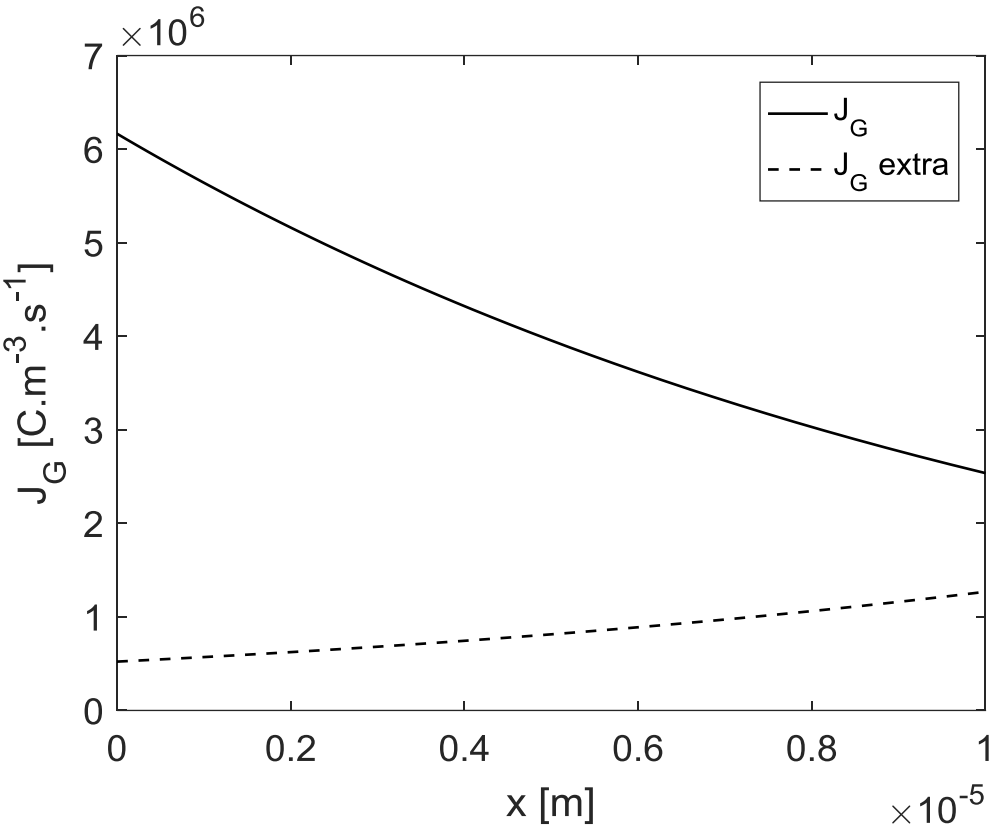

Figure 5.31: Plot showing the modelled generation term, J_G, as a function of x. J_G extra is the extra gain in J_G that results if η_{refl} is 0.5. The figure is calculated for the DSSC made with AFB8-dye.

Figure 5.32 shows the three main terms of the continuity equation, namely the generation term J_G, the recombination term J_R, and the diffusion term J_D. They are plotted as functions of x for the case of short circuit. The recombination term is so small that it barely can be seen, and it is hard to distinguish the diffusion term from the generation term. Practically all the injected electrons diffuse out from the titanium dioxide. This is in great contrast to the figures for the N719 based cell, shown in Figure 5.17 and Figure 5.25, where the recombination term is significant.

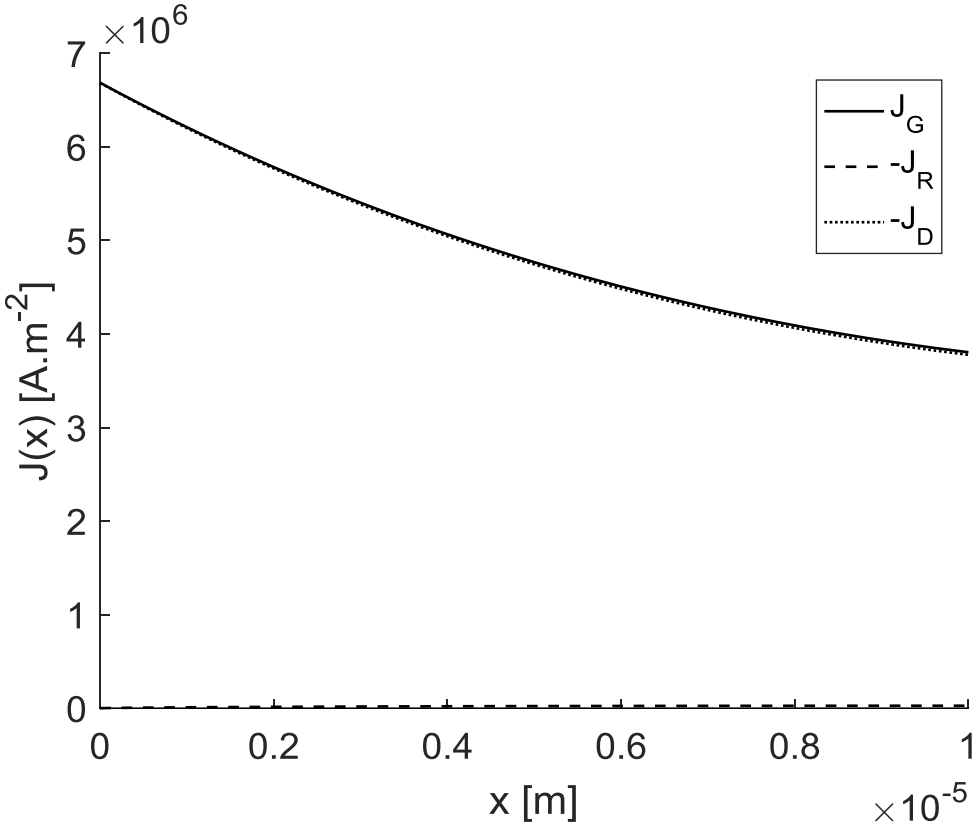

Figure 5.32: Plot showing the modelled generation term (J_G), recombination term (J_R) and diffusion term (J_G), as a function of x. The terms are modelled for short circuit. The figure is calculated for the DSSC made with AFB8-dye.

Figure 5.33 shows the generation term J_G, the recombination term J_R, and the diffusion term J_D, plotted as functions of x for the case of open circuit. The diffusion term and the generation term have nearly identical shapes, explaining why the concentration profile is flat in Figure 5.30. The flat concentration profile in Figure 5.30 also explains the flat recombination profile in Figure 5.33. Lastly, it can be noticed that Figure 5.33 and Figure 5.26 are very similar, and considerably different from Figure 5.18.

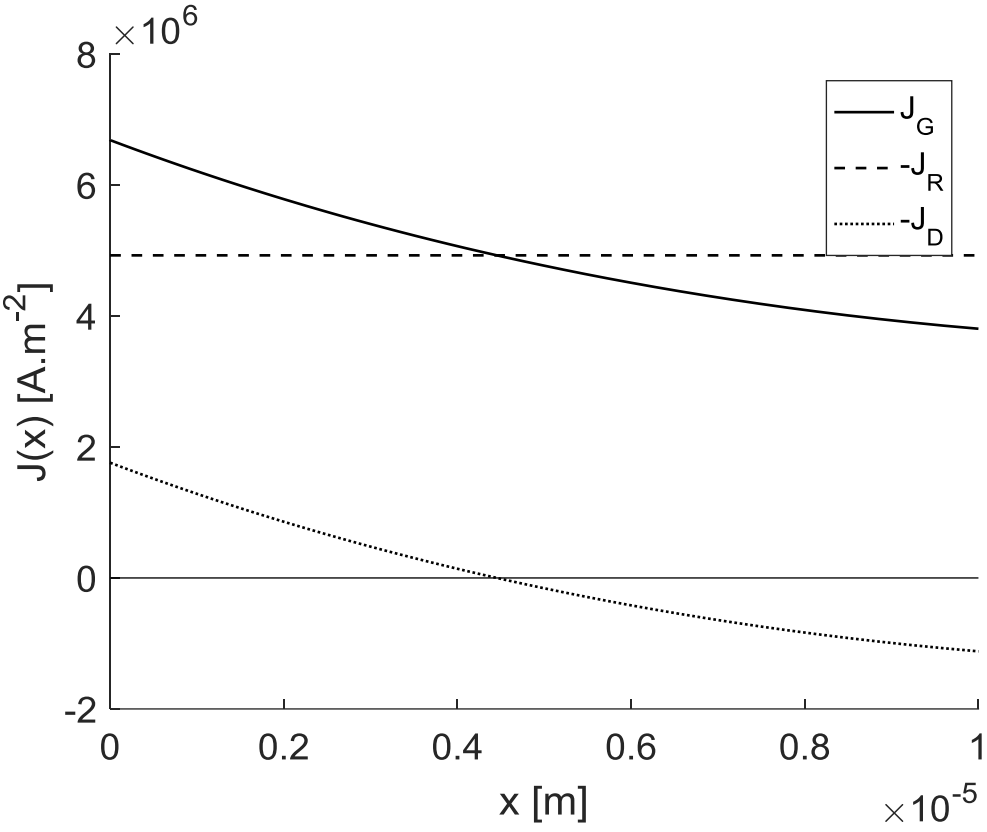

Figure 5.33: Plot showing the modelled generation term (J_G), recombination term (J_R) and diffusion term (J_G), as a function of x. The terms are modelled for the case of open circuit. The figure is calculated for the DSSC made with AFB8-dye.

Figure 5.34 shows how much of the incident light which has been absorbed and injected into the titanium dioxide for a given x. The profile is almost linear compared to Figure 5.18, and is quite similar to Figure 5.27. As expected, ~70% of the light is captured. This was as expected because the injection efficiency was set to 1, the IPCE was measured to 70%, and the previous figures in this section have shown that there is little recombination.

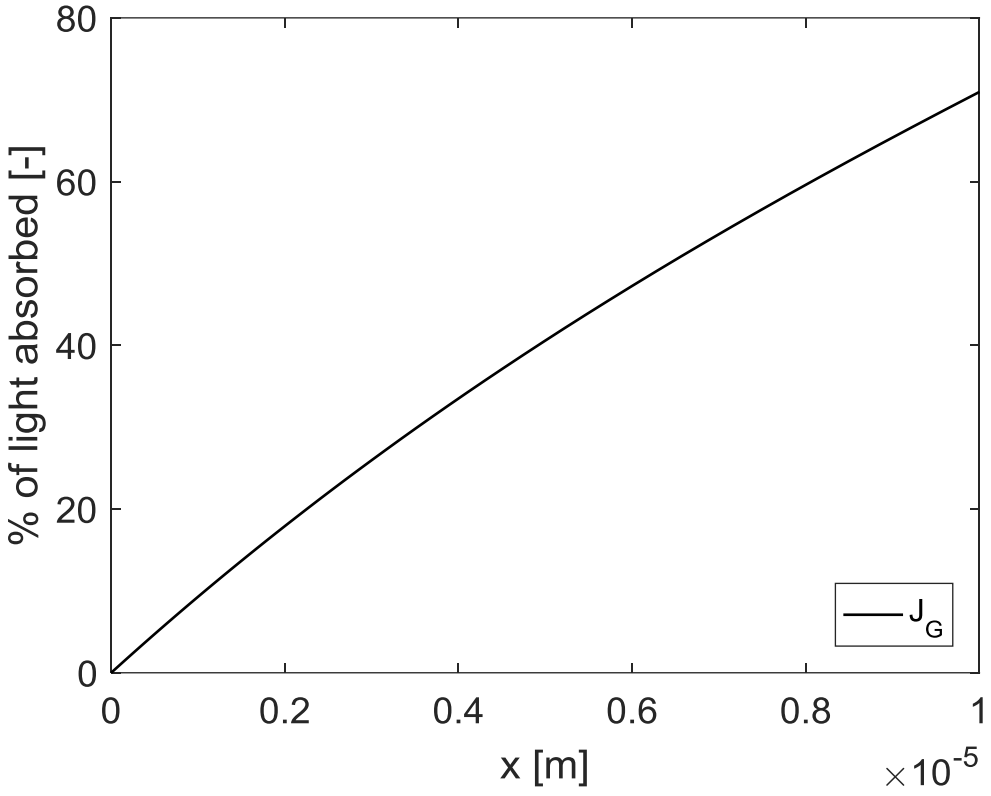

Figure 5.34: Plot showing how many percent of the incident light which has been absorbed at a given depth in the cell, given by x. The plot is calculated from the model for the DSSC made with AFB8-dye.

Figure 5.35 shows the total amount of electrons that recombine, are injected, and the current from the DSSC. There is practically no recombination for potentials below 0.4 V, in contrast to Figure 5.20 and Figure 5.28. All the electrons that are injected at short circuit results in a current.

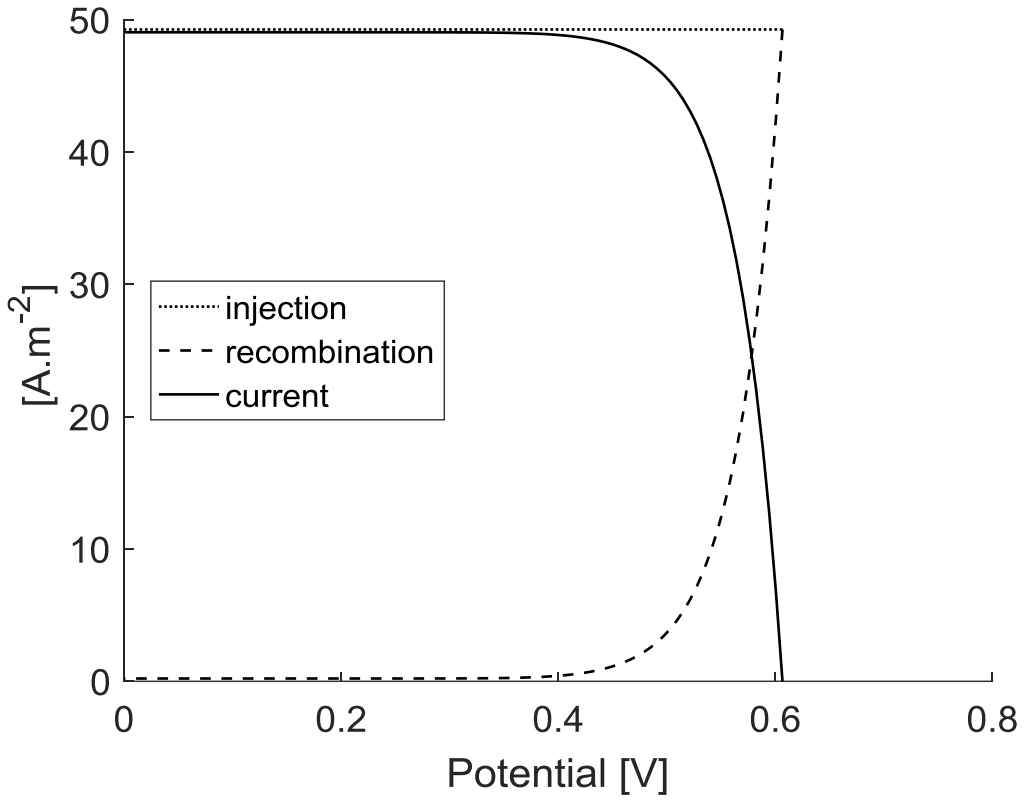

Figure 5.35: Plot showing how many electrons that are injected into the cell, how many which result in a current going out from the cell and how many which recombine as a function of the potential over the cell. The figure is calculated for the DSSC made with AFB8-dye.

Figure 5.36 shows the modelled power conversion efficiency as a function of d. The AFB8 DSSC will have an improved efficiency by increasing the thickness. The optimum thickness appears to be thicker than 35 µm according to the model. It can seem like the efficiency goes asymptotically towards about 15 % with increasing thickness.

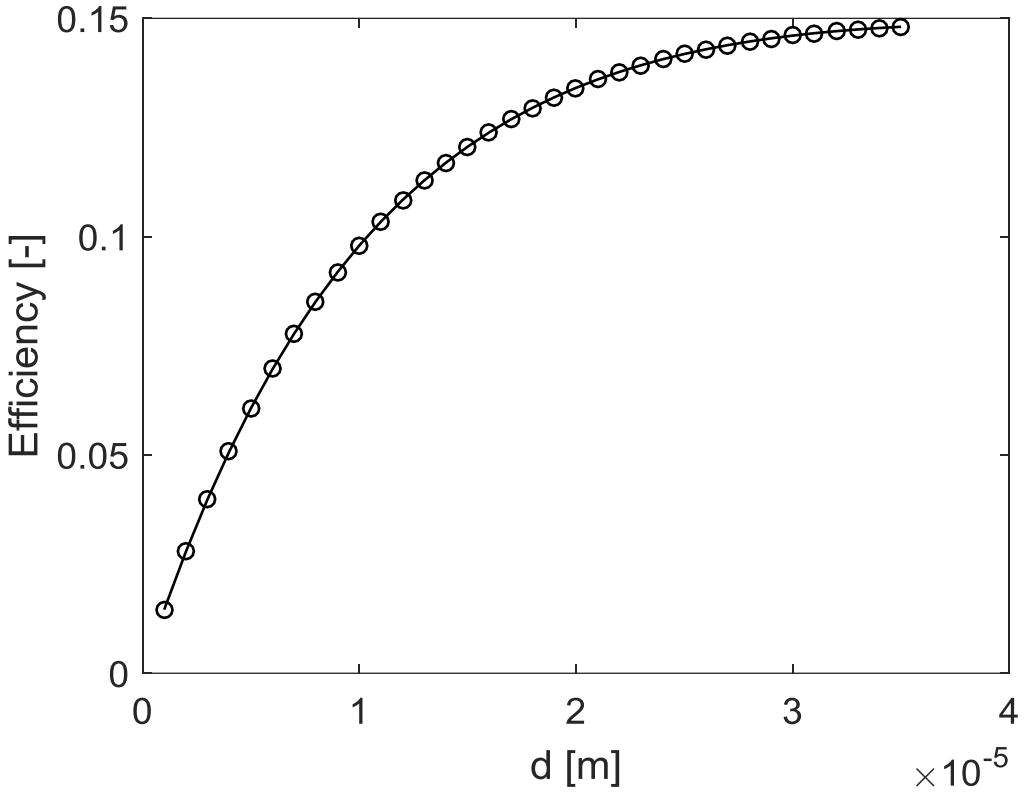

Figure 5.36: Plot showing the efficiency for a DSSC based on AFB8 as a function of the titanium dioxide layer thickness, for the case of η_{refl} 0.5.

5.2.4 Selected parameters' effect on the IV-characteristic

The effect on the IV-characteristic when the parameters k_0, D_0, α and β are varied is studied in this section. The model for both the AFB8-cell and the N719-cell is studied. The parameters are set as shown in Table 5.2.

Figure 5.37 shows the effect of varying k_0 by a factor of 100 in the model for the AFB8-cell. All other parameters were kept constant. Decreasing k_0 by a factor of 10 results in a considerably higher obtainable potential, but no change in the maximum obtainable current. Increasing k_0 by a factor of 10, results in a somewhat lower current, and a considerably lower potential.

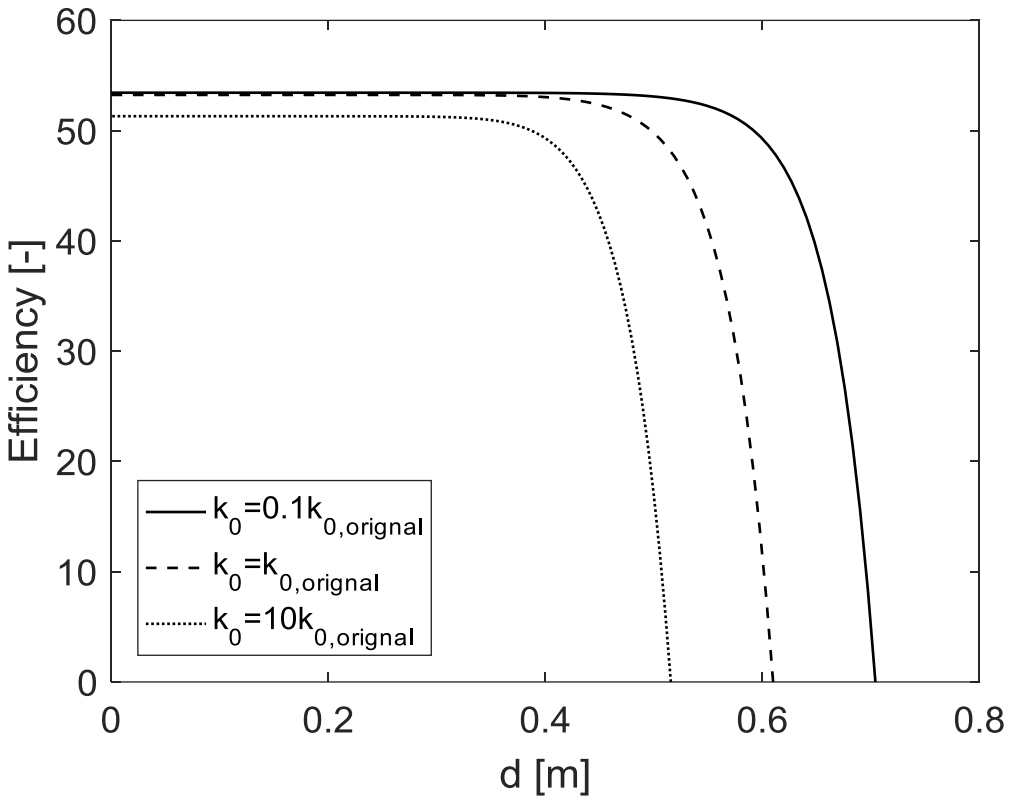

Figure 5.37: Plot showing the modelled IV-characteristic for a DSSC based on AFB8, for three different values for k_o.

Figure 5.38 shows the effect of varying D_0 by a factor of 100 in the model for the AFB8-cell. All other parameters were kept constant. Decreasing D_0 by a factor of 10 results in a barely noticeable decrease in the maximum current. Increasing D_0 by a factor of 10 has no visible effect.

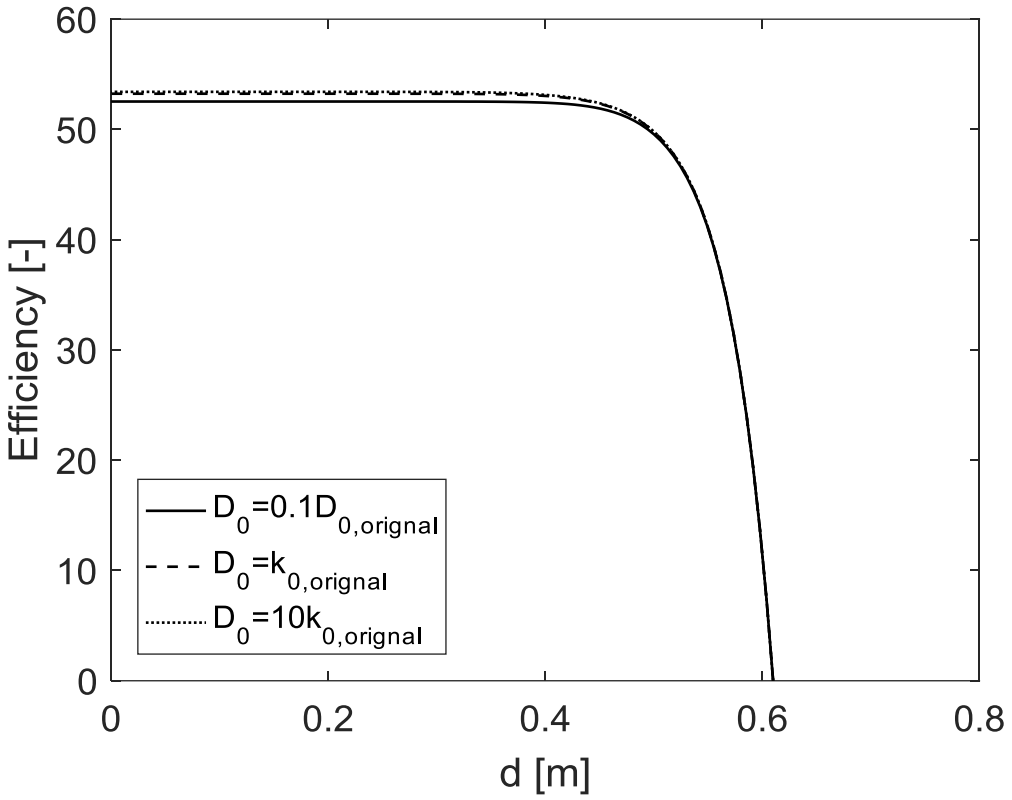

Figure 5.38: Plot showing the modelled IV-characteristic for a DSSC based on AFB8, for three different values for D_0.

Figure 5.39 shows the effect of varying k_0 by a factor of 100 in the model for the N719-cell. All other parameters were kept constant. Decreasing k_0 by a factor of 10 results in greatly increased current and potential. Increasing k_0 by a factor of 10, results in greatly reduced current and potential.

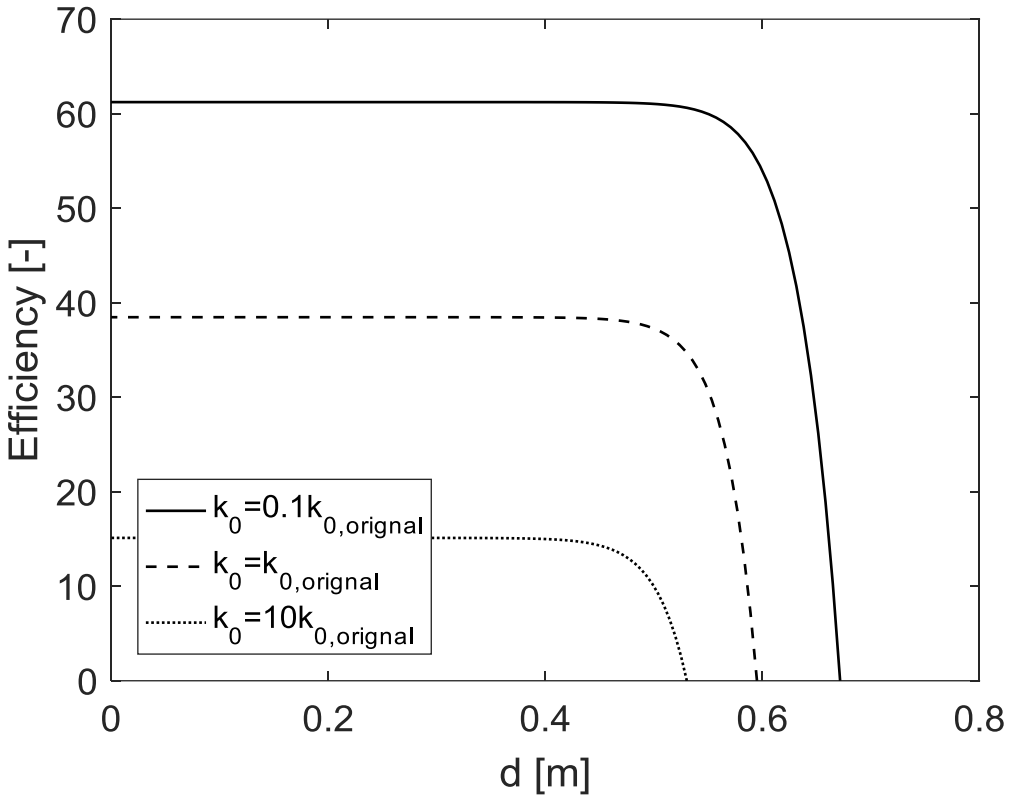

Figure 5.39: Plot showing the modelled IV-characteristic for a DSSC based on N719, for three different values for k_0.

Figure 5.40 shows the effect of varying D_0 by a factor of 100 in the model for the N719-cell. All other parameters were kept constant. Decreasing D_0 by a factor of 10 results in a slight increase in potential, and a large decrease in current. Increasing D_0 by a factor of 10 gives a slight decrease in potential, and a large increase in current.

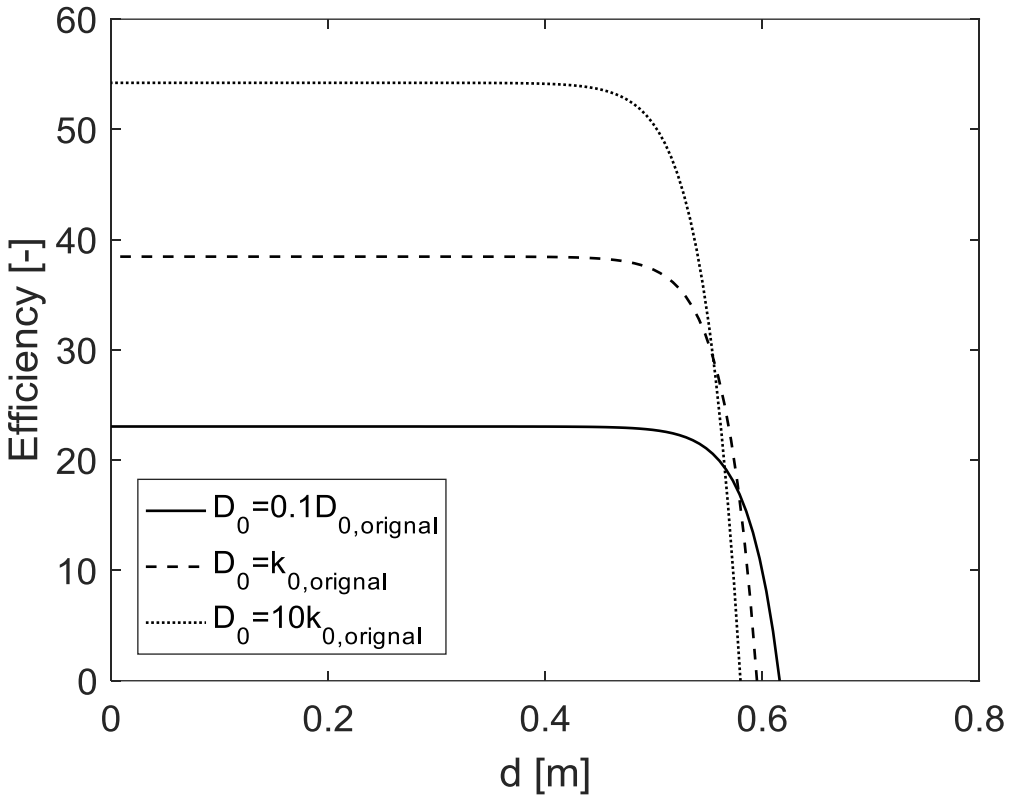

Figure 5.40: Plot showing the modelled IV-characteristic for a DSSC based on N719, for three different values for D_0.

Figure 5.41 shows the experimental IV-characteristic, the default model, and the model where β has been varied from 0.33 to 0.75. The parameters ϵ, n_0, k_0 and D_0 were adjusted anew as described in section 3.4.2.3. Decreasing β decreased the fill factor, but not in such a way that the experimental curve and the modelled curve ended up overlapping. The model became unstable if β was set larger than 0.75 or lower than 0.33.

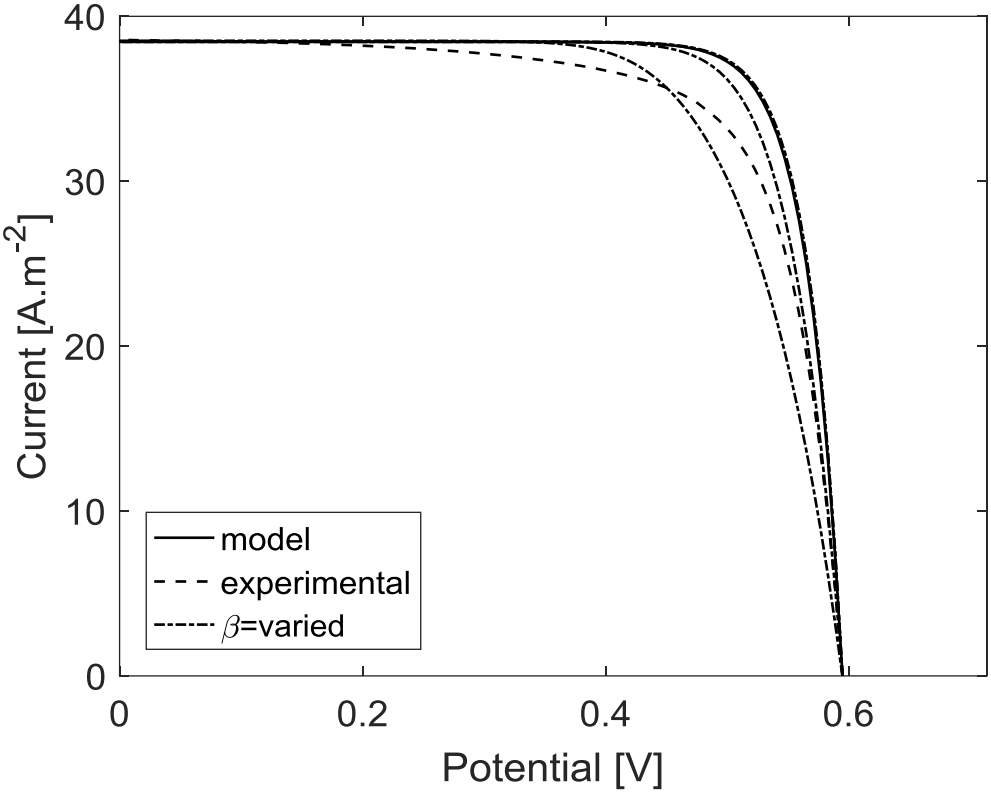

Figure 5.41: Plot showing the modelled IV-characteristic for a DSSC based on N719, for four different values of β. The values used for β were 0.33, 0.5, 0.75, in addition to the original value of 0.63. The curves for β = 0.33 and 0.5 can be seen to the left of the original model, with 0.33 being to furthest to the left. The value of 0.74 can hardly be distinguished from the original model.

α was also varied slightly, in the same way as β. However, it did not influence the shape of the IV-characteristic, and the figure is therefore omitted.

6 Discussion

6.1 Extension of model to include small amplitude perturbation

This section discusses whether the extension of the diffusion model to include small amplitude perturbation was successful or not. Both experimental and modelled results are discussed to do so.

6.1.1 Experimental and modelled small amplitude perturbation

This sub-section discusses how the modelled IMPS and IMVS spectra compare to the experimental IMVS and IMPS spectra.

Both the modelled IMPS spectrum and the modelled IMVS spectrum fit well with experimental data for the N719-cell, but the IMVS spectrum has the best fit, ref Figure 5.7 and Figure 5.10. Both spectra fit better when the titanium dioxide thickness d is reduced to 10 μm, ref Figure 5.8 and Figure 5.11. The IMVS spectrum becomes slightly narrower with the reduction of d, while the IMPS spectrum broadens and has a change of shape at its lower part, as can be seen in Figure 5.9. The model manages to reproduce the non-symmetrical shape of the experimental IMPS spectrum, except for at the highest frequencies. The mismatch at the highest frequencies is however attributed to experimental error, since positive IMPS response has not been reported in the literature earlier as far as the author knows.

The modelled IMPS spectra fit better with 10 μm than with 15 μm, but still not excellently. This might be due to simplifications in the model, or it could be because neither 10 nor 15 μm is the correct value for the thickness parameter. It is however hard to know which of these reasons is the correct one. One way to determine whether it is the model or the thickness, would be to perform profilometer measurements with a higher accuracy. The accuracy of the thickness measurement used in this work is too low to conclude why the fit is not better, when the measured thickness of 15 μm has an uncertainty giving a lower bound at 10 μm. Another way to determine whether it is the simplifications in the model or the uncertain thickness that cause the non-perfect fit, would be to calculate the IMPS-spectrum for all relevant values of d. It would then be possible to see whether any of the spectra give a very good fit.

Calculating IMPS-spectra for many values of d might also prove to be an indirect way of estimating d. If the spectra for the different values of d are distinct in shape, and only one matches the experimental spectrum, then that would give an indication of what the value of d is. Figure 5.7, Figure 5.8 and Figure 5.9 show that the shape of IMPS-spectra have a large dependency on d, suggesting that the shape might be used as a "fingerprint" to find the correct d. Calculating the IMPS-spectrum for a given value of d does however demand a complete fitting of all the parameters. This is a time consuming process, and was therefore only done with 10 μm and 15 μm. The process in Figure 3.1 would need to automated before it would be practical to use the model to determine d.

The parameter η_{refl} was unknown, and was a potential source of uncertainty. It was briefly investigated, as mentioned at the end of section 5.2.1.2. Varying η_{refl} had practically no

effect on neither the modelled IMVS nor the modelled IMPS spectrum for the N719-cell. This can be explained from considering Figure 5.16. Figure 5.16 shows that practically all the light is absorbed on its way through the titanium dioxide layer, and putting on a reflective layer will have minimal effect, because there is a minimal amount of light that can be reflected.

On the AFB8-cell however, based on brief measurements, varying η_{refl} had the same effect as varying Φ_{ss} or ϵ. The minimum of the IMPS and IMVS spectrum was moved horizontally to higher frequencies when η_{refl} was increased. This was as expected, since Figure 5.31 shows that an increase in η_{refl} will increase the generation term. These details on η_{refl} are unfortunately not prioritized in this thesis. What is worth noticing about η_{refl} is however that it did not influence the shape nor the width of the IMPS and IMVS-spectra. This is important, as that it increases the likelihood that the shape of the spectra can be used to determine d. If both η_{refl} and d were unknown, and both influenced the shape of the spectra, then it would be a chance that several combinations of η_{refl} and d that could give the same shape. When only d influences the shape however, then there is a much higher chance that a certain value of d can be linked to a certain shape of the spectra, so that d can be determined. η_{refl} on the other hand, seems hard to separate from ϵ, because they have same effect on all the experimental data presented in this thesis.

All in all, the model seems capable of reproducing experimental IMVS and IMPS spectra. This supports that the extension of the model presented by Anta et al. to include small amplitude perturbation was successful. The slight mismatch between experimental and modelled IMPS-spectra may be due to the large uncertainty in the thickness parameter d. The shape and width of the IMPS-spectrum showed an interesting and somewhat unexpected dependency on d. This dependency might be possible to utilize to determine the value of d from IMPS. This would however demand a faster way of fitting the model to the parameters, and more experimental data would be needed to investigate it further.

6.1.2 Electrochemical impedance spectroscopy

The EIS-measurements gave half-ellipse curves instead of the expected half-circle curves, when Z_{Im} was plotted versus Z_{Re}, as can be seen in Figure 5.4. This is however a common aberration, and it was ignored. The recombination resistance was determined from the maximum value of Z_{Im}, as if the curve had been a half circle[29]. The elliptical shape suggests that the theory which is used is incomplete or too simplified to describe the DSSC. The error which is gained from this is assumed to be tolerable.

The values for α and β that were calculated for the N719 and AFB8-based cells, ended up being identical to two digits, ref Table 5.2. This might be due to the relatively low resolution used in the experimental measurement, as can be seen in Figure 5.4. The lower the resolution, the higher can the difference in two cells be, while still ending up having their maximum value at the same frequency. This might have caused the two different cells to be measured with more similar values than what they actually have. This also suggests that the uncertainty in the measured α and β can be significant.

6.1.3 Current-potential characteristics

This sub-section discusses how well the model compares to the experimental current-potential characteristic for the DSSC based on N719.

The modelled IV-characteristic fits well with the experimental IV-characteristic, as evident from Figure 5.12. The model has a fill factor that is a little too high, but this can to a good extent be corrected by introduction of a shunt resistance and a series resistance, ref Figure 5.13. The fit is still not perfect however. This can in part be because the fill factor and shunt resistance was used to correct the model, instead of being part of the model. A proper implementation of the resistances into the model, would yield slightly different corrections than simply subtracting the potential loss and current loss as described in section 3.5. The series and shunt resistance should preferably be determined experimentally as well, and not simply left as open parameters as was the case for the correction. Further, as discussed in section 6.1.2, there are some uncertainties in the experimental basis for α and β. As seen in Figure 5.41, an uncertainty in β implies an uncertainty in the fill factor as well. Lastly, there is also an extra uncertainty in both k_0 and D_0, especially due to the uncertainty in d. This is because the value of d influences the value the k_0 and D_0 end up with when a complete fit with all the parameters is performed. And both k_0 and D_0 can influence the fill factor. Thus, a better experimental foundation for β and d, together with proper introduction of shunt and series resistance might give a better fit between experimental and modelled IV-characteristics.

It is assumed that the uncertainties in the measurements of d, α and β are considerably larger than the other experimental uncertainties. It is hard to quantify how large the uncertainties of d, α and β are. Therefore, the validation of the model in this thesis is built on the fact that it can reproduce the IV-characteristic and the IMPS and IMVS spectra to a large degree. The validity of the model is further increased by the fact that it does a decent job at predicting light intensities lower than 193 $\mathrm{W.m^{-2}}$, as evident from Figure 5.14. However, further validation could be obtained by performing EIS with higher resolution, and measuring d more accurately, and see whether the model fits the experimental data better.

6.2 Characterization, comparison, and optimization

6.2.1 N719-dye

This sub-section discusses how the model can be used to characterize and optimize the DSSC made with N719. The connection between the recombination, the absorption, the electron concentration, and the thickness of the titanium dioxide is examined to do so.

6.2.1.1 Power conversion efficiency

The cell made with N719 would be more efficient if it had a thinner titanium dioxide layer, according to Figure 5.21. Several other figures must be examined, to understand why it is so. First, Figure 5.15 shows that the electron concentration profile is unfavorable. Whether the gradient of the profile is positive or negative determines which way the electrons diffuse. In an ideal cell, there would be no recombination, and every electron would have to diffuse towards the TCO. This implies that the gradient would be positive over the whole system, leading all electrons to the TCO. The concentration profiles in Figure 5.15 on the other hand,

contain both negative and positive gradients. The concentration profile has a peak value somewhere between $x = 0$ and $x = d$, and all the electrons which are injected to the right of this peak will experience a gradient which makes them diffuse away from the TCO, and they will thus not be collected. Thus, it can be suspected that the N719 cell has considerable room for improvement, already from judging the concentration profile.

The N719-cell has a strikingly different concentration profile when its thickness is reduced to 4 μm, ref Figure 5.23. The gradient is approximately zero for the highest potentials, and positive for the rest. This implies that all the electrons which are injected into the 4 μm cell will diffuse towards the TCO to be collected. There is still a chance though that the electron will recombine during the timespan it takes to diffuse to the TCO and be collected. However, it is guaranteed that the electron will end up recombining if it diffuses away from the TCO.

Figure 5.20 and Figure 5.28 shows that for potentials up to 0.5 V there is less than half as much recombination for the cell with 4 μm thick titanium dioxide, compared to the cell with 15 μm thick titanium dioxide. However, the figures also show that the generation rate reduces from about 70 $\mathrm{A.m^{-2}}$ to 60 $\mathrm{A.m^{-2}}$. This illustrates the tradeoff between the absorption and the recombination. A thicker layer of dye-coated titanium dioxide will absorb more light, but it will also have increased recombination. Figure 5.17 illustrates this further for the N719 cell. The generation and recombination term equal each other at $x = 7$ μm. For $x > 7$ μm, the recombination term is larger than the generation term. In other words, the amount of electrons which is injected at the backmost half of the cell, is smaller than the amount that recombines. This would suggest that the optimal thickness would be 7 μm, by keeping the part of the cell where the generation term is larger than the recombination term. However, it is not quite that simple. Both the recombination term and generation term depends on the thickness d, and Figure 5.17 is only valid for open circuit.

The only way which was considered good enough to find the optimal thickness, was to calculate the IV-characteristic for several values of d. The power conversion efficiency was then calculated for each d from the potential and current giving the largest power in the IV-characteristic. The result can be seen in Figure 5.21 for the cell made with N719. The optimum thickness is 6 and 4 μm for the case with 0% reflection and 75% reflection respectively, in both cases considerably less than the 15 μm which was used under manufacture. The optimum thickness is as expected shorter for the case with reflection, than for the case without reflection. A titanium dioxide layer with reflection can be thinner than a layer without reflection and still capture the same amount of light. And as already explained, a shorter layer will have less recombination, thus giving the highest power conversion efficiency. Too short a titanium dioxide layer will however capture too little of the light, and give a very low efficiency. All in all, there are strong indications that the N719-cell would gain higher efficiency with smaller d, though it is hard to tell how small the optimum thickness d would be, as long as the reflection efficiency is unknown.

6.2.1.2 Other efficiencies and the effect of k_0 and D_0

The power conversion efficiency is perhaps the most important parameter for a DSSC. However, three other important efficiencies are the charge collection efficiency, the injection

efficiency, and the absorption efficiency, which combined make up the IPCE, ref equation (1). The IPCE of the N719-cell was measured to 55%, ref Table 5.1. The charge collection efficiency that is calculated by the model is only 57%, due to the high recombination. It follows from equation (1) that the product of the injection efficiency and the absorbance efficiency must be 96%. This suggests that the assumption of the injection efficiency being 100% is good. It also means that the cell cannot have significant benefit from increased thickness, since it already absorbs at least 96% of the incoming light, which indeed is what the model predicts.

Figure 5.39 and Figure 5.40 shows that the DSSC made with N719 will benefit from both slower recombination and quicker diffusion, respectively. This is as expected. There are significant recombination problems with the cell, leading to large current losses. Providing a quicker diffusion through a higher D_0, lowers the average time it takes for an electron to diffuse to the TCO, as explained in section 2.3. And the less time an electron spends in the titanium dioxide, the less is the chance for recombination. This reduced recombination results in the cell providing considerably higher current, ref Figure 5.40. However, there is a slight decrease in the maximum potential. This can be understood from looking at Figure 5.15. The potential is measured at the junction between the TCO and the titanium dioxide, namely at $x = 0$. This is also were the electron concentration is highest in the cell. There is a build up of electrons at the junction due to the slow diffusion, and the fact that the generation term is largest at $x = 0$, ref Figure 5.16. This build up will flatten out when the diffusion is increased, thus lowering the measured potential slightly. The average potential in the titanum dioxide may be the same though, it is only the measured potential at the junction which is lowered. This lowering of potential is far smaller than the increase in current due to reduced recombiantion.

Slowing down the recombination increases both the potential and the current significantly, as evident from Figure 5.39. The increased current from slower recombination, can be explained the same way as the increased current from quicker diffusion. The average timespan an electron can "live" in the titanium dioxide increases when k_0 is lowered. Thus, more electrons get enough time to diffuse to the TCO, increasing the charge capture efficiency and the current. Lowering k_0 increases the potential also, ref Figure 5.39. This can be explained from equation (16) and (17). The recombination must equal the diffusion and generation for a given current in the IV-characteristic. And the lower the k_0, the higher the electron concentration n must be. The electron concentration which is in equilibrium with diffusion and generation increases with decreasing k_0, leading to higher potential, ref equation (10).

Overall, the most important finding is that the cell made with N719 has a problem with low charge capture efficiency. Alternatively, it can be said that it has a too high fraction of electrons recombining. The simplest way to reduce this problem would be to reduce the thickness parameter d, as suggested by several figures drawn from the model. Another way to reduce the problem would be to lower k_0 or increase D_0, though this is not done as easily as changing the thickness.

The assumption that the injection efficiency is 100% is considered good, because the measured IPCE and calculated charge capture efficiency implies that the injection efficiency must be at least 97%. There was a high uncertainty in the measured thickness of the titanium dioxide layer d. From section 4.1 it was suggested that the value for d might in fact be as low as 10 μm. The predicted optimum thickness in Figure 5.21 might have been different if the figure had been calculated with a smaller d. This uncertainty comes in addition to the uncertainty due to the reflection efficiency being unknown. The optimum thickness for the cell is thus hard to accurately determine, except for that it should be shorter than in its current state. A more accurately determined d could increase the usefulness of the model. However, experimental data from several cells made with different thicknesses would be the only way to know whether the model works at predicting efficiencies.

6.2.2 AFB8-dye

The AFB8 cell exhibits a strikingly different behavior than the N719-cell. Figure 5.30 shows that the electron concentration profile is flat for almost all potentials, indicating a very quick diffusion. The recombination is negligible, except for the highest potentials, ref Figure 5.35. This is as expected, because the IMPS spectrum has its minimum at a considerably higher frequency than the IMVS spectrum, as summarized in Table 5.1. A minimum at a high frequency, suggests that it is a fast process. And the amount of electrons that recombine will be low when the diffusion is much faster than the recombination process, as discussed in section 2.3. The low recombination rate also helps explain the high IPCE of 70%, ref Table 5.1. Practically no recombination at short circuit means that the charge collection efficiency must be ~100%. The product of the injection efficiency and the absorption efficiency must then equal the IPCE, as a consequence of equation (1). This sets the lower limit for the injection efficiency and recombination efficiency at 70%. It has not been found a way in this work to determine whether it is insufficient absorption, insufficient injection or both that results in the 30% loss in the IPCE. It could be assumed that the absorption efficiency should be approximately 100%, because the absorption measurement shows that AFB8 has a stronger absorption than N719, ref Figure 5.1. And since it was shown that N719's absorption efficiency was 97% or higher in the previous section, it follows that AFB8 should have a higher absorption efficiency than 100%. This is however not a valid way to estimate the absorption efficiency of the cell with AFB8. A dye needs both to absorb light well, and adsorb well onto the titanium dioxide. Thus, it is impossible to know whether it is the injection efficiency or the adsorption/absorption properties that needs to be improved. It can however be asked whether a very large difference in adsorption might explain the very unexpected result that the diffusion coefficients were a factor 10^4 different, ref Table 5.2. But this amounts to nothing more than speculation, and will not be discussed further.

The efficiency as a function of titanium dioxide thickness d was computed for the AFB8 cell in the same way as for the N719 cell. The assumption of 100% injection efficiency was used, and the result is given in Figure 5.36. It shows that the AFB8 cell benefits from increased thickness, in contrast to the N719 cell in Figure 5.21. This suggests that the benefit from increased absorption with increasing d outweighs increased recombination. The efficiency seems to flatten out. This could be explained from assuming that the AFB8 cell's absorption

goes towards 100% in the same way as the N719 cell did in Figure 5.19. It is also worth noticing that there is no optimal thickness for the range of thicknesses in figure Figure 5.36. An explanation could be that the diffusion is so quick, that even though the recombination is increased with increasing d, it still amounts to practically nothing.

Figure 5.38 further supports that the diffusion is indeed quicker than what is strictly necessary to avoid recombination. It can barely be seen in the IV-characteristic when D_0 is lowered by a factor of 10. Increasing D_0 by a factor 10 does not give any noticeable difference in the IV-characteristic, further suggesting that quick diffusion is only beneficial up to a certain point. Lowering k_0 a factor 10 gives a slightly lower current, suggesting some recombination, while increasing k_0 a factor 10 has no effect on the current. The potential is however widely dependent on k_0, presumably for the same reasons as discussed in the end of section 6.2.1.

All in all, it seems clear that the cell made with AFB8-dye has an excellent charge collection efficiency. The model predicts that the charge collection efficiency is so good, that there will be no recombination penalty from increasing the thickness. It can however be a gain from increased absorption, if the thickness is increased. This is however uncertain, since it is unclear how good the injection efficiency is. The measured IPCE is high at 70%, and the increase in efficiency from increased absorption is therefore limited to go from 70% to 100%. The model predicts that the thicker the titanium dioxide, the closer to 100% absorption efficiency is achieved. However, a very thick titanium dioxide layer might start to make the potential losses in the electrolyte substantial. As with the N719-cell, it would be very useful to have AFB8 cells made with varying thickness. From this it would be possible to gain more information as to whether it is the injection efficiency or the absorption efficiency that limits the performance. It might also make it possible to estimate η_{refl}, if Figure 5.36 had an experimental counterpart which could be used to adjust η_{refl}.

6.3 The absorbance and the incident photon to electron conversion efficiency

There is a discrepancy between the IPCE in Figure 5.2 and the IPCE calculated from the short circuit current in Figure 5.3. The IPCE for N719 is only 20% according to Figure 5.2, while it is 55% based on the IV-characteristic in Figure 5.3. The value for the IPCE for the N719-cell is reported to be approximately 55% in [28], suggesting that the values in Figure 5.2 are misleading or wrong. One reason for this could be that the IPCE might have been recorded with very low light intensities, and that the IPCE is considerably lower for such low intensities. However, this cannot be known, since it was impossible to access the intensity used for the IPCE measurement.

The absorbance measurement and the IPCE have different profiles, ref Figure 5.1 and Figure 5.2. If it is assumed that the IPCE measurement can be trusted, then this suggests that the charge collection efficiency or injection efficiency is dependent on the wavelength in ways that are not treated in this work.

The N719-cell was calculated to have approximately 100% absorption, even though Figure 5.1 shows that the 453 nm is a wavelength where N719-dye has a relatively poor absorption. This would suggest that the N719-cells' titanium dioxide layer could be made even thinner

than suggested previously, if it is to be optimized for wavelengths were the dye has a larger absorption. This is because the higher absorption the dye has, the less dye is needed, and a smaller d implies less dye. It would be the opposite with the AFB8-dye, since it has a relatively high absorption at 453 nm. This means that if the absorption efficiency is poor at 453, then it would be even more critical with a thicker titanium dioxide layer to enhance absorption at other wavelengths. Thus, Figure 5.1 suggests that the necessity of decreased thickness for the N719-cell and increased thickness for the AFB8-cell might be even more beneficial than suggested in section 6.2.1 and 6.2.2, if the cells are to be used for other wavelengths than 453 nm.

The quantitative optimization presented in section 6.2.1 and 6.2.2 is thus not necessarily valid if the DSSC is to be optimized for the solar spectrum, which contains significant energy over the whole visible spectrum. The simplest way to optimize a DSSC for the solar spectrum would be to use illumination with the solar spectrum when conducting the measurements. Another way would be to measure the DSSC's several times with different wavelengths of monochromatic light.

7 Conclusion

Anta et al.'s numerical version of the diffusion model was successfully implemented for steady state and extended to small amplitude perturbations. It reproduced the experimental IV-characteristics well, but had a somewhat lower fill factor. This was mostly contributed to the lack of series resistance and shunt resistance in the model, but may also be due to somewhat low accuracy in the EIS-measurements and the measurement of the titanium dioxide layer's thickness. The modelled and experimental IMVS spectra fitted excellently, while the IMPS spectra had a good fit. The non-excellent fit of the IMPS spectra was attributed to uncertainties in the measurement of the titanium dioxide layer's thickness.

The interpretation of the model gave useful information, ref Figure 1.1. The DSSC made with the ruthenium dye N719 had a low charge collection efficiency at 57% at short circuit, while the injection and absorption efficiencies were 97% or greater. This contrasted to the DSSC made with the ruthenium-free dye AFB8, which had a 100% charge collection efficiency at short circuit. The superior charge collection efficiency of the AFB8-cell was attributed to its superior diffusion properties over the N719-cell. The AFB8-cell did however have inferior absorption efficiency and/or injection efficiency. It was determined that the product of the efficiencies was 70%, but it was not possible to determine how much each of the efficiencies contributed to the loss.

The model did also suggest ways for which the DSSC's could be optimized, ref Figure 1.1. The cell made with N719 would benefit from decreased titanium dioxide layer thickness. It would also benefit from increased diffusion coefficient (D_0) in the form of increased current, and benefit from lower recombination coefficient (k_0) in the form of both increased current and potential. The cell made with AFB8 might benefit from increased titanium dioxide layer thickness, in contrast to the N719-cell. The AFB8-cell would not benefit from increased diffusion coefficient, but it would benefit from lower recombination coefficient in the form of increased potential. The model would be able to give more precise predictions for both cells if experimental data for cells with varying thickness had been accessible.

All in all, the model shows great promise. It reproduces experimental results well, and provides useful information on how the DSSC's behave differently, and how they might be optimized.

8 Further work

Suggestions for further work, both with the model and with the experimental techniques, is summarized below:

-The model would be both more useful and practical if the fitting of IMVS and IMPS spectra was done automatically. Automatic fitting would enable to investigate the model further, and perhaps enable determination of d without profilometer. And of course, it would be very time saving.

-The model could quite easily be modified to include shunt resistance and series resistance. This could especially be useful if experimental techniques are used to determine what the resistances are.

-The model could also be modified to include a potential dependent injection efficiency. This would however introduce a free parameter, or the problem of finding a way to determine how the potential dependency is.

-The model could be expanded to include specific losses at the cathode and in the electrolyte.

-The model does only work for small amplitude perturbation, due to the simplification which was done from equation (45) to (46). It would be interesting to solve the same equations without the approximation, and see whether the model can be used to simulate large amplitude perturbation.

-It would be interesting to compare the presented model versus the analytical models in [20] and [27].

-The EIS-measurements should be done with significantly higher resolution, to further investigate whether the α and β parameters are as similar for the two different dyes as it seems.

-The profilometer measurements should be done with a much higher accuracy. This would be of great help in further validation of the model.

-The work in this thesis should be tried on several identical DSSC's, to confirm reproducibility of the results.

-The model could be further validated if cells made with different thicknesses were investigated. This might also lead the model to give information on the reflection efficiency, the injection efficiency or the absorption efficiency.

-The IMPS-spectrums dependency on the thickness parameter d should be further investigated, both experimentally and with modelling.

-The model was only tested with blue light with relatively low intensity. The measurements would be more valuable if the same measurements were done with a solar simulator as a light source.

-And last, but not least, should the very interesting result that the diffusion coefficients were so different be investigated further.

References

1. Anta, J.A., et al., *A continuity equation for the simulation of the current-voltage curve and the time-dependent properties of dye-sensitized solar cells.* Physical Chemistry Chemical Physics, 2012. **14**(29): p. 10285-10299.
2. *Paris Agreement*. 2016; Available from: http://unfccc.int/resource/docs/2015/cop21/eng/l09r01.pdf.
3. Hasan, M.A. and K. Sumathy, *Photovoltaic thermal module concepts and their performance analysis: A review.* Renewable & Sustainable Energy Reviews, 2010. **14**(7): p. 1845-1859.
4. Gong, J.W., J. Liang, and K. Sumathy, *Review on dye-sensitized solar cells (DSSCs): Fundamental concepts and novel materials.* Renewable & Sustainable Energy Reviews, 2012. **16**(8): p. 5848-5860.
5. Ondersma, J.W. and T.W. Hamann, *Recombination and redox couples in dye-sensitized solar cells.* Coordination Chemistry Reviews, 2013. **257**(9-10): p. 1533-1543.
6. Hagfeldt, A., et al., *Dye-Sensitized Solar Cells.* Chemical Reviews, 2010. **110**(11): p. 6595-6663.
7. Shalini, S., et al., *Status and outlook of sensitizers/dyes used in dye sensitized solar cells (DSSC): a review.* International Journal of Energy Research, 2016. **40**(10): p. 1303-1320.
8. Sulaeman, U. and A.Z. Abdullah, *The way forward for the modification of dye-sensitized solar cell towards better power conversion efficiency.* Renewable & Sustainable Energy Reviews, 2017. **74**: p. 438-452.
9. McGehee, M.D., *Paradigm Shifts in Dye-Sensitized Solar Cells.* Science, 2011. **334**(6056): p. 607-608.
10. Bertoluzzi, L. and S.A. Ma, *On the methods of calculation of the charge collection efficiency of dye sensitized solar cells.* Physical Chemistry Chemical Physics, 2013. **15**(12): p. 4283-4285.
11. Oregan, B. and M. Gratzel, *A LOW-COST, HIGH-EFFICIENCY SOLAR-CELL BASED ON DYE-SENSITIZED COLLOIDAL TIO2 FILMS.* Nature, 1991. **353**(6346): p. 737-740.
12. Hagfeldt, A. and M. Gratzel, *LIGHT-INDUCED REDOX REACTIONS IN NANOCRYSTALLINE SYSTEMS.* Chemical Reviews, 1995. **95**(1): p. 49-68.
13. Mishra, A., M.K.R. Fischer, and P. Bauerle, *Metal-Free Organic Dyes for Dye-Sensitized Solar Cells: From Structure: Property Relationships to Design Rules.* Angewandte Chemie-International Edition, 2009. **48**(14): p. 2474-2499.
14. Shockley, W. and H.J. Queisser, *DETAILED BALANCE LIMIT OF EFFICIENCY OF P-N JUNCTION SOLAR CELLS.* Journal of Applied Physics, 1961. **32**(3): p. 510-&.
15. Martineau, D., *"DYE SOLAR CELLS FOR REAL" The Assembly Guide for Making YourOwn Solar Cells*. 2012, Solaronix.
16. Cherepy, N.J., et al., *Ultrafast electron injection: Implications for a photoelectrochemical cell utilizing an anthocyanin dye-sensitized TiO2 nanocrystalline electrode.* Journal of Physical Chemistry B, 1997. **101**(45): p. 9342-9351.
17. Shalini, S., et al., *Review on natural dye sensitized solar cells: Operation, materials and methods.* Renewable & Sustainable Energy Reviews, 2015. **51**: p. 1306-1325.
18. Koops, S.E., et al., *Parameters Influencing the Efficiency of Electron Injection in Dye-Sensitized Solar Cells.* Journal of the American Chemical Society, 2009. **131**(13): p. 4808-4818.

19. Kruger, J., et al., *Charge transport and back reaction in solid-state dye-sensitized solar cells: A study using intensity-modulated photovoltage and photocurrent spectroscopy.* Journal of Physical Chemistry B, 2003. **107**(31): p. 7536-7539.
20. Kern, R., et al., *Modeling and interpretation of electrical impedance spectra of dye solar cells operated under open-circuit conditions.* Electrochimica Acta, 2002. **47**(26): p. 4213-4225.
21. Schlichthorl, G., N.G. Park, and A.J. Frank, *Evaluation of the charge-collection efficiency of dye-sensitized nanocrystalline TiO2 solar cells.* Journal of Physical Chemistry B, 1999. **103**(5): p. 782-791.
22. Peter, L.M. and K.G.U. Wijayantha, *Electron transport and back reaction in dye sensitised nanocrystalline photovoltaic cells.* Electrochimica Acta, 2000. **45**(28): p. 4543-4551.
23. Sodergren, S., et al., *THEORETICAL-MODELS FOR THE ACTION SPECTRUM AND THE CURRENT-VOLTAGE CHARACTERISTICS OF MICROPOROUS SEMICONDUCTOR-FILMS IN PHOTOELECTROCHEMICAL CELLS.* Journal of Physical Chemistry, 1994. **98**(21): p. 5552-5556.
24. Cao, F., et al., *Electron transport in porous nanocrystalline TiO2 photoelectrochemical cells.* Journal of Physical Chemistry, 1996. **100**(42): p. 17021-17027.
25. Ferber, J., R. Stangl, and J. Luther, *An electrical model of the dye-sensitized solar cell.* Solar Energy Materials and Solar Cells, 1998. **53**(1-2): p. 29-54.
26. Halme, J., et al., *Device Physics of Dye Solar Cells.* Advanced Materials, 2010. **22**(35): p. E210-E234.
27. Dloczik, L., et al., *Dynamic response of dye-sensitized nanocrystalline solar cells: Characterization by intensity-modulated photocurrent spectroscopy.* Journal of Physical Chemistry B, 1997. **101**(49): p. 10281-10289.
28. Cappelluti, F., et al., *Consistent static and small-signal physics-based modeling of dye-sensitized solar cells under different illumination conditions.* Physical Chemistry Chemical Physics, 2013. **15**(35): p. 14634-14646.
29. Carl H. Hamann, A.H., Wolf Vielstich, *Electrochemistry*. 2007: Wiley-VCH.
30. Halme, J., *Linking optical and electrical small amplitude perturbation techniques for dynamic performance characterization of dye solar cells.* Physical Chemistry Chemical Physics, 2011. **13**(27): p. 12435-12446.

Appendix A : Experimental work by Audun Formo Buene

This section contains the experimental procedure of assembling the DSSC's used in this thesis, as written by Audun Formo Buene:

"TEC-8 FTO glass supplied by Dyenamo was washed with Deconex 21 (2 g/L H_2O) in an ultrasonic bath for 45 min, and then rinsed with deionized water and ethanol before air drying.

Five layers of transparent TiO_2 paste (20 nm, 18NR-T, Dyesol) were screen printed on the FTO glass (mesh count 250, active area diameter 5.5 mm). Between each layer the electrodes were heated to 125 °C for 5 min. Finally, a scattering layer (WER2-O, Dyesol) was screen printed, and the electrodes were sintered at 500 °C for 30 minutes. Determining the thickness of the sintered layer was done with a profilometer (Veeco, Dektak 150).

When cooled to 80 °C, the electrodes were placed in the staining solution, which had a dye concentration of 5×10^{-4} M and 5 mM of CDCA in a mixture of acetonitrile/THF (47:53, v/v). Staining times were 16-18 hours, before the electrodes were rinsed in ACN and air dried before sealing with counter electrodes from Solaronix (Platinum electrodes, predrilled). DuPont Surlyn (25 μm thick) was used for sealing.

The electrolyte (Iodolyte HI-30, Solaronix) was injected by vacuum backfilling before the filling hole was sealed with DuPont Surlyn and a circular glass disc. The contacts for the anode and cathode were painted with a conductive silver paint (Electrolube, SCP) before characterization."

Appendix B : Additional information on the thickness parameter d

One day before this thesis was submitted, new and more exact measurements of the active titanium dioxide layer was performed by Audun Formo Buene. The measurements were done with profilometer, and determined the thickness parameter d to be 12.75 +/- 1 μm.

Appendix C : MATLAB code

The scripts presented below should work if it is run in MATLAB 2016a, and if the functions below are saved. There are mainly four scripts, one for IMPS, one for IMVS, one for the IV-characteristic, and one for automatic iteration on n_0 and ϵ.

The functions used in the scripts for calculating IV, IMPS and IMVS

```
% Z_Re=F_Re, Z_Im=F_Im, C is used instead of n for electron
% concentration
% ya=[C_Re, Z_Re, C_Im, Z_Im] [C_Re, dC_Redx, C_Im, dC_Imdx]
% yb=[C_Re, Z_Re, C_Im, Z_Im] [C_Re, dC_Redx, C_Im, dC_Imdx]

function res=ANTA_bcs_IMPS(ya,yb)
res=[ya(1)-0; ya(3)-0; yb(2)-0; yb(4)-0];

function res=ANTA_bcs_IMVS(ya,yb)
res=[ya(2)-0; ya(4)-0; yb(2)-0; yb(4)-0];
```

```
function dYdx=ANTA_deriv_ss_v2(x,Y)

global k_0 e Phi_ss b a Beta Alpha D_0 C_0 n_inj n_refl d K_G
dYdx(1)=Y(2)/(D_0*(Y(1)/C_0).^a);
dYdx(2)=Beta/Alpha*k_0*(Y(1)/C_0)^b*Y(1)     -
n_inj.*K_G.*e*Phi_ss*(exp(-e*x)+n_refl*exp(e*(x-2*d)));
end


function dYdx=ANTA_deriv_t_v2(x,Y)
global k_0 e Phi_ss b a D_0 omega K_G Phi_A sol_ss C_0 K_D K_R
n_inj n_refl d
P_Re=Y(1);
Z_Re=Y(2);
P_Im=Y(3);
Z_Im=Y(4);

y=deval(sol_ss,x);
C_ss=y(1,:);
Z_ss=y(2,:);
dC_ssdx=Z_ss/(D_0*(C_ss/C_0)^a);

dYdx(1)=-P_Re*a*C_ss.^-1*dC_ssdx + Z_Re/C_ss.^a;
dYdx(2)= -Phi_A*n_inj*e*K_G*(exp(-e*x)/K_D+n_refl*exp(e*(x-
2*d)))    +     K_R/K_D*C_ss^b*P_Re*(1+b)-omega*P_Im/K_D;
dYdx(3)=Z_Im/C_ss^a - P_Im*a*C_ss^-1*dC_ssdx;
dYdx(4)=K_R/K_D*C_ss^b*P_Im*(1+b)+omega*P_Re/K_D;

end


function res=bcs_ss_IV(ya,yb)
global n_LB
res=[ya(1)-n_LB; yb(2)-0]; % open circuit
```

Code for calculating the IV-characteristic

```
clear y omega_grid save_alpha save_V_mod save_Z save_C x
save_x_IV n_omega_mesh J_R_int V_IV
global e Phi_ss C_0 d Beta Alpha n_LB n_refl n_inj b a D_0 k_0
K_G guess_LB K_D K_R omega Phi_A sol_ss
n_xmesh=100;
IV_mesh=100;
plot_on=0;
iv_on=1;
IV_plot_on=1;
```

```
d=10*10^-6;
%The following 4 lines creates the mesh in x
direction/thickness of TiO2
x1=(0:n_xmesh);
x=x1.^4+1; %How much denser mesh at the LeftBoundary? exp(x1)
is extremely dense, x.^3 less dense, x.^2 even less dense and
so on
x=x/max(x)*d;
x=[0, x]; %x does now starts at x=0, and ends at x=d, with
most gridpoints close to x=0.
%Pre allocating
save_C_Re=zeros(n_omega_mesh,length(x));
save_Z_Re=zeros(n_omega_mesh,length(x));
save_C_Im=zeros(n_omega_mesh,length(x));
save_Z_Im=zeros(n_omega_mesh,length(x));
V_Re_mod=zeros(n_omega_mesh,length(x));
V_Im_mod=zeros(n_omega_mesh,length(x));
save_omega=zeros(1,n_omega_mesh);
save_C=zeros(IV_mesh+1,length(x));
save_Z=zeros(IV_mesh+1,length(x));
save_x_IV=zeros(IV_mesh+1,length(x));

%% steady state
I_sc_mod=38.5;
save_C(1)=1;
Phi_ss=190;
R_shunt=0.1;
R=2*10^-3;
Alpha=0.4344;
Beta=0.6274; %Recombination %0.6 (målt til 0.72(3pkt) og
0.46(4pkt), )
a=(1-Alpha)/Alpha; %Since (1-Alpha)/Alpha is used mostly
b=(Beta-Alpha)/Alpha; % Since (Beta-Alpha)/Alpha is used
mostly
%%eksp input:
K_boltzmann= 1.38064852*10^-23;
e_charge=1.60217662*10^-19;
t_rec=0.027;
omega_eksp_IMVS=t_rec^-1;
t_trans=0.00862;
V_eksp=0.595;
I_sc_eksp=38.5;

n_refl=0;
n_inj=1;
Phi_A=Phi_ss*0.05;

K_D=D_0/C_0^a;
K_R=Beta*k_0/(Alpha*C_0^b);
K_G=0.3654; %Antall coloumb per watt
```

```
guess_LB= (K_G*Phi_ss*(1-exp(-e*d))/(d*K_R))^(1/(1+b)); %
Guess for value of c at left boundary. Needs to be good.
guess_RB= (K_G*Phi_ss*(1-exp(-e*d))/(d*K_R))^(1/(1+b));% Guess
for value of c at right boundary

for i=1:IV_mesh+1 %preallocating
save_x_IV(i,:)=x;
end

%THE CORE----------------------------------------
solinit = bvpinit([0,d],[guess_LB, guess_RB]); %edit, hvorfor
er ikke gjett_b global?
solinit.x=x; %[x x x x x x x x]
solinit.y=[0*x+(guess_LB+guess_RB)/2 ; 0*x]; %[c c c c c c c
c; z z z z z z z ]
sol_ss=bvp4c(@ANTA_deriv_ss_v2,@bcs_ss_Voc, solinit);
y=deval(sol_ss,x);
save_C(1,:)=y(1,:);
save_Z(1,:)=y(2,:);
C_ss=y(1,:);
Z_ss=y(2,:);
%The core end

if plot_on==1
    figure
plot(x,save_C(1,:),'k-*')
xlabel('x')
ylabel('c')
end

%kontroll
J_R_tot=Beta/Alpha*k_0*(save_C(1)/C_0)^b*save_C(1)*d;
J_G_tot=n_inj*Phi_ss*K_G*(1-exp(-e*d));%trapz(-
n_inj.*K_G.*e*Phi_ss*(exp(-e*x)));
n_n_0_ratio=save_C(1)/C_0;
V_mod_oc=log(save_C(1)/C_0)*K_boltzmann*298/(Alpha*e_charge);
t_rec_anta_k_0=(k_0*(save_C(1)/C_0)^b*save_C(1))^-1;
v__omega=(k_0*(save_C(1)/C_0)^b*save_C(1));
v__C1=save_C(1);

%% END STEADY STATE

%% IV-CURVE
if iv_on==1 %% finne resten av IV-kurven

temp=1:1:IV_mesh;
V_IV=V_mod_oc-temp/IV_mesh*V_mod_oc;

for i=1:IV_mesh

    n_LB=C_0*exp(Alpha*e_charge*V_IV(i)/K_boltzmann/298);
```

```
    solinit = bvpinit([0,d],[guess_LB, guess_RB]);
    solinit.x=x; %[x x x x x x x x]
    solinit.y=[y(1,:) ; y(2,:)]; %[c c c c c c c c; z z z z z
z z ]
    sol_ss=bvp4c(@ANTA_deriv_ss_v2,@bcs_ss_IV, solinit);
    y=deval(sol_ss,x);
    save_C(i+1,:)=y(1,:);
    save_Z(i+1,:)=y(2,:);
end
I_sc_mod=save_Z(end,1);

end
V_IV=[V_mod_oc V_IV];
I_IV=save_Z(:,1);


%% plot IV
if IV_plot_on==1
figure
plot(V_IV,I_IV,'b-')
xlabel('V [V]')
ylabel('I [A.m^-^2]')

hold on
plot(x_IV_eksp,y_IV_eksp,'k-')
xlabel('V [V]')
ylabel('I [A.m^-^2]')
set(gca,'FontSize',font_size_axis)
xlim([0,V_eksp*1.2]);
ylim([0, 40])
```

Code for calculating the IMVS-specter

```
%%
clear y omega_grid save_alpha save_V_mod save_Z save_C x
save_x_IV n_omega_mesh
global e Phi_ss C_0 d Beta Alpha n_LB n_refl n_inj b a D_0 k_0
K_G guess_LB K_D K_R omega Phi_A sol_ss %k_rec k_abs phi_0
Beta Alpha D_0 gjett_a_2 omega Phi_x sol_ss
n_xmesh=100; %grid points x
n_omega_mesh=100; %grid points IMVS

omega_min=2*pi*10^-1; %start"frekvens"
omega_max=2*pi*10^4;
plot_on=0; %PLot over steady state elektronkonsentrasjon
iv_on=0;   %This cannot be turned on if IMVS is to be turned
on. EDIT
IMVS_on=1;
```

```
d=10*10^-6;
%The following 4 lines creates the mesh in x
direction/thickness of TiO2
x1=(0:n_xmesh);
%x=exp(x1);
x=x1.^4+1;
x=x/max(x)*d;
x=[0, x];
save_C_Re=zeros(n_omega_mesh,length(x));
save_Z_Re=zeros(n_omega_mesh,length(x));
save_C_Im=zeros(n_omega_mesh,length(x));
save_Z_Im=zeros(n_omega_mesh,length(x));
V_Re_mod=zeros(n_omega_mesh,length(x));
V_Im_mod=zeros(n_omega_mesh,length(x));
save_omega=zeros(1,n_omega_mesh);
save_C=zeros(IV_mesh+1,length(x));
save_Z=zeros(IV_mesh+1,length(x));
save_x_IV=zeros(IV_mesh+1,length(x));

Phi_ss=190;
R=2*10^-3;
Alpha=0.4344;
Beta=0.6274; %Recombination %0.6 (målt til 0.72(3pkt) og
0.46(4pkt), )
a=(1-Alpha)/Alpha; %Since (1-Alpha)/Alpha is used mostly
b=(Beta-Alpha)/Alpha; % Since (Beta-Alpha)/Alpha is used
mostly
%%eksp input:
K_boltzmann= 1.38064852*10^-23;%8.617*10^-5;
e_charge=1.60217662*10^-19;
t_rec=0.027;%0.027;
omega_eksp_IMVS=t_rec^-1;
t_trans=0.00862;
V_eksp=0.595;
I_sc_eksp=39;
n_n_0=exp(Alpha*e_charge*V_eksp/(K_boltzmann*298)); %0.6 ble m


n_refl=1;
n_inj=1;
Phi_A=Phi_ss*0.05;%*0.0115;

K_D=D_0/C_0^a;
K_R=Beta*k_0/(Alpha*C_0^b);
K_G=0.3654; %Antall coloumb per watt

guess_LB= (K_G*Phi_ss*(1-exp(-e*d))/(d*K_R))^(1/(1+b));
guess_RB= (K_G*Phi_ss*(1-exp(-e*d))/(d*K_R))^(1/(1+b));% Guess
for value of c at right boundary
```

```
for i=1:IV_mesh+1
save_x_IV(i,:)=x;
end

%% steady state V_oc

%THE CORE----------------------------------------
solinit = bvpinit([0,d],[guess_LB, guess_RB]); %edit, hvorfor
er ikke gjett_b global?
solinit.x=x; %[x x x x x x x x]
solinit.y=[0*x+(guess_LB+guess_RB)/2 ; 0*x]; %[c c c c c c c
c; z z z z z z z ]
sol_ss=bvp4c(@ANTA_deriv_ss_v2,@bcs_ss_Voc, solinit);
y=deval(sol_ss,x);
save_C(1,:)=y(1,:);
save_Z(1,:)=y(2,:);
C_ss=y(1,:);
Z_ss=y(2,:);
%The core end

if plot_on==1
    figure
plot(x,save_C(1,:),'k-*')
xlabel('x')
ylabel('c')
end

%kontroll
J_R_tot=Beta/Alpha*k_0*(save_C(1)/C_0)^b*save_C(1)*d;
J_G_tot=n_inj*Phi_ss*K_G*(1-exp(-e*d));%trapz(-
n_inj.*K_G.*e*Phi_ss*(exp(-e*x)));
n_n_0_ratio=save_C(1)/C_0;
V_mod_oc=log(save_C(1)/C_0)*K_boltzmann*298/(Alpha*e_charge);
t_rec_anta_k_0=(k_0*(save_C(1)/C_0)^b*save_C(1))^-1;
v__omega=(k_0*(save_C(1)/C_0)^b*save_C(1));
v__C1=save_C(1);


%% END STEADY STATE V_oc
%% Calculate IMVS-"STEADY STATE"
%The same as earlier, excpet that the light intensity is a
little bit higher
Phi_ss=Phi_ss+Phi_A;
solinit = bvpinit([0,d],[guess_LB, guess_RB]);
solinit.x=x; %[x x x x x x x x]
solinit.y=[0*x+(guess_LB+guess_RB)/2 ; 0*x]; %[c c c c c c c
c; z z z z z z z ]
sol_IMVS=bvp4c(@ANTA_deriv_ss_v2,@bcs_ss_Voc, solinit);
y=deval(sol_IMVS,x);
C_m=y(1,:);
```

```
Z_m=y(2,:);
Phi_ss=Phi_ss-Phi_A;

%% END IMVS-"STEADY STATE"

 if IMVS_on==0

     return
 end
 telle_omega=0;
%% IMVS
temp=(0 : log(omega_max/omega_min)/n_omega_mesh :
log(omega_max/omega_min));
omega_grid=omega_min*exp(temp);

for i=1:n_omega_mesh+1
    omega=omega_grid(i);
    telle_omega=telle_omega+1;

if i==1 %må ha omega såpass lav at C_Re=C_Im=~0
    solinit = bvpinit([0,d],[guess_LB, guess_RB]); %edit
,spiller ingen rolle hva som står her
    solinit.x=x; %[x x x x x x x]
    solinit.y=[C_m-C_ss; 0*x; 0*x ; 0*x]; %[P_Re ; Z_Re; P_Im
    sol=bvp4c(@ANTA_deriv_t_v2,@ANTA_bcs_IMVS, solinit);
    y_first=deval(sol,x);
    y=deval(sol,x);
    C_Re_guess=y_first(1,:);
    dC_Redx_guess=y_first(2,:);
    C_Im_guess=y_first(3,:);
    dC_Imdx_guess=y_first(4,:);

else
    solinit = bvpinit([0,d],[C_Re_guess(1), C_Re_guess(end)]);
%edit ,spiller ingen rolle hva som står her
    solinit.x=x; %[x x x x x x x]
    solinit.y=[C_Re_guess ; dC_Redx_guess; C_Im_guess ;
dC_Imdx_guess]; %[C_Re ; dC_Redx; C_Im ; dC_Imdx;][C_Re C_Re
C_Re C_Re; Z_Re Z_Re Z_Re Z_Re ; C_Im C_Im C_Im C_Im C_Im;
Z_Im Z_Im Z_Im Z_Im ]
    sol=bvp4c(@ANTA_deriv_t_v2,@ANTA_bcs_IMVS, solinit);
    y=deval(sol,x);
    y_first=deval(sol,x);
    C_Re_guess=y(1,:);
    dC_Redx_guess=y(2,:);
    C_Im_guess=y(3,:);
    dC_Imdx_guess=y(4,:);
end
save_C_Re(i,:)=y(1,:);
save_Z_Re(i,:)=y(2,:);
save_C_Im(i,:)=y(3,:);
```

```
save_Z_Im(i,:)=y(4,:);
save_omega(i)=omega;
V_Re_mod(i,:)=log((save_C_Re(i,:)+C_ss)./C_ss)*K_boltzmann*298
/(Alpha*e_charge);
V_Im_mod(i,:)=log((save_C_Im(i,:)+C_ss)./C_ss)*K_boltzmann*298
/(Alpha*e_charge);

end

figure
semilogx(omega_grid/(2*pi),V_Im_mod(:,1),'-k')
xlabel('Frequency [Hz]')
ylabel('Im(Potential) [V.W^-^1.m^-^2]')
hold on
semilogx(x_IMVS,y_IMVS*3.5,'ok-
','LineWidth',line_width,'MarkerFaceColor','k')
xlim([10^-1,10^4])
set(gca,'FontSize',font_size_axis) % bruker 14 i rapport

f_min_eksp=Beta/Alpha*k_0*(C_ss(1)/C_0)^b*1/(2*pi);
```

Code for calculating the IMPS-specter

```
%%
clear y omega_grid save_alpha save_V_mod save_Z save_C x
save_x_IV n_omega_mesh J_R_int
global e Phi_ss C_0 d Beta Alpha n_LB n_refl n_inj b a D_0
k_0 K_G guess_LB K_D K_R omega Phi_A sol_ss %k_rec k_abs phi_0
Beta Alpha D_0 gjett_a_2 omega Phi_x sol_ss

figure
for w=1:1
n_xmesh=100; %antall gridpunkter
n_omega_mesh=100; %antall frekvsener som brukes i IMVS
IV_mesh=10;
omega_min=2*pi*10^-1; %start"frekvens"
omega_max=2*pi*10^4;
plot_on=0;
iv_on=1;
IMPS_on=1;
IV_plot_on=0;

d=10*10^-6;
x1=(0:n_xmesh);
x=x1.^4+1; %How much denser mesh at the LeftBoundary? exp(x1)
is extremely dense, x.^3 less dense, x.^2 even less dense and
so on
x=x/max(x)*d;
```

```
x=[0, x]; %x does now starts at x=0, and ends at x=d
save_C_Re=zeros(n_omega_mesh,length(x));
save_Z_Re=zeros(n_omega_mesh,length(x));
save_C_Im=zeros(n_omega_mesh,length(x));
save_Z_Im=zeros(n_omega_mesh,length(x));
V_Re_mod=zeros(n_omega_mesh,length(x));

save_omega=zeros(1,n_omega_mesh);
save_C=zeros(IV_mesh+1,length(x));
save_Z=zeros(IV_mesh+1,length(x));
save_x_IV=zeros(IV_mesh+1,length(x));

%% steady state
save_C(1)=1;
Phi_ss=190;

R=2*10^-3;
Alpha=0.4344;
Beta=0.6274; %Recombination %0.6 (målt til 0.72(3pkt) og
0.46(4pkt), )
a=(1-Alpha)/Alpha; %Since (1-Alpha)/Alpha is used mostly
b=(Beta-Alpha)/Alpha; % Since (Beta-Alpha)/Alpha is used
mostly
%%eksp input:
K_boltzmann= 1.38064852*10^-23;%8.617*10^-5;
e_charge=1.60217662*10^-19;
t_rec=0.027;%0.027;
omega_eksp_IMVS=t_rec^-1;
t_trans=0.00862;
omega_eksp_IMPS=t_rec^-1;
V_eksp=0.595;
I_sc_eksp=39.5;
n_n_0=exp(Alpha*e_charge*V_eksp/(K_boltzmann*298)); %0.6 ble m

n_refl=0;
n_inj=1;
Phi_A=Phi_ss*0.05;

K_D=D_0/C_0^a;
K_R=Beta*k_0/(Alpha*C_0^b);
K_G=0.3654; %Antall coloumb per watt

guess_LB= (K_G*Phi_ss*(1-exp(-e*d))/(d*K_R))^(1/(1+b)); %
Guess for value of c at left boundary. Needs to be good.
guess_RB= (K_G*Phi_ss*(1-exp(-e*d))/(d*K_R))^(1/(1+b));% Guess
for value of c at right boundary

for i=1:IV_mesh+1
save_x_IV(i,:)=x;
end
```

```
%THE CORE----------------------------------------------
solinit = bvpinit([0,d],[guess_LB, guess_RB]); %edit, hvorfor
er ikke gjett_b global?
solinit.x=x; %[x x x x x x x x]
solinit.y=[0*x+(guess_LB+guess_RB)/2 ; 0*x]; %[c c c c c c c
c; z z z z z z z ]
sol_ss=bvp4c(@ANTA_deriv_ss_v2,@bcs_ss_Voc, solinit);
y=deval(sol_ss,x);
save_C(1,:)=y(1,:);
save_Z(1,:)=y(2,:);
C_ss=y(1,:);
Z_ss=y(2,:);
%The core end

if plot_on==1
    figure
plot(x,save_C(1,:),'k-*')
xlabel('x')
ylabel('c')
end

%kontroll
J_R_tot=Beta/Alpha*k_0*(save_C(1)/C_0)^b*save_C(1)*d;
J_G_tot=n_inj*Phi_ss*K_G*(1-exp(-e*d));%trapz(-
n_inj.*K_G.*e*Phi_ss*(exp(-e*x))); Edit, mangler refleksjon
n_n_0_ratio=save_C(1)/C_0;
V_mod_oc=log(save_C(1)/C_0)*K_boltzmann*298/(Alpha*e_charge);
t_rec_anta_k_0=(k_0*(save_C(1)/C_0)^b*save_C(1))^-1;
v__omega=(k_0*(save_C(1)/C_0)^b*save_C(1));
v__C1=save_C(1);


%% END STEADY STATE

Phi_ss=Phi_ss+Phi_A;
solinit = bvpinit([0,d],[guess_LB, guess_RB]);
solinit.x=x; %[x x x x x x x x]
solinit.y=[0*x+(guess_LB+guess_RB)/2 ; 0*x]; %[c c c c c c c
c; z z z z z z z ]
sol_IMVS=bvp4c(@ANTA_deriv_ss_v2,@bcs_ss_Voc, solinit);
y=deval(sol_IMVS,x);
C_m=y(1,:);
Z_m=y(2,:);
Phi_ss=Phi_ss-Phi_A;


%% IV-CURVE
if iv_on==1 %% finne resten av IV-kurven

temp=1:1:IV_mesh;
V_IV=V_mod_oc-temp/IV_mesh*V_mod_oc;
```

```
for i=1:IV_mesh

    n_LB=C_0*exp(Alpha*e_charge*V_IV(i)/K_boltzmann/298);

    solinit = bvpinit([0,d],[guess_LB, guess_RB]);
    solinit.x=x; %[x x x x x x x x]
    solinit.y=[y(1,:) ; y(2,:)]; %[c c c c c c c c; z z z z z
z z ]
    sol_ss=bvp4c(@ANTA_deriv_ss_v2,@bcs_ss_IV, solinit);
    y=deval(sol_ss,x);
    save_C(i+1,:)=y(1,:);
    save_Z(i+1,:)=y(2,:);
end

V_IV=[V_mod_oc V_IV]; %Få med spenningen ved åpen krets også
if IV_plot_on==1
figure
plot(V_IV,save_Z(:,1),'ksq')
xlabel('V [V]')
ylabel('I [A.m^-^2]')

hold on
V_ny=V_IV-save_Z(:,1)'*R;
plot(V_ny,save_Z(:,1),'m*')
xlim([0,V_eksp*1.2]);

figure
plot(save_x_IV',save_C','r-')
xlabel('x')
ylabel('C')

%Calculating how much of the injected electrons recombine
Y=save_C; %Pre allocating
for i=1:IV_mesh+1
Y(i,:)=K_R*save_C(i,:).^(b+1);
J_R_int(i)=trapz(x,Y(i,:));
end

%Plotting a comparison to see that recombination is neglible
at sc.
figure
hold on
plot(V_IV,J_R_int,'r*')
plot(V_IV,save_Z(:,1),'c*')
plot(V_IV,V_IV*0+J_G_tot,'g*')
plot(V_IV,J_R_int+save_Z(:,1)',['k-')
end
end
%% END IV-CURVE
```

```
 if IMPS_on==0

     return
 end

%% IMPS
temp=(0 : log(omega_max/omega_min)/n_omega_mesh :
log(omega_max/omega_min));
omega_grid=omega_min*exp(temp);

for i=1:n_omega_mesh+1
    omega=omega_grid(i);

if i==1
    solinit = bvpinit([0,d],[guess_LB, guess_RB]);
    solinit.x=x; %[x x x x x x x x]
    solinit.y=[C_m-C_ss; Z_m-Z_ss; 0*x ; 0*x]; %[P_Re ; Z_Re;
P_Im ; Z_IM;]
    %edit, fix over
    sol=bvp4c(@ANTA_deriv_t_v2,@ANTA_bcs_IMPS, solinit);
    y_first=deval(sol,x);
    y=deval(sol,x);
    C_Re_guess=y_first(1,:);
    dC_Redx_guess=y_first(2,:);
    C_Im_guess=y_first(3,:);
    dC_Imdx_guess=y_first(4,:);

else
    solinit = bvpinit([0,d],[C_Re_guess(1), C_Re_guess(end)]);
    solinit.x=x; %[x x x x x x x x]
    solinit.y=[C_Re_guess ; dC_Redx_guess; C_Im_guess ;
dC_Imdx_guess]; %[C_Re ; dC_Redx; C_Im ; dC_Imdx;][C_Re C_Re
C_Re C_Re; Z_Re Z_Re Z_Re Z_Re ; C_Im C_Im C_Im C_Im C_Im;
Z_Im Z_Im Z_Im Z_Im ]
    sol=bvp4c(@ANTA_deriv_t_v2,@ANTA_bcs_IMPS, solinit);
    y=deval(sol,x);
    y_first=deval(sol,x);
    C_Re_guess=y(1,:);
    dC_Redx_guess=y(2,:);
    C_Im_guess=y(3,:);
    dC_Imdx_guess=y(4,:);
end
save_C_Re(i,:)=y(1,:);
save_Z_Re(i,:)=y(2,:);
save_C_Im(i,:)=y(3,:);
save_Z_Im(i,:)=y(4,:);
save_omega(i)=omega;

end
```

```
I_Im_plot=K_D*save_Z_Im(:,1);
semilogx(omega_grid/(2*pi),K_D*save_Z_Im(:,1),'k-')
xlabel('Frequency [Hz]')
ylabel('A.W^-^1.m^-^2')
hold on

f_min_Anta_way_model=Beta/Alpha*k_0*(C_ss(1)/C_0)^b*1/(2*pi);

end
%% END IMVS
semilogx(x_IMPS,10.5*y_IMPS/(9.62*10^-6),'k-o')
set(gca,'FontSize',font_size_axis)
xlim([10^-1, 10^4])
```

Iterative scheme for determination of ϵ and n_0

```
clear y omega_grid J_G_int save_alpha save_V_mod save_Z save_C
x save_x_IV n_omega_mesh J_R_int V_IV
global e Phi_ss C_0 d Beta Alpha n_LB n_refl n_inj b a D_0 k_0
K_G guess_LB K_D K_R omega Phi_A sol_ss %k_rec k_abs phi_0
Beta Alpha D_0 gjett_a_2 omega Phi_x sol_ss
n_xmesh=100; %antall gridpunkter
n_omega_mesh=100; %antall frekvsener som brukes i IMVS
IV_mesh=10;
omega_min=2*pi*10^-1; %start"frekvens"
omega_max=2*pi*10^4;
plot_on=0; %PLot over steady state elektronkonsentrasjon
iv_on=1;
IMPS_on=0; %Regne ut IMVS-spekter?
IV_plot_on=0;


d=10*10^-6;
x1=(0:n_xmesh);
%x=exp(x1);
x=x1.^4+1; %How much denser mesh at the LeftBoundary? exp(x1)
is extremely dense, x.^3 less dense, x.^2 even less dense and
so on
x=x/max(x)*d;
x=[0, x]; %x does now starts at x=0, and ends at x=d, with
most gridpoints close to x=0.
%preallokere plass
save_C_Re=zeros(n_omega_mesh,length(x));
save_Z_Re=zeros(n_omega_mesh,length(x));
save_C_Im=zeros(n_omega_mesh,length(x));
save_Z_Im=zeros(n_omega_mesh,length(x));
V_Re_mod=zeros(n_omega_mesh,length(x));
V_Im_mod=zeros(n_omega_mesh,length(x));
save_omega=zeros(1,n_omega_mesh);
save_C=zeros(IV_mesh+1,length(x));
```

```
save_Z=zeros(IV_mesh+1,length(x));
save_x_IV=zeros(IV_mesh+1,length(x));


%% steady state
I_sc_mod=38;
%e=9.1702*10^4;%2.2331*10^5;%1*3*5.4316*10^4;
I_sc_eksp=38.5;
e_0=0;
C_0_old=0;
V_mod_oc=0;

save_C(1)=1;
telle_C_0=0;
telle=0;
while abs(I_sc_mod-I_sc_eksp)>10^-1
telle=telle+1;
Phi_ss=190;

R=2*10^-3;
Alpha=0.4344;
Beta=0.6274; %Recombination %0.6 (målt til 0.72(3pkt) og
0.46(4pkt), )
a=(1-Alpha)/Alpha; %Since (1-Alpha)/Alpha is used mostly
b=(Beta-Alpha)/Alpha; % Since (Beta-Alpha)/Alpha is used
K_boltzmann= 1.38064852*10^-23;%8.617*10^-5;
e_charge=1.60217662*10^-19;
t_rec=0.027;%0.027;
omega_eksp_IMVS=t_rec^-1;
t_trans=0.00862;
V_eksp=0.595;

n_n_0=exp(Alpha*e_charge*V_eksp/(K_boltzmann*298)); %0.6 ble m

V_mod_oc=10000;

while abs(V_mod_oc-V_eksp)>10^-5
C_0_old=C_0;
C_0=save_C(1)*n_n_0^-1;%n_n_0^-1 * I_sc_eksp*t_rec*Alpha/Beta
;%0.001;%
telle_C_0=telle_C_0+1;

n_refl=0;
n_inj=1;
Phi_A=Phi_ss*0.01;

K_D=D_0/C_0^a;
K_R=Beta*k_0/(Alpha*C_0^b);
K_G=0.3654; %Antall coloumb per watt
```

```
guess_LB= (K_G*Phi_ss*(1-exp(-e*d))/(d*K_R))^(1/(1+b)); %
Guess for value of c at left boundary. Needs to be good.
guess_RB= (K_G*Phi_ss*(1-exp(-e*d))/(d*K_R))^(1/(1+b));% Guess
for value of c at right boundary

for i=1:IV_mesh+1
save_x_IV(i,:)=x;
end

%THE CORE----------------------------------------
solinit = bvpinit([0,d],[guess_LB, guess_RB]); %edit, hvorfor
er ikke gjett_b global?
solinit.x=x; %[x x x x x x x x]
solinit.y=[0*x+(guess_LB+guess_RB)/2 ; 0*x]; %[c c c c c c c
c; z z z z z z z ]
sol_ss=bvp4c(@ANTA_deriv_ss_v2,@bcs_ss_Voc, solinit);
y=deval(sol_ss,x);
save_C(1,:)=y(1,:);
save_Z(1,:)=y(2,:);
C_ss=y(1,:);
Z_ss=y(2,:);
%The core end

if plot_on==1
    figure
plot(x,save_C(1,:),'k-*')
xlabel('x')
ylabel('c')
end

%kontroll
J_R_tot=Beta/Alpha*k_0*(save_C(1)/C_0)^b*save_C(1)*d;
J_G_tot=n_inj*Phi_ss*K_G*(1-exp(-e*d));%trapz(-
n_inj.*K_G.*e*Phi_ss*(exp(-e*x)));
n_n_0_ratio=save_C(1)/C_0;
V_mod_oc=log(save_C(1)/C_0)*K_boltzmann*298/(Alpha*e_charge);
t_rec_anta_k_0=(k_0*(save_C(1)/C_0)^b*save_C(1))^-1;
v__omega=(k_0*(save_C(1)/C_0)^b*save_C(1));
v__C1=save_C(1);

%% END STEADY STATE
end

%% IV-CURVE
if iv_on==1 %% finne resten av IV-kurven

temp=1:1:IV_mesh;
V_IV=V_mod_oc-temp/IV_mesh*V_mod_oc;

for i=1:IV_mesh
```

```
    n_LB=C_0*exp(Alpha*e_charge*V_IV(i)/K_boltzmann/298);

    solinit = bvpinit([0,d],[guess_LB, guess_RB]); %edit,
hvorfor er ikke gjett_b global?
    solinit.x=x; %[x x x x x x x x]
    solinit.y=[y(1,:) ; y(2,:)]; %[c c c c c c c c; z z z z z
z z ]
    sol_ss=bvp4c(@ANTA_deriv_ss_v2,@bcs_ss_IV, solinit);
    y=deval(sol_ss,x);
    save_C(i+1,:)=y(1,:);
    save_Z(i+1,:)=y(2,:);
end
I_sc_mod=save_Z(end,1);
e_0=e;
e=e+(1-I_sc_mod/(I_sc_eksp))*(e);   %Beregnet

end
V_IV=[V_mod_oc V_IV]; %Få med spenningen ved åpen krets også

end

%% plot IV
if IV_plot_on==1
figure
plot(V_IV,save_Z(:,1),'ksq')
xlabel('V [V]')
ylabel('I [A.m^-^2]')

hold on
V_ny=V_IV-save_Z(:,1)'*R;
plot(V_ny,save_Z(:,1),'m*')
xlim([0,V_eksp*1.2]);

figure
plot(save_x_IV',save_C','r-')
xlabel('x')
ylabel('C')

%Calculating how much of the injected electrons recombine
Y=save_C; %Pre allocating
Y_G=Y;
for i=1:IV_mesh+1
Y(i,:)=K_R*save_C(i,:).^(b+1);
Y_G(i,:)=n_inj*Phi_ss*K_G*e*(exp(-e*x)+n_refl*exp(e*(x-2*d)));
J_R_int(i)=trapz(x,Y(i,:));
J_G_int(i)=trapz(x,Y_G(i,:));
end

figure
hold on
plot(V_IV,J_G_int,'g*')
```

```
plot(V_IV,J_R_int,'r*')
plot(V_IV,save_Z(:,1),'c*')
plot(V_IV,J_R_int+save_Z(:,1)','k-')
end
%% END IV-CURVE
```